

**STUDIES ON ABOVEGROUND STORAGE TANKS SUBJECTED TO
SEISMIC EXCITATION AND FOUNDATION SETTLEMENT**

by

Harsh Bohra

A Thesis

Submitted to the Faculty of Purdue University

In Partial Fulfillment of the Requirements for the degree of

Master of Science in Civil Engineering



Lyles School of Civil Engineering

West Lafayette, Indiana

May 2020

THE PURDUE UNIVERSITY GRADUATE SCHOOL
STATEMENT OF COMMITTEE APPROVAL

Dr. Sukru Guzey, Chair

Lyles School of Civil Engineering

Dr. Mark D. Bowman

Lyles School of Civil Engineering

Dr. Ayhan Irfanoglu

Lyles School of Civil Engineering

Approved by:

Dr. Dulcy M. Abraham

Dedicated to my parents

ACKNOWLEDGMENTS

The work of scientific research community laid the foundation of my thesis, therefore my first and foremost acknowledgement goes to them.

I would like to thank my advisor, Dr. Sukru Guzey for his continuous support and guidance throughout my journey. I will always be indebted to Dr. Guzey for having trust in my abilities, having the patience and for always keeping me motivated. I would also like to thank rest of my committee members, Dr. Mark D. Bowman and Dr. Ayhan Irfanoglu for reviewing my work and for their insightful comments and suggestions on my thesis.

I would like to extend my gratitude to my research group for proofreading my work and giving their insights. I would like to thank Yen Chen and Eyas for being an outstanding mentor. I will be always be grateful to Rahul, who inspired me learn scripting in Abaqus.

I would like to express my gratitude to Mr. Baker for offering me the opportunity to work on various industrial projects and for providing me financial support for my graduate studies.

My time at Purdue University would have be uneventful without my friends and colleagues: Tarutal, Rahul, Shubham, Preshit, Deepak, Saurabh and Shreya. Our discussion on politics and engineering have always be delightful.

.

Finally, I would like to thank my parents, who have always been there for me. None of this would be possible without there encouragement and support.

TABLE OF CONTENTS

LIST OF TABLES	7
LIST OF FIGURES	8
ABSTRACT.....	11
1. INTRODUCTION	13
1.1 Thesis Background.....	13
1.2 Objective and Scope	14
1.3 References.....	15
2. SEISMIC ANALYSIS OF OPEN-TOP STORAGE TANKS WITH FLEXIBLE FOUNDATION	17
2.1 Introduction.....	18
2.2 Methodology.....	23
2.2.1 Tank design and geometry.....	24
2.2.2 Loading	25
2.2.2.1 Gravity and hydrostatic loading	25
2.2.2.2 Housner rigid wall model.....	26
2.2.2.3 Jacobsen-Veletsos rigid wall model	27
2.2.3 Finite Element Modelling	29
2.2.3.1 Material Properties	29
2.2.3.2 Finite Element Mesh.....	29
2.2.3.3 Finite Element Step	30
2.2.3.4 Finite Element Loading	30
2.2.3.5 Boundary conditions.....	32
2.3 Results and Discussion	32
2.3.1 Hoop Stress	33
2.3.2 Longitudinal Stress	37
2.3.3 Buckling.....	39
2.4 Conclusions.....	41
2.5 References.....	45

2.6	Tables.....	51
2.7	Figures.....	55
3.	FITNESS-FOR-SERVICE OF OPEN-TOP STORAGE TANKS SUBJECTED TO DIFFERENTIAL SETTLEMENT.....	74
3.1	Introduction.....	75
3.2	Settlement calculation model.....	79
3.2.1	Tank geometry.....	80
3.2.2	Tank Design.....	80
3.2.3	Criterion for the limiting settlement.....	81
3.2.4	FEA procedure.....	83
3.2.5	FEA limiting settlement results.....	84
3.3	Validation of the proposed method.....	86
3.3.1	Tank models for the validation of the proposed method.....	86
3.3.2	Modeling measured actual settlement in FEA.....	86
3.3.2.1	The Fourier transformation of settlement data.....	87
3.3.3	Proposed method for the evaluation of allowable differential settlement.....	89
3.3.4	FEA results for validation.....	91
3.4	Comparison between the existing API method and the proposed method.....	92
3.4.1	API 653 method-1 settlement amplitude.....	93
3.4.2	Proposed method settlement amplitude.....	93
3.4.3	Comparison of the API 653 method-1 and the proposed method.....	94
3.5	Conclusion.....	95
3.6	Appendix A: Shell thickness and wind girder details.....	98
3.7	Appendix B: Example problem to use the proposed method.....	100
3.8	Appendix C: Study on effect of rotational boundary condition.....	102
3.9	Appendix D: Limiting settlement value from FEA.....	103
3.10	Tables.....	105
3.11	Figures.....	111
3.12	References.....	121
4.	CONCLUSION.....	124

LIST OF TABLES

Table 2-1 : Tank geometric properties ^{a, b}	51
Table 2-2: The C_i coefficients, impulsive and convective time periods, and convective acceleration	51
Table 2-3: Top wind girder design in accordance with API 650 ^{a, b, c}	52
Table 2-4: Comparison of hoop stresses in psi (MPa) ^a for tanks.....	52
Table 2-5: Comparison of longitudinal stresses in psi (MPa) ^a for Tank-1	53
Table 2-6 Comparison of longitudinal stresses in psi (MPa)a for Tank-2.....	53
Table 2-7: Comparison of longitudinal stresses in psi (MPa)a for Tank-3.....	54
Table 3-1: Notation to identify tank geometry, aspect ratio and geometric ratio for each tank considered	105
Table 3-2: Constant U_n and p_n of power functions corresponding to limiting settlement for different harmonic wave numbers	106
Table 3-3: Tank-ID and randomly selected design parameters for tank models used in validation of proposed method.....	106
Table 3-4: Measured natural settlement data in mm taken from Gong et al. [21]	107
Table 3-5: Fourier transformation coefficients, C_n , phase angles, ϕ_n , corresponding maximum error and R^2 values for measured settlement data.....	108
Table 3-6: The settlement scaling factor based on method-1 for different tank models and settlement profiles	109
Table 3-7: The settlement scaling factor based on proposed for different tank models and settlement profiles.....	110

LIST OF FIGURES

Figure 2-1: Housner’s “Spring-mass” model [2]	55
Figure 2-2: Haroun-Housner’s “spring-mass” model for flexible tank [15].....	56
Figure 2-3: Wind girder details in accordance with API 650 [54]	57
Figure 2-4: Hydrostatic, impulsive and convective pressure distribution diagrams on tank shell	58
Figure 2-5: Plot for Tank-2 impulsive base pressure and approximate polynomial function	59
Figure 2-6: Stress-strain curve for ASTM A516 Grade 70 and ASTM A36 steel. To convert to MPa, multiply stress in ksi by a factor of 6.9	60
Figure 2-7: Finite element model of Tank-1 using Abaqus CAE.....	61
Figure 2-8: Design Response Spectra using API 650 procedure.....	62
Figure 2-9: Comparison of total hoop stresses in psi for tanks; to convert stress values to MPa multiply stress in ksi by 6.9	63
Figure 2-10: Rotation and uplift of base of Tank 3 for flexible foundation with elevation and plan view of tank bottom plate. Tanks shell is not shown for clarity. Positive values indicate uplift and negative values indicate tank base penetrating or settling to foundation. Uplift is given in inches. To convert uplift values to mm, multiply values in inches with 25.4.....	64
Figure 2-11: Normalized nonlinear radial deformation of Tank-1 and Tank-3 using Riks method. LPF represent the percentage of load applied. Deformation is measured for the topmost point; deformation is normalized to ht of the respective tanks.....	65
Figure 2-12: Comparison of contribution of higher impulsive modes to only first impulsive mode	66
Figure 2-13: Normalized nonlinear uplift of (a) Tank-1 and (b) Tank-3 using Riks method. LPF represent the percentage of load applied. Uplift is measured for the extreme point on tank bottom; uplift is normalized to Rt of the respective tanks	67
Figure 2-14: Normalized nonlinear behaviour of Tank-1 using Riks method. LPF represent the percentage of load applied. Deformation is measured from the point of maximum hoop stress; deformation is normalized to Rt of the respective tank	68
Figure 2-15: (a), Hoop stress and (b) Longitudinal stress with deformation of Tank-1 under hydrostatic, gravity and hydrodynamic loads. Stress values shown are in psi; to convert them to MPa, multiply stress in psi by 6.9×10^{-3}	69
Figure 2-16: Normalized nonlinear behaviour of Tank-2 using Riks method. LPF represent the percentage of load applied. Deformation is measured from the point of maximum hoop stress; deformation is normalized to Rt of the respective tank	70

Figure 2-17: (a), Hoop stress and (b) Longitudinal stress with deformation Tank-2 under hydrostatic, gravity and hydrodynamic loads. Stress values shown are in psi; to convert them to MPa, multiply stress in psi by 6.9×10^{-3}	71
Figure 2-18: Normalized nonlinear behaviour of Tank-3 using Riks method. LPF represent the percentage of load applied. Deformation is measured from the point of maximum hoop stress; deformation is normalized to R_t of the respective tank	72
Figure 2-19: (a), Hoop stress and (b) Longitudinal stress with deformation of Tank-3 under hydrostatic, gravity and hydrodynamic loads. Stress values shown are in psi; to convert them to MPa, multiply stress in psi by 6.9×10^{-3}	73
Figure 3-1: Coordinate system for the cylindrical shell model.....	111
Figure 3-2: Wind girder details in accordance with API 650 [23]	111
Figure 3-3: True stress-strain diagram for A36 and A516 Grade 70 material specifications; to convert stress values to MPa multiply stress in ksi by 6.9.....	112
Figure 3-4: FEA mesh for TK-360 with a close-up view to the top wind girder	112
Figure 3-5: Limiting settlement for different geometric ratios for harmonic wave number $n=2$. The settlement values are shown in inches; to convert settlement values to mm, multiply values in inches with 25.4.	112
Figure 3-6: Limiting settlement for different geometric ratios for harmonic wave number $n= 3$. The settlement values are shown in inches; to convert settlement values to mm, multiply values in inches with 25.4.	113
Figure 3-7: Limiting settlement for different geometric ratios for harmonic wave number $n= 4$. The settlement values are shown in inches; to convert settlement values to mm, multiply values in inches with 25.4.	113
Figure 3-8: Deformed tank TK-90c under application of pure harmonic settlement profile for (a) $n=2$, (b) $n=3$ and (c) $n=4$. The total displacement magnitude values are shown in inches; to convert displacement values to mm, multiply values in inches with 25.4.....	114
Figure 3-9: Von Mises membrane stresses with deformation for tank TK-90c under application of a pure harmonic settlement profile for (a) $n=2$, (b) $n=3$ and (c) $n=4$. The stress values area shown in psi; to convert the stress value to MPa, multiply the stress in psi by 6.9×10^{-3}	115
Figure 3-10: The approximated settlement profile using Fourier transformation and actual measured data for (a) Profile-1, (b) Profile-2, (c) Profile-3, and (d) Profile-4.....	116
Figure 3-11: CDF value at failure settlement profile level of $z_f\theta$ for the set-1 tanks.....	117
Figure 3-12: CDF value at failure settlement profile level of $z_f\theta$ for the set-2 tanks.....	117
Figure 3-13: CDF value at failure settlement profile level of $z_f\theta$ for the set-3 tanks.....	118
Figure 3-14: Normalized settlement scaling factor for (a) Profile-2 and (b) Profile-3 for the set-1 tanks with different aspect ratio. The normalization is done with respect to settlement scaling factor obtained from FEA	119

Figure 3-15: Normalized settlement scaling factor for (a) Profile-2 and (b) Profile-3 for the set-2 tanks with same aspect ratio. The normalization is done with respect to settlement scaling factor obtained from FEA 119

Figure 3-16: Normalized settlement scaling factor for (a) Profile-2 and (b) Profile-4 for the set-3 tanks with different aspect ratio. The normalization is done with respect to settlement scaling factor obtained from FEA 120

ABSTRACT

The author aims to investigate the current design provision for seismic and foundation settlement design of aboveground open-top storage tanks using finite element analysis. The thesis is divided into two independent but closely related studies: (1) seismic analysis of open-top storage tanks with flexible foundation and (2) fitness-for-service of open-top storage tanks subjected to differential settlement.

The present seismic design provisions in American Petroleum Institute's storage tank standard API 650 (2013) assumes the tank foundation is rigid and therefore, ignores the effect of uplift during a seismic excitation. In the first study, the objective was to quantitatively critique rigid foundation assumption and conclude if the assumption is acceptable or not for a given tank geometry. Tanks with three different height to diameter ratio (H/D), i.e aspect ratios, of 0.67, 1.0 and 3.0 representing broad, nominal and slender geometry, respectively, were modelled having both rigid and flexible foundations. The flexible foundation was modelled with series of non-linear compression only springs. Additionally, for each tank model two different hydrodynamic pressure distribution suggested by (1) Housner and (2) Jacobsen-Veletsos were applied which are used by API 650 and Eurocode 8, respectively. Geometric non-linear analysis with non-linear material properties was conducted (GMNA) using Riks algorithm in Abaqus finite element analysis (FEA) program. The hoop stresses, longitudinal stresses, uplift and buckling capacity of each rigid foundation tank model were compared with its respective flexible foundation tank model and corresponding API 650 rule based provisions. It was observed that the assumption of rigid foundation from design point of view is acceptable for the broad tank, however, for the nominal and slender tanks this assumption is not acceptable. The buckling capacity of nominal and slender tanks having flexible foundation are significantly lower compared to rigid foundation. Therefore, the effect of uplift should not be neglected for design purposes for nominal and slender tank geometries.

In the second study, an alternative method for evaluating the structural integrity of storage tank subjected to differential settlement is proposed. The limitations of the existing method in API 653 (2014), currently used in the industry are highlighted. The tank settlement is measured underneath the tank bottom along the tank circumference at discrete locations. The settlement can be transformed into a Fourier series by combining different harmonic components. In the existing API 653 method there is no distinction between the effects of different harmonic components whereas in the proposed method the effects of first five harmonic components are individually accounted and the cumulative damage is evaluated. The proposed method is formulated based on FEA conducted on twenty-one different tank models with each having different tank geometry. The limiting settlement value for each harmonic wave number is found for a given tank geometry by conducting GMNA using Riks algorithm, and a generalized trend is found for each harmonic wave number. The proposed method is further validated by performing numerous FEA simulations. The simulations were conducted for several tank models subjected to four representative actual measured settlement data. A set of tank models used in the validation was generated using random tank geometries and design parameters to have a blind test of the proposed method. Finally, a comparison is made between allowable settlement based on the API 653 method, the proposed method and the FEA. It was observed that the proposed method consistently results in conservative results compared to FEA. In contrast the API 653 method does not always result in conservative results. For some measured settlement data, the API 653 method gives overly conservative values and for others it gives non-conservative values. Moreover, the API 653 method is based on the beam theory which may not capture the true shell behavior. Therefore, the API 653 method requires modifications. The proposed method on the other hand is consistent and is based FEA which can capture the true shell behavior as it is formulated using shell theory. Therefore, it is recommended that the existing method in API 653 shall be replaced with the proposed method to determine the fitness of tank under differential settlement.

1. INTRODUCTION

1.1 Thesis Background

Aboveground storage tanks are widely used for storage of different petroleum products, fertilizers, chemicals and other liquid products. These tanks are cylindrical, vertical, open- or closed-top, aboveground and flat bottom. These tanks are generally built using steel and are cost effective as the required shell thickness is relatively thin. The typical range of tank radius to shell thickness is between 1000-7000. The failure of these tanks can cause enormous economic loss and even led to environmental disaster. These tanks are continuously subjected to different environmental loads and are susceptible to various structural failures. The primary environmental loads are seismic excitation, lateral wind load and foundation settlement. The failure of tank is likely to take place due to yielding or buckling of the tank shell. The thesis focuses on design and analysis provision currently used in the industry for seismic design and foundation settlement.

The Annex E of the API 650 standard [1] governs the seismic design provisions for aboveground, open-top storage tanks. The API 650 design criteria are based on the work done by Housner and coworkers [2, 3]. Housner presented a simple spring-mass analog which splits the complicated dynamic response of tank-liquid system into two different parts: (1) impulsive and (2) convective. Housner's model gives an approximate closed form solution which is simple to understand and use by practicing engineers. Housner's model is widely used across the globe by API 650, ACI 350.3-06 [4], AWWA D-100 [5] and Indian Standard 10987: 1992 [6]. Nonetheless, Housner's model assumes that the tank base is rigid and there is negligible uplift of the tank bottom during the seismic excitation. Researchers such as Clough [7] and Natsiavas and Babcock [8] observed that if the tank uplift allowed the stresses in the tank will increase. The first study in the thesis investigates the effect of flexible foundation using FEA and compares the results with API 650 hand calculation. The FEA is conducted based on Housner's approximate model and using exact solution proposed by Jacobsen-Veletsos model. The study aims to give thorough insights on the applicability of the design philosophy used in API 650 Annex E for seismic design on different tank geometries. The results of this study have been published in ASME Journal of Pressure Vessel Technology [9].

The Annex B of the API 653 [10] governs the fitness-for-service of storage tank subjected to settlement. The tanks are susceptible to settlement because they are typically built on soft soil. Researchers are working to determine the effect of settlement on overall structural integrity and functionality. The settlement can be transformed into Fourier series using different harmonic component [11]. In the last two decades extensive research has been done on influence of different harmonic component on buckling capacity of open-top and closed roof tanks [12-18]. The research indicates that there is a significant difference between the allowable settlement for different harmonic components. Nonetheless, the current design guidelines are still based on prior research findings of Marr et. al [19]. The current method does not differentiate between different harmonic components. In the second study, an alternate method is proposed to bridge the gap between the current research and the current industrial practice. The limiting settlement values are found for different harmonic components. The method is validated using FEA with actual measured settlement data. The study focuses on the limitations of the existing method in API 653 and a practical solution to overcome those limitations.

1.2 Objective and Scope

The objective of the study is to investigate the current design and analysis provisions used in the industry for design of aboveground open-top storage tanks. The assumptions used in the current provision for seismic design are investigated and an alternate analysis method used for determining the fitness-for-service under differential settlement is proposed.

The scope of the study includes: (1) Seismic analysis of open-top storage tanks with flexible foundation and (2) Fitness-for-service of open-top storage tanks subjected to differential settlement.

1.3 References

- [1] American Petroleum Institute (API) Standard 650, *Welded steel tanks for oil storage, 12th Edition*, American Petroleum Institute. 2013.
- [2] G. W. Housner, "Dynamic Pressure on Fluid Containers," in *Technical Information Document (TID) 7024, Chapter 6 and Appendix F*, U.S. Atomic Energy Commission, 1963, ch. Chapter 6, pp. 183-209.
- [3] G. W. Housner, "The dynamic behavior of water tanks," *Bulletin of the seismological society of America*, vol. 53, no. 2, pp. 381-387, 1963.
- [4] American Concrete Institute (ACI), *Seismic Design of Liquid-Containing Concrete Structures and Commentary, ACI 350.3-06*, Farmington Hills, MI, 2006.
- [5] American Water Works Association (AWWA), *Welded Steel Tanks for Water Storage, AWWA D-100*, Denver, CO, 2016.
- [6] B. o. I. Standards, *IS 10987 : Code of practice for design, fabrication, testing and installation of underground/above ground horizontal cylindrical storage tanks for petroleum products*. 1992.
- [7] D. P. Clough, "Experimental evaluation of seismic design methods for broad cylindrical tanks," University of California Earthquake Engineering Research Center, Berkeley, CA, USA, UCB/EERC 77-10,, 1977.
- [8] S. Natsiavas and C. D. Babcock, "Behavior of unanchored fluid-filled tanks subjected to ground excitation," *Journal of Applied Mechanics*, vol. 55, no. 3, pp. 654-659, 1988.
- [9] H. Bohra, E. Azzuni, and S. Guzey, "Seismic analysis of open-top storage tanks with flexible foundation," *Journal of Pressure Vessel Technology*, vol. 141, no. 4, 2019.
- [10] American Petroleum Institute (API) Standard, "API 653: Tank inspection, repair, alteration and reconstruction," 5th ed: American Petroleum Institute, Washington, DC.
- [11] Z. Malik, J. Morton, and C. Ruiz, "Ovalization of cylindrical tanks as a result of foundation settlement," *The Journal of Strain Analysis for Engineering Design The Journal of Strain Analysis for Engineering Design*, vol. 12, no. 4, pp. 339-348, 1977.
- [12] Q.-s. Cao and Y. Zhao, "Buckling strength of cylindrical steel tanks under harmonic settlement," *Thin-Walled Structures*, vol. 48, no. 6, pp. 391-400, 2010.
- [13] J. Gong, W. Cui, S. Zeng, and T. Jin, "Buckling analysis of large scale oil tanks with a conical roof subjected to harmonic settlement," *Thin-Walled Structures*, vol. 52, pp. 143-148, 2012.
- [14] J. Gong, J. Tao, J. Zhao, S. Zeng, and T. Jin, "Buckling analysis of open top tanks subjected to harmonic settlement," *Thin-walled structures.*, vol. 63, pp. 37-43, 2013.

- [15] J. Gong, J. Tao, J. Zhao, S. Zeng, and T. Jin, "Effect of top stiffening rings of open top tanks on critical harmonic settlement," *Thin-Walled Structures*, vol. 65, pp. 62-71, 2013.
- [16] J. G. Gong, Z. Q. Zhou, and F. Z. Xuan, "Buckling strength of cylindrical steel tanks under measured differential settlement: Harmonic components needed for consideration and its effect," *Thin-Walled Structures*, vol. 119, pp. 345-355, 2017.
- [17] M. Jonaidi and P. Ansourian, "Harmonic settlement effects on uniform and tapered tank shells," *Thin-Walled Structures*, vol. 31, no. 1, pp. 237-255, 1998.
- [18] Y. Zhao, Q.-s. Cao, and X.-y. Xie, "Floating-roof steel tanks under harmonic settlement: FE parametric study and design criterion," *J. Zhejiang Univ. - Sci. A Journal of Zhejiang University-SCIENCE A : Applied Physics & Engineering*, vol. 7, no. 3, pp. 398-406, 2006.
- [19] W. A. Marr, J. A. Ramos, and T. W. Lambe, "Criteria for settlement of tanks," *Journal of the Geotechnical Engineering Division*, vol. 108, no. 8, pp. 1017-1039, 1982.

2. SEISMIC ANALYSIS OF OPEN-TOP STORAGE TANKS WITH FLEXIBLE FOUNDATION

Summary

The behavior of aboveground storage tanks subjected to seismic excitation was investigated using numerical methods by taking flexibility of foundation into account. The hydrostatic load due to stored liquid has an axisymmetric distribution on the tank shell and base. However, during seismic events, the hydrodynamic load originating from the seismic acceleration of liquid in the tank start to act in the direction of the earthquake motion. This leads to a non-axisymmetric loading distribution, which may result in buckling and uplifting of the tank structure. Finite element models were created having nonlinear material properties and large deformation capabilities. Three different tank geometries with liquid height to tank radius aspect ratios of 0.67, 1.0 and 3.0 were selected representing broad, nominal and slender tanks. These tanks were subjected to two different hydrodynamic loading based on Housner's and Jacobsen-Veletsos' pressure distributions, which forms the basis of design provisions used in American Petroleum Institute API 650 and Eurocode 8, respectively. These pressure distributions were formulated under the assumption of rigid tank wall and base. Furthermore, each tank for a given geometry was subjected to two different foundations; (1) representing a rigid foundation and (2) representing a flexible foundation. The flexible foundation was created using a series of compression only elastic springs attached to tank base having equivalent soil stiffness. Static analysis corresponding to maximum dynamic force was performed. The finite element results for circumferential and longitudinal stress in the shell were compared with the provisions of API 650. It was found that the effect of foundation flexibility from the practical design point of view may be neglected for broad tanks but should be considered for nominal and slender tanks.

2.1 Introduction

Large aboveground steel storage tanks are generally used for storing variety of liquid products such as water, petroleum products, fertilizers, hazardous chemicals, and other liquids. The structural and mechanical integrity of these tanks are of interest because their failure may cause environmental disasters and economic losses. The storage tanks are vertical, aboveground, cylindrical, closed- or open-top welded tanks with uniformly supported flat bottom plate. These tanks are prone to failure when subjected to lateral wind loads when they are empty or seismic excitation when they store liquid. The damages likely take place due to buckling or yielding of tank shell. Therefore, a considerable amount of research has been conducted for the design and analysis of these tanks under seismic excitation [1-50].

Jacobsen [1] investigated the impulsive hydrodynamic behavior of fluid contained in cylindrical tanks under seismic excitation in as early as 1940s. The aim was to calculate the effective hydrodynamic masses and mass moments due to impulsive horizontal motion under seismic excitation. Jacobsen assumed that the cylindrical boundaries of the tank do not deform as a consequence of motion. Thus, the tank was considered to have rigid walls and foundation.

The hydrodynamic pressure can be divided into two parts, the impulsive pressure and the convective (sloshing) pressure. The impulsive pressure corresponds to the fluid which moves along with the tank; oscillating with the same frequency as that of tank. The convective pressure corresponds to fluid which generates waves when accelerated horizontally against the tank wall, and thus, oscillates independently.

Jacobsen analysis however, considers only impulsive pressure and neglects the effect of convective pressure. His analysis provides the basis for many of the storage tank seismic design standards such as Eurocode 8 [51] and New Zealand Society of Earthquake Engineering (NZSEE) [52]. He derived the expression for velocity potential. The velocity potential must satisfy the Laplace equation in accordance with fluid mechanics principles. The velocity potential function was found using the tank boundary conditions. The expression of impulsive pressure distribution was calculated using the Eq.(1),

$$p = -\gamma_l \frac{d\phi}{dt} \quad (1)$$

where p represents the impulsive pressure, γ_l represents the specific weight of the fluid, t represents time and ϕ represents the velocity potential function.

The solution of the Laplace equation for velocity potential and corresponding impulsive pressure distribution involves infinite series of the modified Bessel functions. Although, Jacobsen approach obtained the theoretical solution, dealing with infinite series of modified Bessel functions was rather sophisticated to use for practicing engineers especially in the pre-computer era.

Later, Housner [2, 3] in the mid-1950s further carried the investigation of hydrodynamic behavior of tanks under seismic excitation using an approximate method which would avoid partial differential equations and infinite series and presents the hydrodynamic behavior in a simple form. The aim was to provide a simple closed form solution which could be used by practicing engineers. Similar to Jacobsen, Housner also assumed the tank to have rigid walls and rigid foundation. Housner created a spring-mass mechanical analog model for liquid storage tanks experiencing seismic loads. The spring-mass analogy in this context was apparently first proposed by Westergaard in early 1930s for a study on fluid-structure interaction of dam-reservoir system subjected to seismic excitation [53].

While Jacobsen was only considering the impulsive motion of the liquid, Housner used a spring-mass mechanical analog, separating the tank-liquid system into two parts: the impulsive mass and the convective (sloshing) mass. The impulsive mass is the lower portion of the liquid which moves along with the tank and is modeled as a “rigidly-tied” portion to the tank at its center of action as shown in Figure 2-1. The convective (sloshing) mass is the upper portion of the liquid which generates waves when accelerated horizontally against the tank wall, and thus, oscillates independently from the tank wall and impulsive liquid mass

Splitting the complicated system of hydrodynamic forces into two different parts made it is easier to analyze the system and then superpose their effects. Housner’s model is widely used by various design documents such as API 650 Standard [54], Indian Standard 10987: 1992 [55], ACI 350.3-06 [56] and AWWA D-100 [57] However, a major drawback of Housner’s spring-mass

mechanical analog model and also Jacobsen's theoretical solution is the assumption of the rigid tank wall and foundation, which is certainly not the case in real-world applications for thin-walled steel aboveground storage tanks.

Veletsos and coworkers [6-8] provided an approximate procedure for evaluating the effect of tank wall flexibility, considering the interaction between the tank wall and stored fluid in 1974. They modified Chopra's [58-60] investigations of reservoir-dam interaction during earthquake. Veletsos and coworkers assumed that there is almost no effect on the convective (sloshing) part due to tank flexibility because the convective effects are characterized by oscillations of much longer periods than those of impulsive effects. Thus, they cannot be influenced significantly by the flexibility of tanks. The effect on wall flexibility on the impulsive part are, however, considerable because of the shorter time period of impulsive motion closer to the tank wall natural period.

Specifically, Veletsos and Yang [8] combined the tank and fluid as single system which vibrates in its own natural modes. They separated the system into a rigid part and a flexible part similar to impulsive and convective components of Housner's spring-mass analogy. The rigid part oscillates with ground motion and the flexible part oscillates with the pseudo acceleration, the acceleration depends on mode of vibration similar to the convective acceleration. The separation was done on the basis of the assumed deflection of the tank under seismic excitation. Initially, the fundamental frequency of empty tank is calculated, and then it is scaled using the effective flexible mass of the combined fluid-tank system. The tank deflection functions are chosen such that they satisfy the shell boundary conditions. Veletsos and Yang concluded that seismic effect in a flexible tank may be significantly greater than those induced in similar excited rigid tanks because the pseudo acceleration can be greater than the ground acceleration. This conclusion follows from both the shell theory and simple beam type analysis of the tank. Veletsos and Yang also concluded that the fundamental natural frequency of the system may be estimated with good accuracy by using Dunkerley's approximation [7]. Initially, Veletsos and Yang assumed that the tank vibrates with the cross section remaining circular [7, 8] and thus analyzed as to be a single degree of freedom system but later this assumption was relaxed assuming it to be a multi degree of freedom system [8].

The natural mode of a cylindrical shell can be defined by two integers n , number of circumferential waves and m , number of waves along tank cylinder axis (vertical axis). It should be noted that only $\cos(\theta)$ -type modes, for which there is a single cosine wave of deflection in the circumferential direction was considered with various vertical modes. It was assumed that only the $\cos(\theta)$ -type modes would be excited significantly by seismic excitation since for a perfect cylindrical tank $\cos(n\theta)$ - type modes cannot be excited by the rigid base motion [1, 5, 7]. Also the assumption that the stresses present in the shell are arising from only vibratory motion are true for $\cos(\theta)$ -type modes because it is insensitive to the existence of initial hoop stress on shell cylinder. The hoop stress has a stiffening effect which can introduce considerable error in calculation of natural frequency for $\cos(n\theta)$ with $n>1$ modes [9]. The Veletsos and Yang's approach hinges on the assumption that the tank is perfectly cylindrical. However, fabrication tolerances permit a some deviation from the nominal circular cross section and thus tends to excite $\cos(n\theta)$ -type modes, therefore, making the effect of initial hoop stress influential. This was proven by the shaking table experiments with aluminum tank models by Clough [10] and Niva [11], and the vibration test of full scale tanks by Haroun and Housner [9, 12].

Following Veletsos and coworkers numerous studies were conducted by various researchers in calculating the pseudo acceleration and the fundamental frequency of tanks [9, 13-17]. Later in the 1980s, Haroun and Housner [15, 18] provided an alternative mass analog taking into account the wall flexibility; having the effective mass correlating to the shell deformation (flexible mass), ground motion (rigid mass) and liquid sloshing (convective mass) which is shown schematically in Figure 2-2. Only the fundamental mode of vibration of the deformable liquid-shell was considered in calculating the flexible and rigid mass. Housner and Haroun also provided an alternative approach for calculating the fundamental frequency of a tank-fluid system [9, 16, 17]- However, the base of tank was still assumed to be rigid.

In order to relax the rigid foundation assumption, researchers also investigated the effect of the tank foundation. Clough [10] and Natsiavas and Babcock [19] showed that the stresses in the tank shell increases if the tank is allowed to uplift from the foundation using analytical and experimental tests. The effect of the tank foundation on storage tank was conducted for vertically excited tanks by various researchers [20-24] in late 1980s. Veletsos, Tang and Malhotra [25-28] had investigated effect of the tank foundation on laterally excited unanchored storage tanks in 1990s. It was found

that the flexibility of the foundation reduces the magnitude of overturning base moment and significantly the axial compressive stresses in the tank wall. However, these reductions are accompanied by increase in magnitude of hoop compressive stresses and base uplift. The base uplift can lead to uneven and permanent settlement around the boundary of the tank. Following this finding, some design standards such as European [51] and New Zealand [52] have included the effect of flexible foundation. In 2000 Malhotra [29] simplified the flexible tank model of Veletsos providing simple procedure for seismic design of cylindrical ground-supported storage tanks.

Meanwhile, there has been a paradigm shift to finite element modelling with advancement in computational power. Several researchers have developed various methods to represent the liquid filled storage tank to an equivalent numerical model which would then be solved as a numerical problem. The methods such as lumped mass method, added mass method or fluid element method were used by researchers [30-41]. These methods were used to confirm the theoretical impulsive and convective time period of vibration, to determine the effect of tank wall flexibility, tank base flexibility, effect of tank anchorage and effect of presence of tank roof on impulsive and convective periods. FEMs have confirmed that impulsive period of vibration increases significantly due to tank wall and tank base flexibility whereas the convective period remains uninfluenced. Recently, nonlinear fluid-structure algorithm of finite element method was used by Ozdemir and coworkers for seismic analysis of both anchored and unanchored [50].

The tanks can be classified into three categories based on their geometries: broad, nominal and slender tank. We define broad tanks as those with an aspect ratio (liquid height to tank radius) less than 1.0, nominal tanks as ones which have aspect ratio between 1.0 and 3.0, and slender tank as those which have aspect ratio greater than 3.0. In the late 1970s, it was observed that the results obtained by the rigid tank assumption are not accurate for some nominal tanks and slender tanks, hence, there is a need to update the design codes [6-8]. However, the API 650 presently uses slightly modified Housner's mechanical mass-analog model proposed by Wozniak and Mitchell [61] for seismic design of tanks. The primary reasons for using Housner's method are its simplicity and accuracy for broad and most nominal tanks, which are the more common geometries for oil storage tanks. The effect of flexible wall and flexible foundation becomes significant only in case of some nominal and slender tanks.

We investigate the effect of flexible foundation under horizontal seismic excitation for large, vertical, aboveground, steel, open-top, flat bottom, unanchored storage tanks using finite element analysis (FEA). The FEA results are compared with current API 650 design procedure for both a rigid foundation as well as for a flexible foundation. The flexible foundation is modelled using series of compression only elastic springs. We apply the hydrodynamic pressure distribution in FEA using two different approaches (1) Housner's rigid wall and rigid foundation idealization and (2) Jacobsen-Veletsos flexible wall and rigid foundation idealization. This study will give insights on the accuracy and applicability of API 650 seismic design philosophy.

2.2 Methodology

The aim of the study is to capture the response of large, vertical, aboveground, steel, open-top, flat bottom liquid storage tanks under horizontal seismic excitation using the finite element method (FEM). Various models were created in Abaqus CAE version 2018 [62] using large deformation capable shell elements and nonlinear material properties for storage tanks. The effect of liquid was modeled in terms of pressure applied on the tank wall and tank base. The seismic response of a storage tank depends primarily on the tank geometry, aspect ratio, shell thickness, material and design of tank, the stored liquid properties, foundation and the ground acceleration. The aspect ratio of a tank is defined as ratio of tank's height to its radius. To find the trend with respect to aspect ratio, the three tanks with different aspect ratio of 0.67, 1.0 and 3.0 were selected to represent broad, nominal and slender tanks.

For a given tank geometry and aspect ratio, four different analyses were performed using combination of two different hydrodynamic pressure distributions and two different foundations. The two pressure distributions correspond to Housner's rigid tank model used in API 650 [54] and Jacobsen-Veletsos rigid tank model used in European Code 8 [51]. Housner's rigid tank model and Jacobsen-Veletsos rigid tank model pressure distribution were selected because they are currently used by practicing engineers. There is also Veletsos flexible wall pressure distribution available in the literature and used by European and New Zealand seismic design documents [51, 52], which captures the effect of wall flexibility. However, the study focuses on flexibility of foundation and the difference of hydrodynamic pressure distribution between rigid and flexible wall assumption is minimal for most of the practical tank geometries, aspect ratios less than 1.0

[42]. Therefore, rigid wall pressure distribution models were selected. The two different foundations were rigid foundation and flexible foundation.

The non-linear springs to simulate flexible foundation with unanchored tanks. The rigid foundation was used to compare the FEM results with theoretical results available in the literature and simulate anchored tanks. The analysis was performed using modified Riks method to capture the nonlinear geometry, material and foundation behavior and to determine the load required to fail due to yielding or buckling of the model. Further, the FEM results such as shell hoop stress and elephant foot buckling loads were compared to rule based API 650 procedure which is based on Housner's mechanical analogy using rigid wall and rigid foundation assumptions.

2.2.1 Tank design and geometry

Three different tank geometries were selected having different aspect ratios. Each of the tank design was sized in accordance with API 650 (2013). These tanks are generally used to store petroleum products which usually have a specific gravity of 0.9. Therefore, the tanks were assumed to contain liquid with specific gravity equal to 0.9. The tanks were assumed to be completely filled. The density of water was taken as 62.4 lbf/ft^3 (1000 kg/m^3).

ASTM A516 Grade 70 [63] steel specification was used to model the shell and ASTM A36 [64] steel specification for the tank base and wind girder. A516 Grade 70 steel has a yield stress, F_y , of 38 ksi (262 MPa), an ultimate tensile strength of 70 ksi (483 MPa), an allowable stress for design, S_d , of 25.3 ksi (174 MPa), and an allowable stress for hydrostatic test, S_t , of 28.5 ksi (197 MPa). ASTM A36 steel has a yield stress of 36 ksi (248 MPa) and an ultimate strength $F_u = 58 \text{ ksi}$ (400 MPa).

The tanks were designed using rules from API 650 [54]. Each of the tanks shell thicknesses were designed using the 1-foot method of API 650. The shell thickness was calculated assuming no corrosion allowance. In order to achieve the elephant foot buckling at the lowest shell course all the time, each of the tanks were designed to have uniform shell thickness. Otherwise, if we have used traditional stepped shell thicknesses for each shell course, sometimes we may obtain elephants foot buckling at the second shell course from the bottom. The base thickness for all tanks was 0.25 in. (6.4 mm). All the shell thicknesses were greater than the base plate thickness as per

API 650 specification. These tanks were assumed to be self-anchored, meaning that there was no mechanical anchorage for the flexible foundation models. The tank has vertical height H , radius R and constant wall thickness t_s . Geometric properties and the design shell thickness of tanks are given in Table 2-1.

Top wind girders were sized using API 650 requirements. Design wind speed, V , was selected as the 3-sec gust design wind speed of 90 mph (40 m/s). This design wind speed corresponds to a typical inland location in the continental of United States. Each of the tanks required to have a top wind girder, none of the tanks were required to have an intermediate wind girder. The broad tank (aspect ratio =0.67) required relatively higher stiffener section modulus. Therefore, “Detail e” was used. For nominal tank (aspect ratio = 1) “Detail d” was used and for slender tank “Detail c” was used. Figure 2-3 shows the wind girder details of c, d and e. The size and the location of top wind girder for each tank are listed in Table 2-3.

2.2.2 Loading

2.2.2.1 Gravity and hydrostatic loading

The storage tanks are primarily designed for hydrostatic loading, wind, seismic loading, and internal and external pressures due to process. Most of the time tanks are subject to only static loads. The static loads include hydrostatic pressure exerted by liquid on the walls of the tank and the gravity load due to its self-weight. The hydrostatic pressure is given in Eq. (2)

$$P_{hydrostatic} = \gamma_l(h - z) \quad (2)$$

where γ_l represents specific weight of the fluid stored, h represents the liquid height and z represents the vertical distance from the tank bottom.

For most of the steel tanks effect of self-weight is negligible comparing with hydrostatic pressure. However, for tanks made using concrete self-weight is more important. The weight of the tanks influences the fundamental natural frequency of oscillation of tank-fluid system under seismic excitation. Although, internal and external pressures due to process may exist in a real tank, we did not model them because each tank would have different internal and external pressures due to specific process. Next, we shall describe the impulsive and convective pressures for the Housner

rigid wall model and the Jacobsen-Veletsos rigid wall model. Figure 2-4 shows schematic view for hydrostatic, impulsive and convective pressure distribution on the tank shell.

2.2.2.2 Housner rigid wall model

Housner used an approximate method for calculating the dynamic response of tank under seismic excitation [2]. His model was based in the assumption that tank wall and tank base do not deform under the seismic action i.e. the tank wall and base are rigid.

For the Housner rigid wall model Eqs. (3) and (4) refer to impulsive wall and base pressure distributions, respectively.

$$P_{wi} = \rho_l A_i h \left(\frac{(h-z)}{h} - \frac{1}{2} \left(\frac{h-z}{h} \right)^2 \right) \sqrt{3} \cos \theta \quad (3)$$

$$P_{bi} = \rho_l A_i h \frac{\sqrt{3}}{2} \cos \theta \frac{(\sinh \frac{\sqrt{3}r}{h})}{\cosh(\frac{\sqrt{3}R}{h})} \quad (4)$$

where the impulsive wall and base pressures are denoted by P_{wi} and P_{bi} , respectively. The parameter A_i is impulsive spectral acceleration response, ρ_l is the density of the liquid, θ is the angle made with respect to horizontal direction of ground motion, h and R are the liquid height and tank radius respectively. The $\cos(\theta)$ component in Eqs. (3) and (4) corresponds to the variation along the circumference of the tank. The wall pressure depends on the vertical distance from the base, z . The base pressure depends on radial position coordinate r .

For the slender tank, the one having $h/R > 1.5$, Eq.(3) is applicable for only upper $1.5R$ portion of the tank wall and the fluid below is assumed to be fully constrained and exerts pressure given in Eq. (5)

$$P_{wi} = \rho_l A_i R \quad (5)$$

The Eqs. (6) and (7) refer to the convective wall and base pressure distributions, respectively.

$$P_{wc} = \frac{15}{16} \rho_l R \cos \theta \left(1 - \frac{(\cos \theta)^2}{3} - \frac{(\sin \theta)^2}{2} \right) \frac{\cosh \left(\sqrt{\frac{27}{8}} \frac{z}{R} \right)}{\cosh \left(\sqrt{\frac{27}{8}} \frac{h}{R} \right)} A_{ch} \quad (6)$$

$$P_{bc} = \frac{15}{16} \rho_l R \cos \theta \left(\frac{r}{R} - \frac{r^2 (\cos \theta)^2}{3R^2} - \frac{r^2 (\sin \theta)^2}{2R^2} \right) \frac{A_{ch}}{\cosh \left(\sqrt{\frac{27}{8}} \frac{h}{R} \right)} \quad (7)$$

where the convective wall and base pressures are denoted using P_{wc} and P_{bc} , respectively. The parameter A_{ch} is convective spectral acceleration response corresponding to Housner's model. The variables ρ_l , θ , z , r , h and R are all the same as defined in Eqns. (3) and (4).

2.2.2.3 Jacobsen-Veletsos rigid wall model

Jacobsen-Veletsos rigid wall model gives the analytical solution for impulsive and convective pressure distribution with rigid wall assumption [1, 42]. We name this model as Jacobsen-Veletsos model because Jacobsen formulated the impulsive pressure distribution and Veletsos formulated the convective pressure distribution. The solution involves infinite series of Bessel and modified Bessel functions making it less attractive to the practicing engineers as opposed to the simpler Housner model. Eurocode [51], however, uses this Jacobsen-Veletsos solution for computation of effective mass and effective mass moment for rigid wall tanks.

For the Jacobsen-Veletsos rigid wall model Eqs. (8) and (9) refer to impulsive wall and the base pressure distributions, respectively.

$$P_{wi} = C_0(R, z) \rho_l A_i R \cos \theta \quad (8)$$

$$P_{bi} = C_0(r, 0) \rho_l A_i R \cos \theta \quad (9)$$

$$C_0(r, z) \quad (10)$$

$$= \frac{8}{\pi^2} \frac{h}{R} \sum_{n=1}^{\infty} \frac{(-1)^{n+1}}{(2n-1)^2} \frac{I_1 \left[\frac{(2n-1)\pi r}{2h} \right]}{I_1' \left[\frac{(2n-1)\pi R}{2h} \right]} \cos \left(\frac{(2n-1)\pi z}{2h} \right)$$

where the parameter $C_0(r, z)$ is a dimensionless coefficient defined in Eq. (10) where index n represents the n th impulsive mode, for the ease of the analysis only the first term of the summation is considered. It is fair to consider only the first term, because the contribution of the first term is already very close to 100% of the full summation. The impulsive wall and base pressures are denoted by P_{wi} and P_{bi} , respectively. The term I_1 is modified Bessel function of the first kind and I_1' is first derivative with respect to radial position coordinate r , of modified Bessel function of the first kind. The term A_i is impulsive spectral acceleration response. The variables ρ_l , θ , z , r , h and R all the same as defined in Eqs. (3) and (4).

The Eqns. (11) and (12) refer to convective wall and base pressure distributions, respectively.

$$P_{wc} = C_j(z)A_j(t) \rho_l R \cos \theta \quad (11)$$

$$P_{bc} = C_j(r)A_j(t) \rho_l R \cos \theta \quad (12)$$

$$C_j(z) = \frac{2 \cosh\left(\frac{\lambda_j z}{R}\right)}{(\lambda_j^2 - 1) \cosh\left(\frac{\lambda_j h}{R}\right)} \quad (13)$$

$$C_j(r) = \frac{2 J_1\left(\frac{\lambda_j r}{R}\right)}{(\lambda_j^2 - 1) J_1(\lambda_j)} \quad (14)$$

where the terms $C_j(z)$ and $C_j(r)$ are dimensionless coefficients defined in Eqns. (13) and (14), respectively where subscript j corresponds to j th convective mode, J_1 is Bessel function of first kind and first order and λ_j are values where the first derivative of J_1 is zero. The convective wall pressure and base pressure are denoted using P_{wc} and P_{bc} , respectively. The term A_j is convective spectral acceleration response corresponding to j th mode. The variables ρ_l , θ , z , r , h and R are the same as defined in Eqs. (3) and (4).

In case of base pressure distribution which involves Bessel function or modified Bessel function an equivalent approximate polynomial function of the fourth order was used in the study when we applied the load in FEM. The approximate polynomial had a minimal deviation from the actual function with a minimum coefficient of determination (R^2) value of 0.99. The coefficient of

determination value represents the statistical measurement of goodness of the fit. The closer coefficient of determination value to 1.0 the better approximation to the actual function is. For example, Figure 2-5 shows the plot for Tank-2 Jacobsen-Veletsos impulsive base pressure and equivalent polynomial function having coefficient of determination value very close to 1.0.

2.2.3 Finite Element Modelling

The finite element analysis was performed using Abaqus CAE 2018 software [62]. Twelve models were analyzed, having three different aspect ratios of 0.67, 1.0 and 3.0. Each of the three tanks was subjected to two different pressure distributions, one corresponding to Housner and the other corresponding to Jacobsen-Veletsos. Also each of the tanks were subjected to two kinds of boundary conditions at the base, one having a rigid base and the other representing compacted sand soil with a subgrade modulus of 250 lbf/in³ (68,000 kN/ m³).

2.2.3.1 Material Properties

Nonlinear material properties were used in the modelling. ASTM A516 Grade 70 steel and ASTM A36 were modelled using the true stress-strain curve as shown in Figure 2-6. The true stress-strain behavior of each material was obtained using the ASME Boiler and Pressure Vessel Code, Section VIII, Division 2 [65]. Both materials were modelled as isotropic materials with modulus of elasticity $E = 2.9 \times 10^4$ ksi (2.0×10^5 MPa), Poisson's ratio $\nu = 0.3$, and density $\rho = 490$ lb/ft³ (7800 kg/m³). The yield stress and the ultimate tensile stress of these materials were given in section 2.2.1.

2.2.3.2 Finite Element Mesh

The four node, doubly curved elements with hourglass control, finite membrane strain and reduced integration formation, S4R elements were used to create the finite element model. The S4R elements were selected to optimizes the number of nodes in the simulation and reduce the computational time. The S4R elements use reduced integration to form the stiffness matrix which means that only center point is used for integration. However, this may produce spurious deformation modes allowing the element to deform without having any change in energy (zero-energy modes). This effect is called hourglass effect and it is avoided in S4R elements by using hourglass control techniques [62]. Figure 2-7 shows the mesh of Tank-1 having an aspect ratio of

0.67. To capture the response of elephant foot buckling finer mesh of size 3 in. (73 mm) by 20 in. (508 mm) along longitudinal and circumferential direction of the element was used. The expected location of elephant for buckling is near the base of the tank. In case of flexible foundation the tank uplift was permitted. Therefore, to capture uplift, finer mesh was also done near the base-shell connection at the base. Rest of the tank had a coarser mesh size of 20 in. (508 mm) by 20 in. (508 mm).

2.2.3.3 Finite Element Step

In Abaqus the analysis is performed in two steps. The loads applied are gravity load, hydrostatic load and hydrodynamic load. No wind load is applied during the analysis. In the first step all the static loads are applied to the structure. The static loads include self-weight of the structure and hydrostatic pressure as mentioned in section 2.2.1.

After the application of static loads, the hydrodynamic loads are applied as described in section 2.2.2 and 2.2.3 using static, Riks method. Riks analysis captures the nonlinear geometry effect (NLgeom). The load in Riks analysis increases gradually from 0 to 100% of the total load. The gradual increase in load enables to calculate the load at which the tank failure/buckling takes place. In Riks method, at every increment of the load, the displacements and stresses are computed.

2.2.3.4 Finite Element Loading

The static loads applied in Abaqus FEA as three different loading stages which are superposed on each other. First, the gravity load was applied. Second, hydrostatic base pressure was applied as uniform pressure on the base depending upon the tank liquid height. The third hydrostatic wall pressure was applied using the analytical field using the function given in Eq. (2).

The hydrodynamic loads were applied as superposition of two loads the base and the wall pressures. The base and the wall pressures were applied as square root of sum of squares (SRSS) of impulsive and convective pressures. Each of the pressure distributions were applied using appropriate function using analytical fields in Abaqus. The functions were defined as given in sections 2.2.2.2 and 2.2.3 for Housner's approach and for Jacobsen-Veletsos approach, respectively.

The impulsive and convective accelerations were calculated using API 650 Annex E. Using United States Geological Survey (USGS) earthquake hazard maps data [66], S_S and S_1 value for a site location were obtained as $S_S = 1.36$ g and $S_1 = 0.68$ g, where the g value refers to acceleration due to gravity. These maps uses a 2%-in-50-year return period (1/2500 probability of occurrence) and a 5% critical damping factor. The response spectrum was plotted using procedure given in API 650 as shown in Figure 2-8. This response spectrum depends on the soil type. The soil type ‘‘Class D’’ was selected corresponding to a site with unknown soil conditions. For given values of S_S and S_1 , modification factors for soil condition, F_a and F_v were 1.0 and 1.5, respectively. The impulsive time period of tanks T_i was calculated using Eq. (15) where, C_i is coefficient for determining impulsive period of tank system obtained from Figure E.1 of Annex E of API 650 [54], ρ is density of fluid, E is elastic modulus of tank material and t_u is the equivalent uniform thickness. The values of C_i and T_i are tabulated in Table 3. The impulsive period of vibration for all tanks was found in the in the plateau region of the response spectra. Thus, the values of impulsive acceleration were same for all tanks equal to 0.259 g. The convective time period for Housner was calculated using Eq. (16) and for Jacobsen-Veletsos was calculated using Eq. (17).

$$T_i = \frac{1}{27.8} \frac{C_i h \sqrt{\frac{\rho}{E}}}{\sqrt{\frac{t_u}{D}}} \quad (15)$$

$$T_c = \frac{1.71}{g} \frac{\sqrt{D}}{\sqrt{\tanh\left(3.68 \frac{h}{D}\right)}} \quad (16)$$

$$T_c(j) = \frac{2\pi}{\sqrt{\frac{\lambda_j g}{R} \tanh\left(\frac{\lambda_j h}{R}\right)}} \quad (17)$$

Annex E of API 650 specifies that if the seismic use group (SUG) is not specified by the purchaser then SUG 1 should be adopted. Hence SUG 1 was adopted and the Importance factor of 1.0 was

used. The response modification factors are $R_{wc}=2.0$ and $R_{wi}=3.5$ for self-anchored tanks as specified in API 650 for convective and impulsive components, respectively.

2.2.3.5 Boundary conditions

The aim of the study is to analyze the difference in behavior under seismic excitation to tank having flexible foundation over rigid foundation. Therefore, each tank was subjected to two kinds of boundary conditions at the base, one having a rigid base and the other representing compacted sand soil with a subgrade modulus of 250 lbf/in^3 ($68,000 \text{ kN/ m}^3$). The rigid base boundary condition represents the rigid foundation approach which is currently used in API 650. The compacted sand soil boundary condition represents the flexible foundation. Results of both the approaches were compared to investigate the impact of having a flexible foundation.

To model the soil with a given subgrade modulus, non-linear compression only elastic springs acting along the vertical direction were attached at the bottom nodes. The non-linear behavior here refers to difference in spring stiffness when the spring is in tension compared to when the spring is in compression. The stiffness of each spring was calculated using the tributary area corresponding to the node it is attached to using Eq. (18). The tributary area was calculated by applying unit uniform pressure of 1.0 psi on the bottom of the tank. The reaction in the vertical direction at the node would give the value of tributary area corresponding to that node. This stiffness is used when the springs are in compression, when springs are in tension the stiffness used is 1 micro lbf/in^3 ($2.72 \times 10^{-4} \text{ kN/ m}^3$) which is almost negligible. This was done because soil can take only compression forces.

$$K_{spring} = A_{tributary} K_{soil} \quad (18)$$

2.3 Results and Discussion

Results of finite element simulations are presented and discussed in this section. Different failure modes are investigated. The material failure primarily depends on the hoop stress and the longitudinal stress in the shell. The material failure results in inelastic deformation of the shell or base which may lead to buckling and uplifting of tank. Therefore, the FEM results of hoop stress, longitudinal stress and buckling for different tanks geometry are compared with API 650 design

provisions. For a given tank geometry (aspect ratio) the hydrodynamic hoop stress and the longitudinal stress corresponding to four different scenario; (1) the Housner's hydrodynamic pressure distribution with fixed foundation, (2) Housner's hydrodynamic pressure distribution with flexible foundation, (3) Jacobsen-Veletsos hydrodynamic pressure distribution with rigid foundation and (4) Jacobsen-Veletsos hydrodynamic pressure distribution with flexible foundation are compared and analyzed.

2.3.1 Hoop Stress

The total hoop stress on tank wall can be divided into two components: the hydrostatic hoop stress and the hydrodynamic hoop stress. The hydrostatic hoop stress depends on the height and density of liquid contained and the tank geometry. The hydrostatic pressure increases linearly with increase in the height of the liquid as in Eq. (2). Thus, as the height of the contained liquid increases there is increase in maximum hoop stress value.

On the other hand, the hydrodynamic hoop stress can also be divided into two components; the impulsive and the convective. At the lower portion of the tank, liquid moves along with the tank. Therefore, the maximum impulsive pressure is at the bottom. Conversely, at the top portion of the tank, liquid moves in convective mode. Thus, the maximum convective pressure is at the top. See Figure 2-4 for a schematic view of hydrostatic and hydrodynamic pressure distributions on the tank shell. The tank radius and liquid height greatly affect the hydrodynamic pressure. Clearly, the liquid moving in the horizontal direction increases with increase in tank radius and the liquid height. Therefore, there is larger horizontal force acting on the tank shell.

The total hydrostatic and hydrodynamic pressure, however, increases nearly linearly with increase in depth from the liquid surface despite non-linear impulsive and convective pressure distribution. This is due to the fact that hydrostatic hoop stress is much larger than the hydrodynamic stress. It can be observed from Table 2-4 that hydrostatic hoop stress contributes almost 60% to 80% of total hoop stress, as the aspect ratio increases the contribution of hydrostatic hoop stress reduces as the hydrodynamic stress value increases. Moreover, the impulsive part contributes to the major part of dynamic stress. The convective stress values are lower primarily because the associated spectral acceleration is lesser comparing with ground acceleration. From Table 2-2, it can be

observed that convective spectral response acceleration varies from 0.28 to 0.50 times the impulsive spectral acceleration as the aspect ratio increases.

The FEM total hoop stress and hydrostatic hoop stress were compared with calculated total hoop stress and hydrostatic hoop stress using API 650 rules. The Eq. (19) is used to compute the total hoop stress in shell.

$$\sigma_t = \sigma_h + \sigma_s = \frac{(N_h + \sqrt{N_i^2 + N_c^2})}{t} \quad (19)$$

where the total hoop stress, σ_t is expressed as sum of hydrostatic hoop stress σ_h and hydrodynamic hoop stress σ_s . The hydrostatic hoop stress is expressed in terms of hydrostatic membrane force N_h . The hydrodynamic stress can be expressed as the sum of the components N_i and N_c , the impulsive and convective hoop membrane forces in tank shell, respectively. The term t is the shell wall thickness at the point of analysis. The terms N_h , N_i and N_c provide results in pounds per inch of the shell thickness and thus divided by thickness t to obtain stresses in psi.

The Eqs. (20) through (24) are taken from API 650 for calculation of hoop and membrane forces N_h , N_i and N_c .

$$N_h = 2.6(h - 1)DG \quad (20)$$

$$N_i = 4.5A_iGDh \left[\frac{Y}{h} - 0.5 \left(\frac{Y}{h} \right)^2 \right] \tanh \left(\frac{0.866D}{h} \right) \quad \text{for } D/h \geq 1.33 \quad (21)$$

$$N_i = 2.77A_iGD^2 \left[\frac{Y}{0.75D} - 0.5 \left(\frac{Y}{0.75D} \right)^2 \right] \quad \text{for } D/h < 1.33, Y < 0.75D \quad (22)$$

$$N_i = 1.39A_iGD^2 \quad \text{for } D/h < 1.33, Y > 0.75D \quad (23)$$

$$N_c = \frac{0.98A_cGD^2 \cosh \left[\frac{3.68(h - Y)}{D} \right]}{\cosh \left(\frac{3.68h}{D} \right)} \quad (24)$$

where the variable G is specific gravity of the liquid ($G=0.9$), Y is distance from the liquid surface to point of analysis in ft, h and D , are the liquid height and the diameter of the tank in ft, and A_i and A_c are the impulsive and convective design response spectral acceleration values.

Table 2-4 shows the calculated value obtained using the API 650 procedure and obtained finite element values of hoop stresses after the application of hydrostatic loading and after the application of hydrostatic and hydrodynamic loading. Figure 2-9 graphically represents the total hoop stress presented in Table 4. For Tank-1 and Tank-2 the values reported corresponds to load proportionality factor (LPF) of 1.0, and for Tank-3 the values correspond to LPF of 0.43. Based on the results it can be observed that the hydrostatic hoop stress is almost same between API 650 and the two other approaches. The hydrostatic stress value for Housner and Jacobsen-Veletsos are very close for both rigid and flexible bases because the methodology for hydrostatic loading and the finite element model are the same. However, there is slight difference, less than 1 percent between the maximum hydrostatic stress values for rigid and flexible bases because of the different boundary conditions at the bases.

The hydrodynamic stress values differ between API 650 and other two approaches. It is observed that the total hoop stress value for Housner and Jacobsen-Veletsos approach deviates more from the value calculated using API 650 procedure with the increase in aspect ratio. Also the contribution of hydrodynamic forces to total hoop stress increases with the increase in aspect ratio. For Tank-1 (aspect ratio=0.67) the total hoop stress is almost the same with respect to different approaches and type of foundation, Jacobsen-Veletsos approach with flexible foundation gives the highest value of total hoop stress with 1.02 times the maximum total hoop stress from API calculation. For Tank-2 (aspect ratio=1.0) it can be seen that both Housner and Jacobsen-Veletsos approaches result in greater stress value compared to stress calculated by API. Also, the flexible foundation results in higher stress value compared to rigid foundation. This is because the flexible foundation allow more rotation at the base as shown in Figure 2-10 resulting in higher hoop stress value comparing with the rigid foundation case. A parallel analogy can be drawn from a beam when there is simple support (flexible) condition at both ends. The deflection at the mid-span would be more comparing with fixed (rigid) supports at both ends. The Figure 2-10 shows the displacement in the Z direction i.e. uplift of the Housner's flexible foundation Tank-3 base, in plan and elevation view to show displacement contour and rotation of the base. There is no rotation or

uplift of the rigid base. To observe the effect of the rotation of the tank base, the normalized radial displacement of the topmost point of the tank is plotted for both flexible and rigid cases as shown in Figure 2-11. The radial displacement of the topmost point is selected primarily because it will experience the maximum effect due to the rotation of the tank base. It is observed from Figure 2-11 that the radial displacement for the flexible tank is always greater than it counter rigid tank irrespective of the aspect ratio. Clearly indicating the effect because of rotation of the tank base. Moreover, Housner's approach lead to higher stress value compared to Jacobsen-Veletsos approach for both types of foundation. Housner flexible foundation was found to give highest total hoop stress with 1.14 times the maximum hoop stress calculated by API procedure. For Tank-3 (aspect ratio=3.0) all the models buckles before reaching the load proportionality factor (LPF) value of 1. Housner tank with flexible foundation buckles at LPF of 0.43 at hoop stress value of 39.6 ksi (273 MPa), Housner rigid tank buckles at LPF of 0.58 at hoop stress value of 36.8 ksi (253 MPa). Veletsos flexible tank buckles at LFP of 0.54 at hoop stress value of 38.9 ksi (268 MPa) and Jacobsen-Veletsos rigid tank buckles at LPF of 0.74 at hoop stress 38.6 ksi (266 MPa). The hoop stress values for all the tanks was found to be 1.45 times the maximum total hoop stress from API calculation. As discussed previously the hoops stress values for flexible foundation are more compared to counter rigid foundation in case of slender tanks as well. The total stress value obtained for slender tanks and nominal tank are greater for Housner flexible foundation instead of Jacobsen-Veletsos flexible foundation, this is because only the first mode for impulsive and convective motion are considered in the analysis of Jacobsen-Veletsos approach. In Figure 2-12 tank aspect ratio (H/R) vs impulsive mass, M_i normalized to the total fluid mass, M , is plotted for different Jacobsen-Veletsos impulsive mode terms and Housner approach. The contribution of higher impulsive modes increases with the increase in aspect ratio as shown in Figure 2-12. Therefore, if higher impulsive modes had been considered then similar results for tank-2 and tank-3 could be observed.

It can be observed that Housner's model gives slightly smaller values for hydrodynamic stresses comparing with that of Jacobsen-Veletsos. Moreover, the flexible foundation has much more total stress value comparing with rigid counterpart, for slender tanks the percentage is as high as 45 percent more even without 100% loading.

2.3.2 Longitudinal Stress

This section focuses on the longitudinal stress developed on tank wall. The longitudinal stress on the tank wall depends on the self-weight and hydrodynamic pressure distribution. The distribution of tank shell self-weight lead to uniformly increasing longitudinal stress as the distance from top increases. However, the longitudinal stress values are much smaller than the hoop stress values. The distribution of hydrodynamic wall and base pressure is non-uniform. Therefore, it led to a non-uniform reaction forces at the base resulting in non-uniform longitudinal stress. The weight of the structure also contributes to longitudinal stress. Higher structure weight increases the vertical force component.

The FEM longitudinal stress values analysis were compared with calculated longitudinal stress using API 650. The Eqs. (25), (26), (27) and (28) are given in Annex E of API 650 used to calculate longitudinal stress value for the selected tanks. The maximum longitudinal compressive stress σ_c depends on anchorage ratio J , total overturning moment acting at the base of tank shell parameter produce by the impulsive, convective and self-weight M_{rw} , the vertical earthquake acceleration A_v , the tank weight acting at the base of shell w_t , the force resisting the uplift in annular region w_a , the thickness of bottom shell course less the corrosion allowance t_s and the diameter D of the tank.

$$\sigma_c = (w_t(1 + 0.4A_v) + \frac{1.273M_{rw}}{D^2}) \frac{1}{12t_s} \quad J < 0.785, \text{ USC Units} \quad (25)$$

$$\sigma_c = (w_t(1 + 0.4A_v) + \frac{1.273M_{rw}}{D^2}) \frac{1}{1000t_s} \quad J < 0.785, \text{ SI Units} \quad (26)$$

$$\sigma_c = (\frac{w_t(1 + 0.4A_v) + w_a}{0.607 - 0.18667[J]^{2.3}} - w_a) \frac{1}{12t_s} \quad J > 0.785, \text{ USC Units} \quad (27)$$

$$\sigma_c = (\frac{w_t(1 + 0.4A_v) + w_a}{0.607 - 0.18667[J]^{2.3}} - w_a) \frac{1}{1000t_s} \quad J > 0.785, \text{ SI Units} \quad (28)$$

API 650 equations for longitudinal stress are applicable for anchorage ratio less than 1.54 for self-anchored tanks. Therefore, the stress values are compared with the acceptable range as shown in Table 2-5, Table 2-6 and Table 2-7 for Tank-1, Tank-2 and Tank-3, respectively. The reported values are corresponding to the node located 1-foot (30 cm) above the base plate for both FEM

and hand calculation for a better comparison. This was done because the FEM results at points near the base are affected due to the boundary conditions and base plate. On the other hand, API hand calculation do not have that issue.

The results show that the stress values from hand calculation matches the FEM values for all three tanks at lower LPF values. At higher LPF values, the hand calculation values are higher than the FEM results for Tank-2 and Tank-3. This is because buckling starts to takes place in FEM resulting in load redistribution to neighboring points. However, API hand calculation which based on linear theory do not capture the buckling and corresponding redistribution of the longitudinal stress values. Thus, giving lesser longitudinal stress values at the given point in FEM results comparing with hand calculation results. The anchorage ratio J is calculated using Eq. (29), all the variables M_{rw} , A_v , w_t , w_a , t_s and D are the same as described earlier. The A_v value is taken as zero, since only horizontal acceleration is considered for analysis. The internal pressure contribution of w_{int} is also zero since the models are open-top tanks.

$$J = \frac{M_{rw}}{D^2[w_t(1 - A_v) + w_a - 0.4w_{int}]} \quad (29)$$

The longitudinal stress values obtained from API procedure and obtained from the FEA analysis have a significant difference at higher LPF values, at lower LPF the values are in much closer to each other. The calculation using API procedure always resulted in greater stress value for all the tank models.

The longitudinal stress value for both Housner and Jacobsen-Veletsos models are in close agreement with each other for both rigid and flexible foundation for Tank 1 and 2 (see Table 5 and Table 6). However, flexible foundation has slightly higher longitudinal stress value compared to its rigid counterpart for Tank 3 (see Table 7). One possible reason may be the flexible foundation allows uplifting of tank as shown in Figure 2-10 and this results in higher reaction at end to balance the net horizontal moment produce by the hydrodynamic forces. A graph for Housner's flexible tank-1 and tank-3 normalized uplift is plotted for comparison as shown in Figure 2-13. In the Figure 2-13, the negative value of uplift is the initial settlement of the tank is due to the hydrostatic and gravity loads. The normalized uplift for tank-3 is significantly larger compared to normalized uplift for tank-1. Reinforcing the fact that the effect of the flexible foundation is significant for

slender tanks. Additionally in Figure 2-13 (b), it can be observed that after reaching the normalized uplift of 0.18 the LPF starts to decrease. This happens because the structure becomes unstable due to the buckling of the shell. To remain in equilibrium the structure releases the strain energy by reducing the load. The release of strain energy results in the load-displacement curve having negative stiffness as seen in Figure 2-13 (b). This is a typical post-buckling behavior, which results in sudden reduction in load bearing capacity after the buckling. For the broad and the nominal tank there is no significant influence of flexible foundation on longitudinal stress. However, for tank-3 the uplift is significant thus, resulting in higher longitudinal stress.

2.3.3 Buckling

This section focuses on tank failure due to buckling. There are two types of buckling generally observed in storage tanks subjected to seismic excitation; one is “elephant’s foot buckling” and the other is “diamond-shape buckling”. The elephant foot buckling occurs at location where there is high internal pressure, causing high hoop tensile stress along with overturning moment, causing high longitudinal compressive stress. The elephant foot buckling is also influenced by uplift in the tank shell; high uplift results into higher longitudinal compressive stress on the opposite side of the tank. The uplift of the tank is influenced by the type of anchorage that is provided. Thus API 650 has different provision for buckling stress depending upon mechanically anchored and self-anchored tanks. Figures 2-14-19 show the deformed shape and LPF v/s normalized radial deformation plots. Elephant foot buckling is one of the most common failure observed in storage tanks subject to earthquake loading and is found near the base of the tank as seen in Figure 2-17 where both the hoop tensile stress and compressive forces are large. Naturally, as the aspect ratio increases the buckling stress increases. Similarly, as the internal stress at bottom increases with increase in height and so does the overturning moment resulting in higher uplift values.

The other kind of buckling observed in tanks in a seismic event is the “diamond-shape buckling” caused by lower internal pressure and high axial compressive forces. Diamond-shape buckling occurs towards the top of the tank much above the location of elephant foot buckling [43]. Diamond-shape buckling typically is not an issue with API 650 storage steel tanks because of minimum shell design thickness requirement of API 650. The minimum thickness is usually

sufficient enough to resist the diamond shape buckling. Thus, there was no diamond shape buckling observed in the analysis.

The Figure 2-14, 16 and 18 show the load proportionality factor (LPF) vs normalized radial displacement plots and FEM hoop stress and longitudinal stress plots for the tanks. The LPF represent the proportion of total load hydrodynamic load applied after the application of static loads. The radial displacement is normalized by square root of shell radius times shell thickness of the tank wall corresponding to the bottom shell course where the elephant foot buckling is likely to take place. The stress plots in Figure 2-15 is from the analysis of Jacobsen-Veletsos pressure distribution with flexible base model for Tank-1. Similarly, the stress plots in Figure 2-17 and Figure 2-19 are from the analysis of Housner pressure distribution with flexible base model for Tank-2 and Tank-3, respectively. It can be observed that the broad tank does not buckle in any of the scenario (Figure 2-14 and Figure 2-15), but nominal (Figure 2-16 and Figure 2-17) and slender (Figure 2-18 and Figure 2-19) tank do buckle.

The broad tank (aspect ratio = 0.67) at LPF value of 1 has maximum normalized radial displacement less than 0.25 for both approaches and type of foundations. The graph between LPF and normalized radial deformation is smooth without any plateau, thus no buckling is observed. However, in Figure 2-15 it can be observed that there is some bulging happening at the bottom of the tank. In case of nominal tank (aspect ratio 1) at LPF value of 1 the maximum normalized radial deformation is more than 0.30. The nominal tank undergoes buckling in all the models at a load close to LPF of 1.0. Finally, in the case of slender tanks (aspect ratio = 3) all the models fail much before reaching the LPF of 1.0, primarily because of slenderness of the tank. Buckling is influenced by uplift as mentioned previously. Therefore, rigid base tank models have higher buckling load comparing with the flexible base tanks because rigid base tanks do not allow uplift. The flexible base tanks for both Housner and Veletsos buckle around LPF value of 0.40 because of the uplift of the tank which results in higher compressive stresses. Thus, the trend with aspect ratio is observed as with the increase in aspect ratio the likelihood of buckling is more at a lower LPF value.

2.4 Conclusions

Several nonlinear finite element models were created to investigate the behavior of large, vertical, aboveground, steel, open-top, flat bottom, unanchored storage tanks under horizontal seismic excitation using Abaqus finite element analysis program. The analysis was carried in two step process. In the first step static loads were applied using static, general method. The second step dynamic loads were applied using static, Riks method. Two different dynamic load configurations were applied one corresponding to Housner's approach and the other corresponding to Jacobsen-Veletsos approach. The analysis was carried for tank on rigid foundation as well as on flexible foundation. Resulting in four different combination for a given tank geometry, all the combinations were then compared. The results were also compared with design procedures presented in API 650. API 650 assumes a rigid tank wall and foundation with linear-elastic material properties using Housner's approach. The finite element provides insight about behavior of tanks with flexible foundation and also compares Jacobsen-Veletsos approach and Housner's approach. Based on the results of the current study following conclusions were drawn.

The effect of foundation flexibility increases with increase in aspect ratio, the ratio of the tank height to radius. For broad tanks (aspect ratio=0.67) the effect is negligible and for design considerations the effect of foundation flexibility can be ignored. However, for nominal (aspect ratio=1.0) and slender (aspect ratio=3.0) size tanks the effect should not be ignored. There is an increase in hoop stress value as the aspect ratio increases for flexible foundation comparing with rigid foundation.

The hoop stress values for Jacobsen-Veletsos's model are much higher comparing with Housner's model for broad tanks. However, in nominal and slender tank Housner's model has higher hoop stress comparing with Jacobsen-Veletsos's model because only single impulsive mode is considered in Jacobsen-Veletsos's approach. The effect of higher mode increases with the increase in aspect ratio. The longitudinal stress values using API 650 are typically much greater comparing with FEM results using Housner and Jacobsen-Veletsos approaches.

The flexibility of the foundation allow the base uplifting which led to increase in hoop stress and finally resulted into failure of tank either by rupture or elephant foot buckling. The flexibility of the foundation increases the longitudinal stresses which are significant only in slender tanks.

The design documents such as API 650 should incorporate the effect of foundation flexibility into the design provisions for nominal and slender tanks. Further studies should also incorporate the pressure distribution corresponding to flexibility of tank wall and higher impulsive modes as the impact of tank flexibility and higher modes is considerable for slender tanks as suggested by the literature.

ACKNOWLEDGMENTS

The authors would like to thank John Spritzer and Andres Rondon for providing guidance for modelling flexible foundation. Authors would also like to thank Office of Corporate and Global Partnerships, Purdue University and Placement Cell of IIT Bombay for providing the opportunity for PURE (Purdue Undergraduate Research Experience) program.

FUNDING

The study was funded by Purdue University under the PURE (Purdue Undergraduate Research Experience) program.

NOMENCLATURE

p	Impulsive pressure	MPa
γ_l	Specific weight	N/m ³
ϕ	Velocity potential function	dimensionless
$P_{hydrostatic}$	Hydrostatic pressure	MPa
H	Height of tank	m
h	Height of liquid level	m
z	Vertical distance from tank bottom	m
Y	Y is distance from the liquid surface	m
P_{wi}	Impulsive wall pressure	MPa
P_{bi}	Impulsive base pressure	MPa
P_{wc}	Convective wall pressure	MPa
P_{bc}	Convective base pressure	MPa
ρ_l	Fluid density	Kg/m ³
A_i	Impulsive spectral acceleration	g-force
A_c	Convective spectral acceleration	g-force
r	Radial position coordinate	m
R	Radius of tank	m
D	Diameter of tank	m
θ	Angle made with respect to horizontal direction	Radian
A_{ch}	Housner's convective spectral acceleration	g-force
A_j	J th mode convective spectral acceleration	g-force
C_0	-	dimensionless
C_j	-	dimensionless
I_1	Modified Bessel function of the first kind	dimensionless
J_1	Bessel function of first kind	dimensionless
K_{spring}	Stiffness of spring	N/m
$A_{tributary}$	Tributary area	m ²

σ_t	Total hoop stress	MPa
σ_h	Hydrostatic hoop stress	MPa
σ_s	Hydrodynamic hoop stress	MPa
N_h	Hydrostatic membrane force	N/mm
N_i	Impulsive hoop stress	N/mm
N_c	Convective hoop stress	N/mm
t	Thickness of shell	M
G	Specific gravity	dimensionless
σ_c	Maximum longitudinal compressive stress	MPa
w_t	Tank weight acting at the base of shell	N/m
A_v	Vertical earthquake acceleration	m/s ²
M_{rw}	Overtopping base moment	N-m
w_a	Force resisting uplift in annular region	N/m
t_s	Thickness of shell	Mm
J	Anchorage ratio	dimensionless

2.5 References

- [1] L. S. Jacobsen, "Impulsive hydrodynamics of fluid inside a cylindrical tank and of fluid surrounding a cylindrical pier," *Bulletin of the Seismological Society of America*, vol. 39, no. 3, pp. 189-204, 1949.
- [2] G. W. Housner, "Dynamic pressures on accelerated fluid containers," *Bulletin of the seismological society of America*, vol. 47, no. 1, pp. 15-35, 1957.
- [3] G. W. Housner, "The dynamic behavior of water tanks," *Bulletin of the seismological society of America*, vol. 53, no. 2, pp. 381-387, 1963.
- [4] G. W. Housner, "Dynamic Pressure on Fluid Containers," in *Technical Information Document (TID) 7024, Chapter 6 and Appendix F, U.S. Atomic Energy Commission*, 1963, pp. 183-209.
- [5] N. W. Edwards, "A procedure for the dynamic analysis of thin walled cylindrical liquid storage tanks subjected to lateral ground motions," Ph.D. dissertation, University of Michigan, 1969.
- [6] A. S. Veletsos, "Seismic effects in flexible liquid storage tanks," in *Proceedings of the 5th world conference on earthquake engineering*, 1974, vol. 1, pp. 630-639.
- [7] A. S. Veletsos and J. Auyang, "Earthquake response of liquid storage tanks," in *Advances in Civil Engineering through Engineering Mechanics*, 1977, pp. 1-24: ASCE.
- [8] J. Y. Yang, "Dynamic behavior of fluid tank systems," Ph.D. dissertation, Rice University, 1976.
- [9] M. A. Haroun, "Dynamic analyses of liquid storage tanks," California Institute of Technology, Pasadena, California, 1980.
- [10] D. P. Clough, "Experimental evaluation of seismic design methods for broad cylindrical tanks," University of California Earthquake Engineering Research Center, Berkeley, CA, USA, UCB/EERC 77-10, 1977.
- [11] A. Niwa, "Seismic behavior of tall liquid storage tanks," U.C. Berkeley, Report No. UCB/EERC-78/04, 1978.
- [12] M. A. Haroun, "Vibration studies and tests of liquid storage tanks," *Earthquake Engineering & Structural Dynamics*, vol. 11, no. 2, pp. 179-206, 1983.

- [13] C. I. Wu, T. Mouzakis, W. A. Nash, and J. M. Colonell "Natural frequencies of cylindrical liquid storage containers," University of Massachusetts, Amherst, MA,1975.
- [14] S. H. Shaaban and W. A. Nash, "Finite element analysis of a seismically excited cylindrical storage tank, ground supported, and partially filled with liquid," University of Massachusetts, Department of Civil Engineering, 1976.
- [15] M. A. Haroun and G. W. Housner, "Seismic design of liquid storage tanks," *Journal of the Technical Councils of ASCE*, vol. 107, no. 1, pp. 191-207, 1981.
- [16] M. A. Haroun and G. W. Housner, "Complications in free vibration analysis of tanks," *Journal of the Engineering Mechanics Division*, vol. 108, no. 5, pp. 801-818, 1982.
- [17] M. A. Haroun and G. W. Housner, "Dynamic characteristics of liquid storage tanks," *Journal of the Engineering Mechanics Division*, vol. 108, no. 5, pp. 783-800, 1982.
- [18] G. W. Housner, "Earthquake response of deformable liquid storage tanks," *Journal of Applied Mechanics*, vol. 48, no. 2, pp. 411-418, 1981.
- [19] S. Natsiavas and C. D. Babcock, "Behavior of unanchored fluid-filled tanks subjected to ground excitation," *Journal of Applied Mechanics*, vol. 55, no. 3, pp. 654-659, 1988.
- [20] N. Hori Ii, "Earthquake response analysis of tanks including hydrodynamic and foundation interaction effects," in *Proc. 8th world conf. earthquake eng.*, San Francisco, California, 1984, vol. III, pp. 817 – 824.
- [21] F. D. Fischer and R. Seeber, "Dynamic response of vertically excited liquid storage tanks considering liquid-soil interaction," *Earthquake engineering & structural dynamics*, vol. 16, no. 3, pp. 329-342, 1988.
- [22] A. S. Veletsos and Y. Tang, "Dynamics of vertically excited liquid storage tanks," *Journal of Structural Engineering*, vol. 112, no. 6, pp. 1228-1246, 1986.
- [23] M. A. Haroun and E. A. Abdel-Hafiz, "A simplified seismic analysis of rigid base liquid storage tanks under vertical excitation with soil-structure interaction," *Soil Dynamics and Earthquake Engineering*, vol. 5, no. 4, pp. 217-225, 1986.
- [24] A. S. Veletsos and Y. Tang, "Interaction effects in vertically excited steel tanks," in *Dynamic Response of Structures*, 1986, pp. 636-643: ASCE.
- [25] Y. Tang and A. S. Veletsos, "Soil-structure interaction effects for laterally excited liquid-tank system," presented at the American Society of Mechanical Engineers (ASME) pressure vessels and piping conference, New Orleans, LA (United States), 1992.

- [26] A. S. Veletsos and Y. Tang, "Soil-structure interaction effects for laterally excited liquid storage tanks," *Earthquake Engineering & Structural Dynamics*, vol. 19, no. 4, pp. 473-496, 1990.
- [27] P. K. Malhotra and A. S. Veletsos, "Uplifting response of unanchored liquid-storage tanks," *Journal of Structural Engineering*, vol. 120, no. 12, pp. 3525-3547, 1994.
- [28] P. K. Malhotra, "Seismic response of soil-supported unanchored liquid-storage tanks," *Journal of Structural Engineering*, vol. 123, no. 4, pp. 440-450, 1997.
- [29] P. K. Malhotra, T. Wenk, and M. Wieland, "Simple procedure for seismic analysis of liquid-storage tanks," *Structural Engineering International*, vol. 10, no. 3, pp. 197-201, 2000.
- [30] N. Buratti and M. Tavano, "Dynamic buckling and seismic fragility of anchored steel tanks by the added mass method," *Earthquake Engineering & Structural Dynamics*, vol. 43, no. 1, pp. 1-21, 2014.
- [31] M. R. Maheri and R. T. Severn, "Experimental added-mass in modal vibration of cylindrical structures," *Engineering Structures*, vol. 14, no. 3, pp. 163-175, 1992.
- [32] H. E. Estekanchi and M. Alembagheri, "Seismic analysis of steel liquid storage tanks by Endurance Time method," *Thin-Walled Structures*, vol. 50, no. 1, pp. 14-23, 2012.
- [33] R. Livaoglu and A. Dogangun, "Simplified seismic analysis procedures for elevated tanks considering fluid-structure-soil interaction," *Journal of fluids and structures*, vol. 22, no. 3, pp. 421-439, 2006.
- [34] J. M. Spritzer and S. Guzey, "Nonlinear numerical evaluation of large open-top aboveground steel welded liquid storage tanks excited by seismic loads," *Thin-Walled Structures*, vol. 119, pp. 662-676, 2017.
- [35] M. Ormeño, T. Larkin, and N. Chouw, "Influence of uplift on liquid storage tanks during earthquakes," *Coupled systems mechanics*, vol. 1, no. 4, pp. 311-324, 2012.
- [36] J. C. Virella, L. E. Suárez, and L. A. Godoy, "A static nonlinear procedure for the evaluation of the elastic buckling of anchored steel tanks due to earthquakes," *Journal of Earthquake Engineering*, vol. 12, no. 6, pp. 999-1022, 2008.
- [37] W. Wunderlich and C. Seiler, "Nonlinear treatment of liquid-filled storage tanks under earthquake excitation by a quasistatic approach," *Computers & Structures*, vol. 78, no. 1, pp. 385-395, 2000.

- [38] M. R. Maheri, M. E. Karbaschi, and M. Mahzoon, "Analytical evaluation of dynamic characteristics of unanchored circular ground-based steel tanks," *Thin-Walled Structures*, vol. 109, pp. 251-259, 2016.
- [39] T. Balendra and W. A. Nash, *Earthquake analysis of a cylindrical liquid storage tank with a dome by finite element method*. Department of Civil Engineering, University of Massachusetts at Amherst, 1978.
- [40] M. S. Sobhan, F. R. Rofooei, and N. K. A. Attari, "Buckling behavior of the anchored steel tanks under horizontal and vertical ground motions using static pushover and incremental dynamic analyses," *Thin-Walled Structures*, vol. 112, pp. 173-183, 2017.
- [41] M. A. Haroun and A. A. El-Zeiny, "Nonlinear transient response of unanchored liquid storage tanks," in *Fluid Sloshing and Fluid-Structure Interaction*, Honolulu, Hawaii, 1995, vol. 314, pp. 51-58: American Society of Mechanical Engineers.
- [42] A. S. Veletsos, "Seismic response and design of liquid storage tanks," in *Guidelines for the seismic design of oil and gas pipeline systems*: ASCE New York, NY, 1984, pp. 255-370.
- [43] F. H. Hamdan, "Seismic behaviour of cylindrical steel liquid storage tanks," *Journal of Constructional steel research*, vol. 53, no. 3, pp. 307-333, 2000.
- [44] M. A. Goudarzi, "Seismic Design of a Double Deck Floating Roof Type Used for Liquid Storage Tanks," *Journal of Pressure Vessel Technology*, vol. 137, no. 4, p. 041302, 2015.
- [45] T. Taniguchi and Y. Katayama, "Masses of Fluid for Cylindrical Tanks in Rock With Partial Uplift of Bottom Plate," *Journal of pressure vessel technology*, vol. 138, no. 5, p. 051301, 2016.
- [46] H. Sakai, A. Uemichi, A. Takai, Y. Yamasaki, and S. Kaneko, "Sloshing in a Horizontal Cylindrical Tank Subjected to Pitching Excitation and Damping Effects by Perforated Plates," *Journal of Pressure Vessel Technology*, vol. 139, no. 4, p. 041302, 2017.
- [47] M. D'Amico and N. Buratti, "Observational Seismic Fragility Curves for Steel Cylindrical Tanks," *Journal of Pressure Vessel Technology*, 2018.
- [48] H. N. Phan, F. Paolacci, and S. Alessandri, "Enhanced seismic fragility analysis of unanchored steel storage tanks accounting for uncertain modeling parameters," *Journal of Pressure Vessel Technology*, 2018.
- [49] A. Musa and A. A. El Damatty, "Capacity of liquid-filled steel conical tanks under vertical excitation," *Thin-walled structures*, vol. 103, pp. 199-210, 2016.

- [50] Z. Ozdemir, M. Souli, and Y. M. Fahjan, "Application of nonlinear fluid–structure interaction methods to seismic analysis of anchored and unanchored tanks," *Engineering Structures*, vol. 32, no. 2, pp. 409-423, 2010.
- [51] C. E. d. Normalisation, *Eurocode 8: Design provision of earthquake resistance of structures, Part 4: Silos, tanks and pipelines, CEN EN 1998-4*. Brussels, Belgium, 2006.
- [52] *New Zealand Society of Earthquake Engineering (NZSEE), Seismic Design of Storage Tanks: 2009*.
- [53] H. M. Westergaard, "Water pressures on dams during earthquakes," *Transactions of the American Society of Civil Engineers*, vol. 98, no. 2, pp. 418-433, 1933.
- [54] *American Petroleum Institute (API) Standard 650, Welded steel tanks for oil storage, 12th Edition, American Petroleum Institute*. 2013.
- [55] B. o. I. Standards, *IS 10987 : Code of practice for design, fabrication, testing and installation of underground/above ground horizontal cylindrical storage tanks for petroleum products*. 1992.
- [56] *American Concrete Institute (ACI), Seismic Design of Liquid-Containing Concrete Structures and Commentary, ACI 350.3-06, Farmington Hills, MI, 2006*.
- [57] *American Water Works Association (AWWA), Welded Steel Tanks for Water Storage, AWWA D-100, Denver, CO, 2016*.
- [58] A. K. Chopra, "Reservoir-dam interaction during earthquakes," *Bulletin of the Seismological Society of America*, vol. 57, no. 4, pp. 675-687, 1967.
- [59] A. K. Chopra, "Earthquake behavior of reservoir-dam systems," *Journal of the Engineering Mechanics Division*, vol. 94, no. 6, pp. 1475-1500, 1968.
- [60] A. K. Chopra, "Earthquake response of concrete gravity dams," *Journal of the Engineering Mechanics Division*, vol. 96, no. 4, pp. 443-454, 1970.
- [61] R. S. Wozniak and W. W. Mitchell, "Basis of seismic design provisions for welded steel oil storage tanks," in *Adv storage tank des API, refin 43rd midyear meet*, Toronto, Ontario, Canada, 1978.
- [62] *ABAQUS, 2018, Abaqus Analysis User's Manual Version 2018, Dassault Systems Simulia Corp., Providence, RI*.

- [63] *ASTM International, 2015, "Standard Specification for Pressure Vessel Plates, Carbon Steel, for Moderate- and Lower-Temperature Service," ASTM International, West Conshohocken, PA, Standard No. ASTM A516/A516M-10.*
- [64] *ASTM, 2008, "Standard Specification for Carbon Structural Steel," ASTM International, West Conshohocken, PA, Standard No. ASTM A36.*
- [65] *ASME Boiler and Pressure Vessel Code, 2015, "Section VIII, Alternative Rules for Construction of Pressure Vessels, Division 2," American Society of Mechanical Engineers, New York, NY.*
- [66] United States Geological Survey (USGS), 2011, Worldwide Seismic Design Tool (Beta). Available: (<http://earthquake.usgs.gov/hazards/designmaps/>).

2.6 Tables

Table 2-1 : Tank geometric properties ^{a, b}

Tank	Height h , ft	Radius R , ft	Aspect ratio h/R	Shell thickness t in.
Tank-1	40	60	0.67	0.433
Tank-2	40	40	1.0	0.289
Tank-3	72	24	3.0	0.315

^a To convert to meters (m) multiply the value in feet (ft) by 0.3048

^b To convert to millimeters (mm) multiply the value in inches (in.) by 25.4

Table 2-2: The C_i coefficients, impulsive and convective time periods, and convective acceleration

	Tank-1		Tank-2		Tank-3	
	Housner	Jacobsen -Veletsos	Housner	Jacobsen -Veletsos	Housner	Jacobsen -Veletsos
C_i	7.00	7.00	6.35	6.35	7.05	7.05
Impulsive time period, T_i (s)	0.23	0.23	0.21	0.21	0.17	0.17
Convective time period, T_c (s)	6.90	6.89	5.30	5.29	4.00	4.00
Convective acceleration (g)	0.074	0.074	0.096	0.096	0.127	0.127

Table 2-3: Top wind girder design in accordance with API 650^{a, b, c}

Tank	S_x Required in ³	S_x Provided in ³	Detail type	Leg “b” width in.	Angle size in.
Tank-1	32.4	33.3	e	12	-
Tank-2	14.4	16.6	d	-	5 x 3 x 5/16
Tank-3	9.33	11.6	c	-	6 x 4 x 3/8

^a All top wind girders are located 12 inch (305 mm) below from the top of the shell course

^b To convert section modulus value to cubic millimeter (mm³) multiply the value in cubic inches (in³) by 16,400

^c To convert the leg width and angle size value to millimeters (mm) multiply the value in inches (in) by 25.4

Table 2-4: Comparison of hoop stresses in psi (MPa)^a for tanks

	Housner		Jacobsen-Veletsos	
	Maximum Hydrostatic Stress (ksi)	Maximum Total Hoop Stress (ksi)	Maximum Hydrostatic Stress (ksi)	Maximum Total Hoop Stress (ksi)
Tank-1, Aspect Ratio: 0.67				
Hand Calculation	25.3	31.2	25.3	31.2
FEM Rigid Base	24.2	31.4	24.2	31.3
FEM Flexible Base	24.5	31.5	24.5	31.7
Tank-2, Aspect Ratio: 1.0				
Hand Calculation	25.3	30.7	25.3	30.7
FEM Rigid Base	24.9	34.8	24.9	33.7
FEM Flexible Base	25.0	34.9	25.0	33.8
Tank-3, Aspect Ratio: 3.0				
Hand Calculation	25.3	27.2	25.3	27.2
FEM Rigid Base	25.6	29.2	25.6	28.3
FEM Flexible Base	25.7	39.6	25.7	29.6

^a To convert stress values to MPa multiply stress in ksi by 6.9

Table 2-5: Comparison of longitudinal stresses in psi (MPa)^a for Tank-1

			Maximum Longitudinal Stress (psi)	
LPF		J Value	Housner	Jacobsen-Veletsos
1	Hand Calculation	1.07	1,042	
	FEM Rigid Base		1003	946
	FEM Flexible Base		840	810
0.8	Hand Calculation	0.867	771	
	FEM Rigid Base		797	778
	FEM Flexible Base		695	679
0.7	Hand Calculation	0.762	688	
	FEM Rigid Base		706	687
	FEM Flexible Base		624	614

^aTo convert stress values to MPa multiply stress in psi by 6.9×10^{-3}

Table 2-6 Comparison of longitudinal stresses in psi (MPa)^a for Tank-2

			Maximum Longitudinal Stress (psi)	
LPF		J Value	Housner	Jacobsen-Veletsos
0.95	Hand Calculation	1.473	4,521	
	FEM Rigid Base		1,688	1,584
	FEM Flexible Base		1,537	1,441
0.8	Hand Calculation	1.246	1,988	
	FEM Rigid Base		1,449	1,351
	FEM Flexible Base		1,315	1,230
0.49	Hand Calculation	0.776	911	
	FEM Rigid Base		947	881
	FEM Flexible Base		872	820

^aTo convert stress values to MPa multiply stress in psi by 6.9×10^{-3}

Table 2-7: Comparison of longitudinal stresses in psi (MPa)^a for Tank-3

			Maximum Longitudinal Stress (psi)	
LPF		<i>J</i> Value	Housner	Jacobsen-Veletsos
0.24	Hand Calculation	1.507	7,396	
	FEM Rigid Base		2,037	1,583
	FEM Flexible Base		2,457	1,751
0.2	Hand Calculation	1.28	2,957	
	FEM Rigid Base		1,761	1,379
	FEM Flexible Base		2,024	1,488
0.1	Hand Calculation	0.711	1,189	
	FEM Rigid Base		1,012	827
	FEM Flexible Base		1098	871

^aTo convert stress values to MPa multiply stress in psi by 6.9×10^{-3}

2.7 Figures

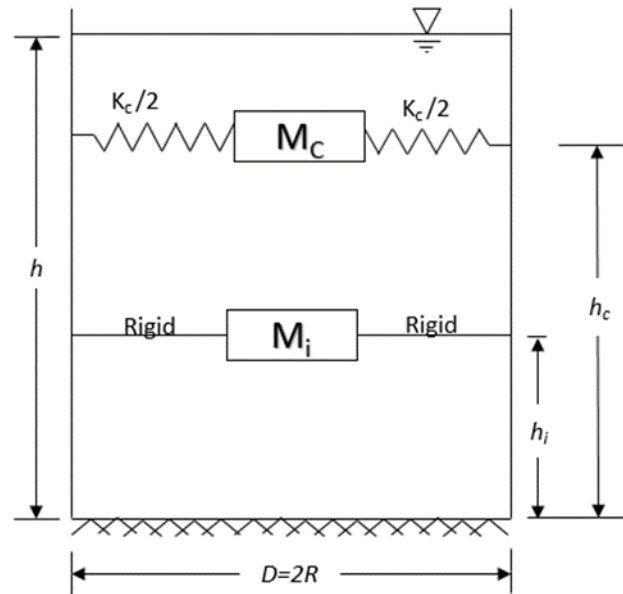


Figure 2-1: Housner's "Spring-mass" model [2]

This figure is originally presented in H. Bohra, E. Azzuni, and S. Guzey, "Seismic Analysis of Open-Top Storage Tanks With Flexible Foundation," *Journal of Pressure Vessel Technology*, vol. 141 no. 4, p. 041801, 2019. Reproduction of the figure has been permitted by ASME. The author would like to acknowledge ASME for granting the permission.

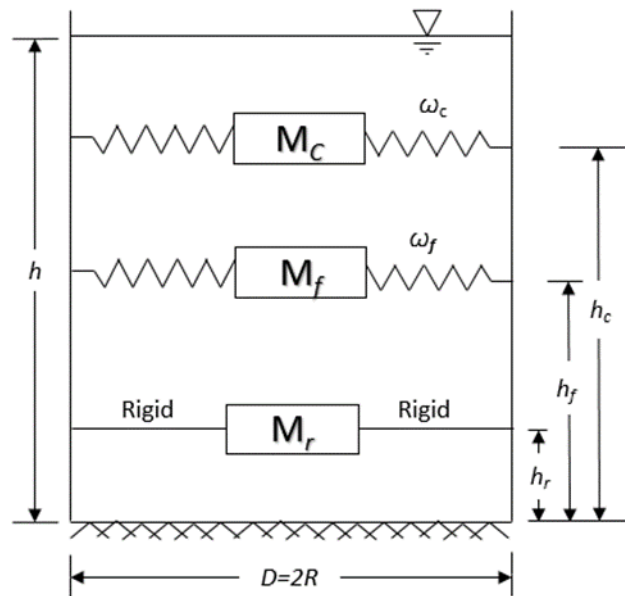


Figure 2-2: Haroun-Housner's "spring-mass" model for flexible tank [15]

This figure is originally presented in H. Bohra, E. Azzuni, and S. Guzey, "Seismic Analysis of Open-Top Storage Tanks With Flexible Foundation," *Journal of Pressure Vessel Technology*, vol. 141 no. 4, p. 041801, 2019. Reproduction of the figure has been permitted by ASME. The author would like to acknowledge ASME for granting the permission.

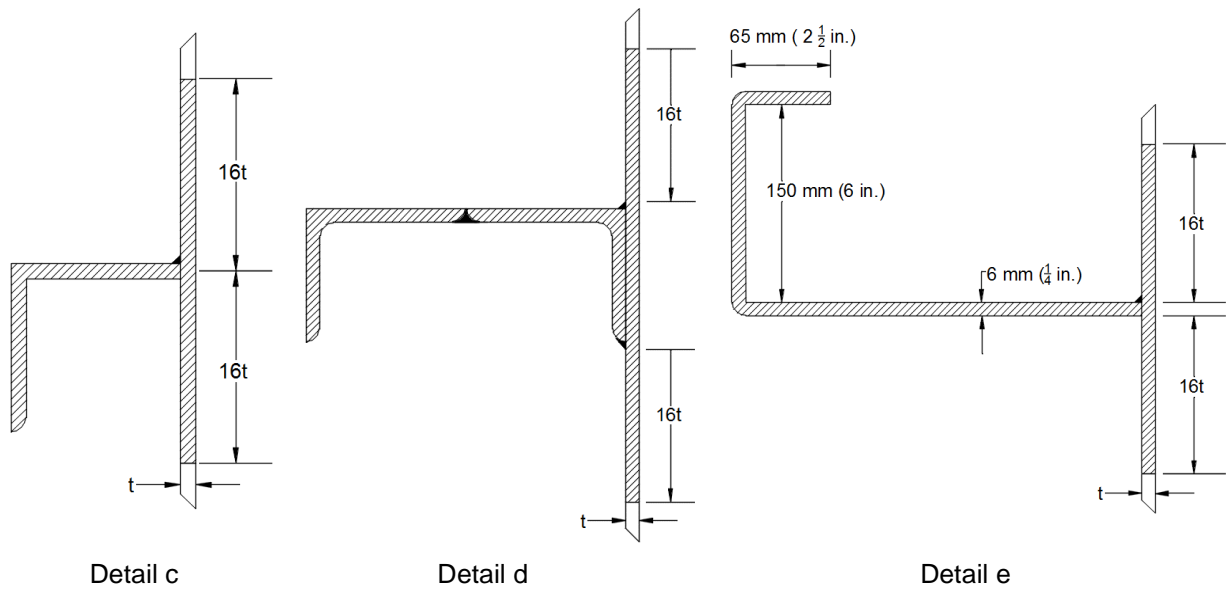


Figure 2-3: Wind girder details in accordance with API 650 [54]

This figure is originally presented in H. Bohra, E. Azzuni, and S. Guzey, "Seismic Analysis of Open-Top Storage Tanks With Flexible Foundation," *Journal of Pressure Vessel Technology*, vol. 141 no. 4, p. 041801, 2019. Reproduction of the figure has been permitted by ASME. The author would like to acknowledge ASME for granting the permission.

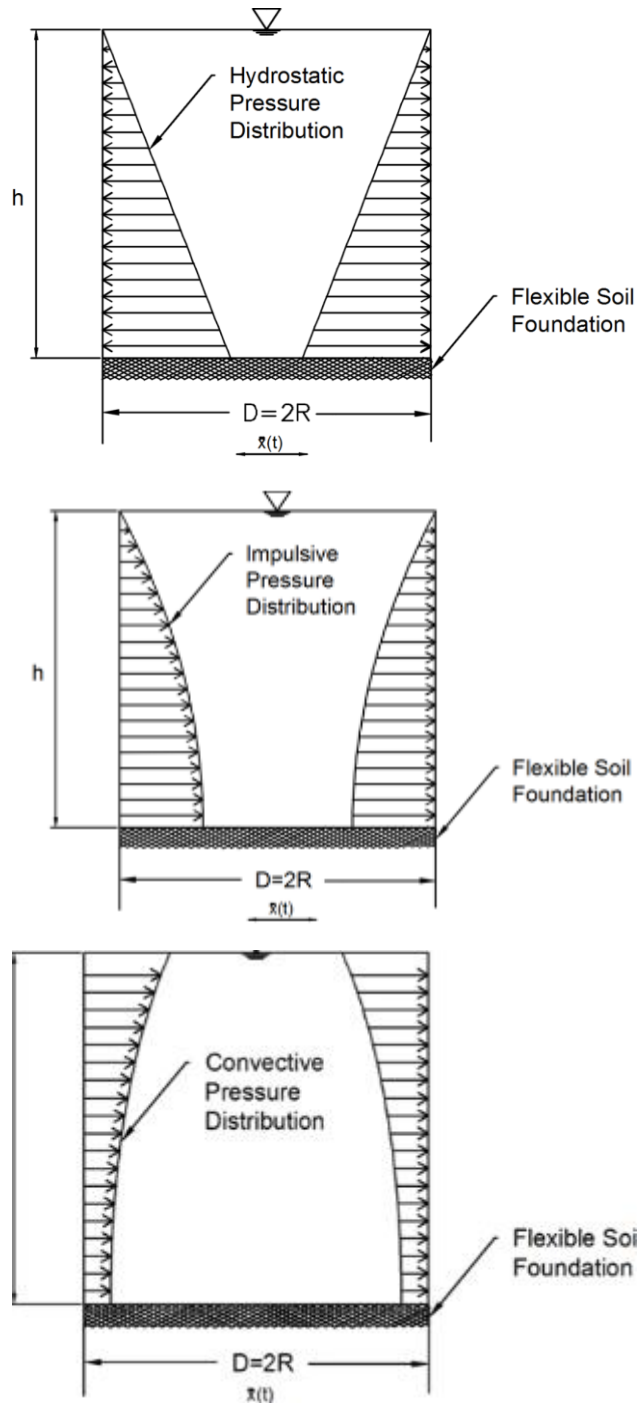


Figure 2-4: Hydrostatic, impulsive and convective pressure distribution diagrams on tank shell

This figure is originally presented in H. Bohra, E. Azzuni, and S. Guzey, "Seismic Analysis of Open-Top Storage Tanks With Flexible Foundation," *Journal of Pressure Vessel Technology*, vol. 141 no. 4, p. 041801, 2019. Reproduction of the figure has been permitted by ASME. The author would like to acknowledge ASME for granting the permission.

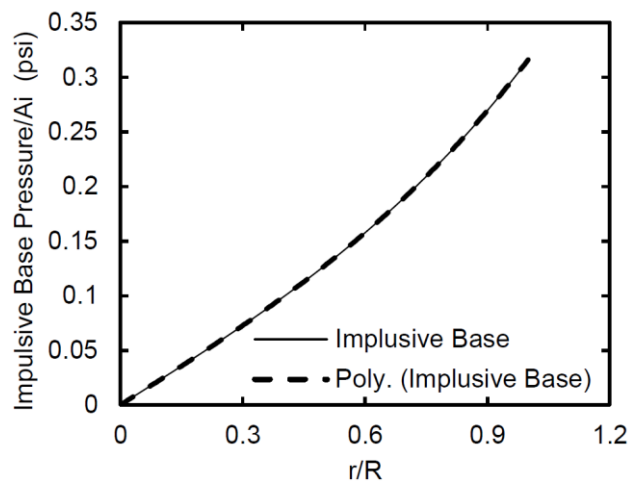


Figure 2-5: Plot for Tank-2 impulsive base pressure and approximate polynomial function

This figure is originally presented in H. Bohra, E. Azzuni, and S. Guzey, "Seismic Analysis of Open-Top Storage Tanks With Flexible Foundation," *Journal of Pressure Vessel Technology*, vol. 141 no. 4, p. 041801, 2019. Reproduction of the figure has been permitted by ASME. The author would like to acknowledge ASME for granting the permission.

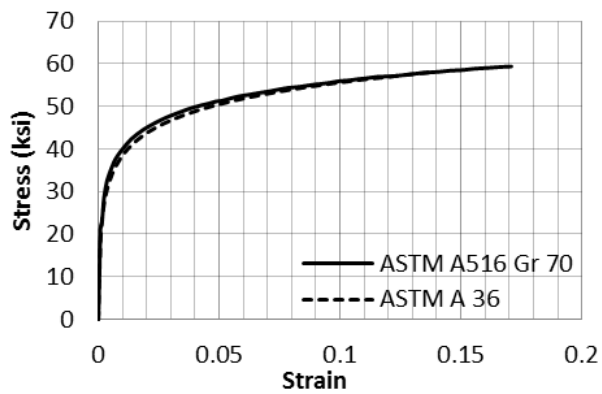


Figure 2-6: Stress-strain curve for ASTM A516 Grade 70 and ASTM A36 steel. To convert to MPa, multiply stress in ksi by a factor of 6.9

This figure is originally presented in H. Bohra, E. Azzuni, and S. Guzey, "Seismic Analysis of Open-Top Storage Tanks With Flexible Foundation," *Journal of Pressure Vessel Technology*, vol. 141 no. 4, p. 041801, 2019. Reproduction of the figure has been permitted by ASME. The author would like to acknowledge ASME for granting the permission.

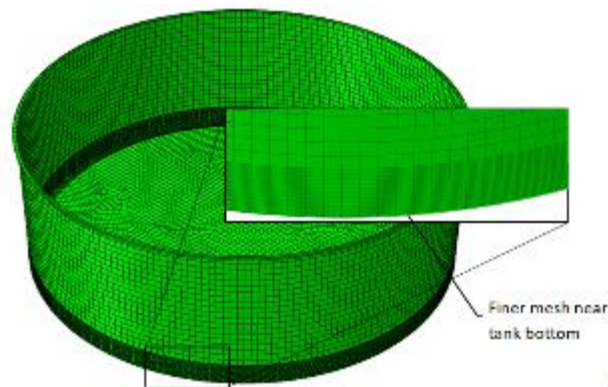


Figure 2-7: Finite element model of Tank-1 using Abaqus CAE

This figure is originally presented in H. Bohra, E. Azzuni, and S. Guzey, "Seismic Analysis of Open-Top Storage Tanks With Flexible Foundation," *Journal of Pressure Vessel Technology*, vol. 141 no. 4, p. 041801, 2019. Reproduction of the figure has been permitted by ASME. The author would like to acknowledge ASME for granting the permission.

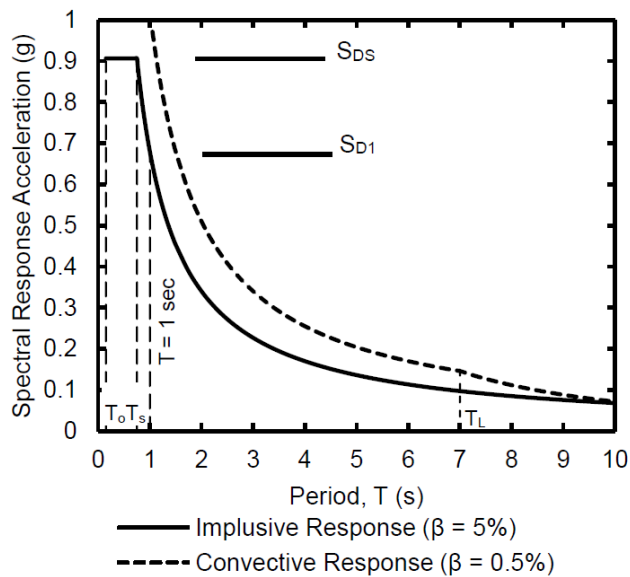


Figure 2-8: Design Response Spectra using API 650 procedure

This figure is originally presented in H. Bohra, E. Azzuni, and S. Guzey, "Seismic Analysis of Open-Top Storage Tanks With Flexible Foundation," *Journal of Pressure Vessel Technology*, vol. 141 no. 4, p. 041801, 2019. Reproduction of the figure has been permitted by ASME. The author would like to acknowledge ASME for granting the permission.

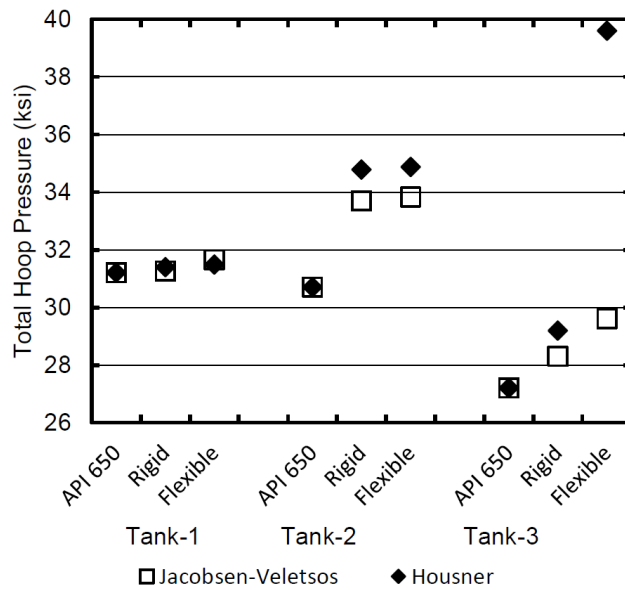


Figure 2-9: Comparison of total hoop stresses in psi for tanks; to convert stress values to MPa multiply stress in ksi by 6.9

This figure is originally presented in H. Bohra, E. Azzuni, and S. Guzey, "Seismic Analysis of Open-Top Storage Tanks With Flexible Foundation," *Journal of Pressure Vessel Technology*, vol. 141 no. 4, p. 041801, 2019. Reproduction of the figure has been permitted by ASME. The author would like to acknowledge ASME for granting the permission.

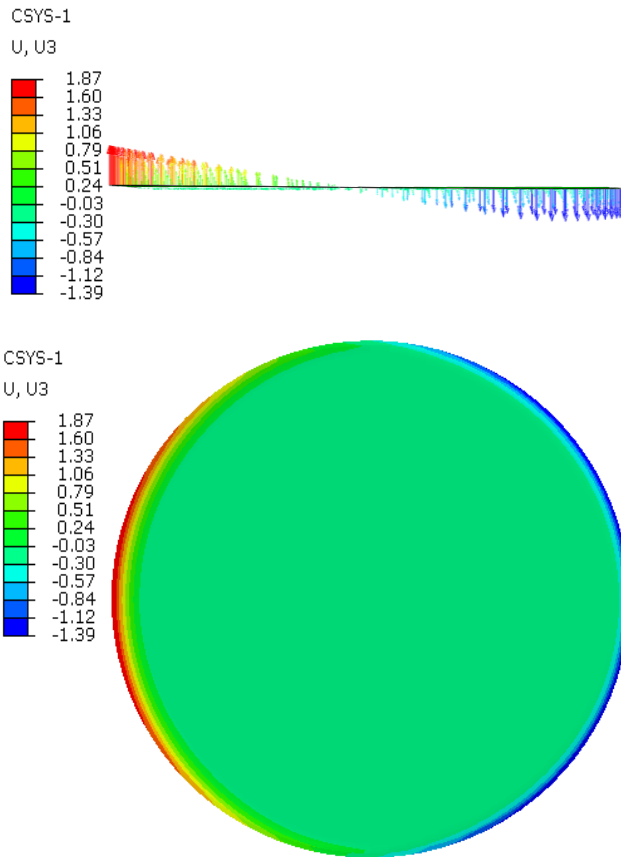


Figure 2-10: Rotation and uplift of base of Tank 3 for flexible foundation with elevation and plan view of tank bottom plate. Tanks shell is not shown for clarity. Positive values indicate uplift and negative values indicate tank base penetrating or settling to foundation. Uplift is given in inches.

To convert uplift values to mm, multiply values in inches with 25.4.

This figure is originally presented in H. Bohra, E. Azzuni, and S. Guzey, "Seismic Analysis of Open-Top Storage Tanks With Flexible Foundation," *Journal of Pressure Vessel Technology*, vol. 141 no. 4, p. 041801, 2019. Reproduction of the figure has been permitted by ASME. The author would like to acknowledge ASME for granting the permission.

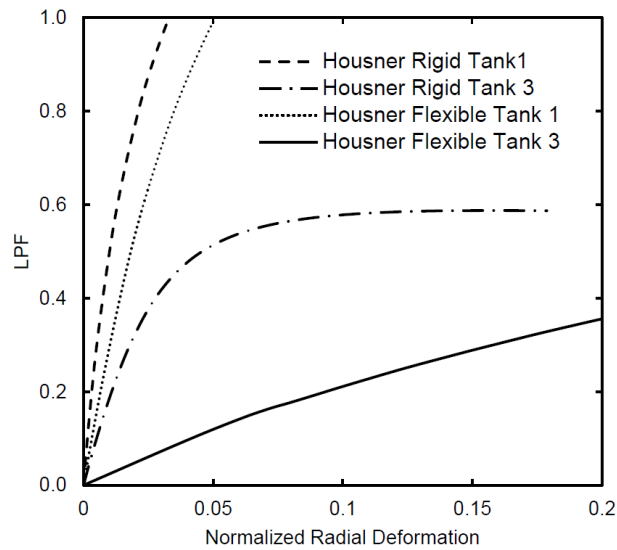


Figure 2-11: Normalized nonlinear radial deformation of Tank-1 and Tank-3 using Riks method. LPF represent the percentage of load applied. Deformation is measured for the topmost point; deformation is normalized to \sqrt{ht} of the respective tanks

This figure is originally presented in H. Bohra, E. Azzuni, and S. Guzey, "Seismic Analysis of Open-Top Storage Tanks With Flexible Foundation," *Journal of Pressure Vessel Technology*, vol. 141 no. 4, p. 041801, 2019. Reproduction of the figure has been permitted by ASME. The author would like to acknowledge ASME for granting the permission.

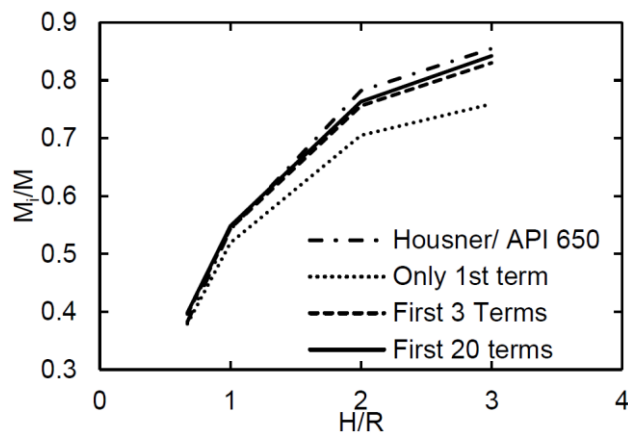


Figure 2-12: Comparison of contribution of higher impulsive modes to only first impulsive mode

This figure is originally presented in H. Bohra, E. Azzuni, and S. Guzey, "Seismic Analysis of Open-Top Storage Tanks With Flexible Foundation," *Journal of Pressure Vessel Technology*, vol. 141 no. 4, p. 041801, 2019. Reproduction of the figure has been permitted by ASME. The author would like to acknowledge ASME for granting the permission.

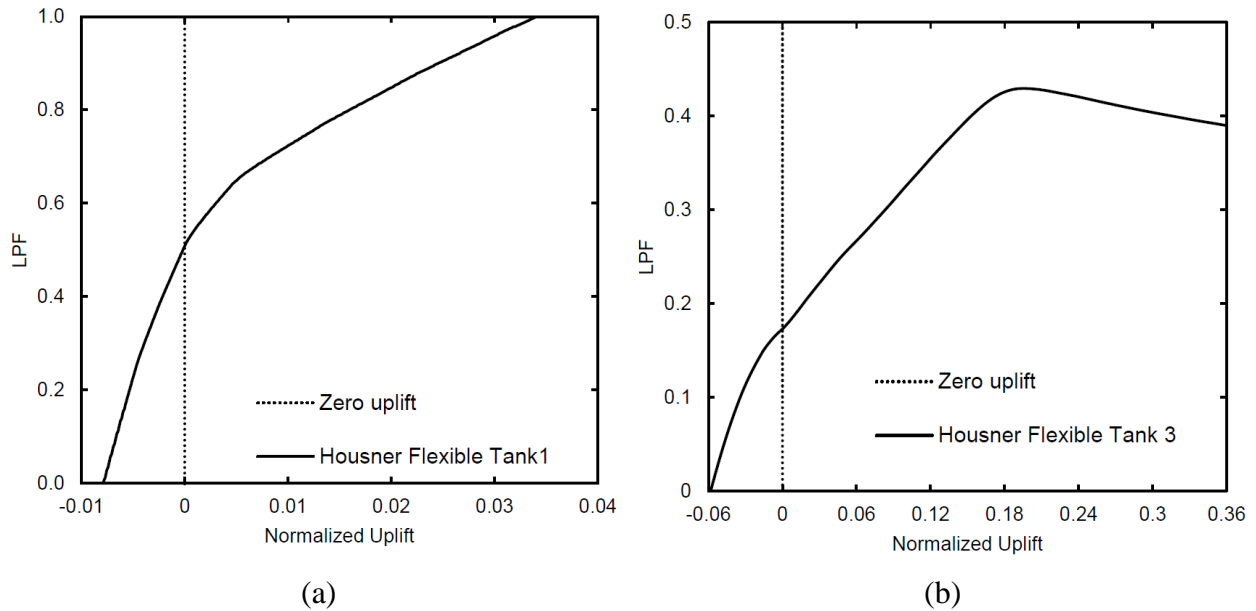


Figure 2-13: Normalized nonlinear uplift of (a) Tank-1 and (b) Tank-3 using Riks method. LPF represent the percentage of load applied. Uplift is measured for the extreme point on tank bottom; uplift is normalized to \sqrt{Rt} of the respective tanks

This figure is originally presented in H. Bohra, E. Azzuni, and S. Guzey, "Seismic Analysis of Open-Top Storage Tanks With Flexible Foundation," *Journal of Pressure Vessel Technology*, vol. 141 no. 4, p. 041801, 2019. Reproduction of the figure has been permitted by ASME. The author would like to acknowledge ASME for granting the permission.

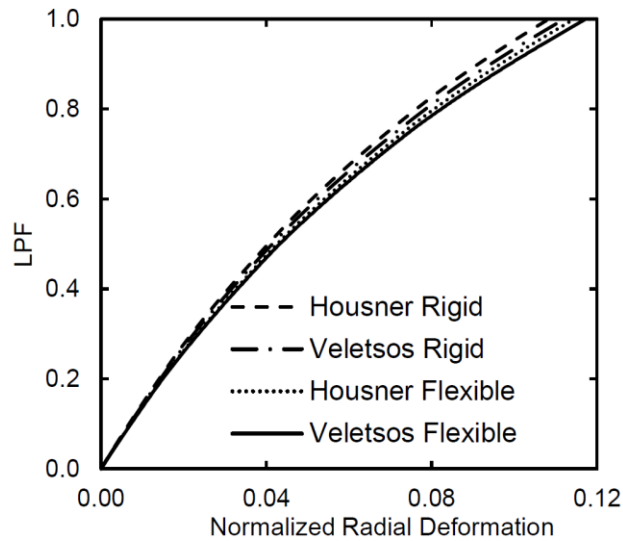


Figure 2-14: Normalized nonlinear behaviour of Tank-1 using Riks method. LPF represent the percentage of load applied. Deformation is measured from the point of maximum hoop stress; deformation is normalized to \sqrt{Rt} of the respective tank

This figure is originally presented in H. Bohra, E. Azzuni, and S. Guzey, "Seismic Analysis of Open-Top Storage Tanks With Flexible Foundation," *Journal of Pressure Vessel Technology*, vol. 141 no. 4, p. 041801, 2019. Reproduction of the figure has been permitted by ASME. The author would like to acknowledge ASME for granting the permission.

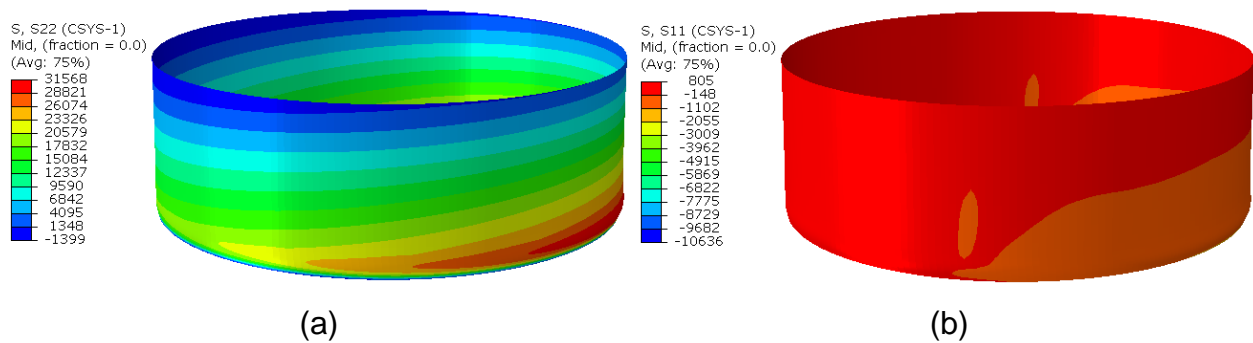


Figure 2-15: (a), Hoop stress and (b) Longitudinal stress with deformation of Tank-1 under hydrostatic, gravity and hydrodynamic loads. Stress values shown are in psi; to convert them to MPa, multiply stress in psi by 6.9×10^{-3}

This figure is originally presented in H. Bohra, E. Azzuni, and S. Guzey, "Seismic Analysis of Open-Top Storage Tanks With Flexible Foundation," *Journal of Pressure Vessel Technology*, vol. 141 no. 4, p. 041801, 2019. Reproduction of the figure has been permitted by ASME. The author would like to acknowledge ASME for granting the permission.

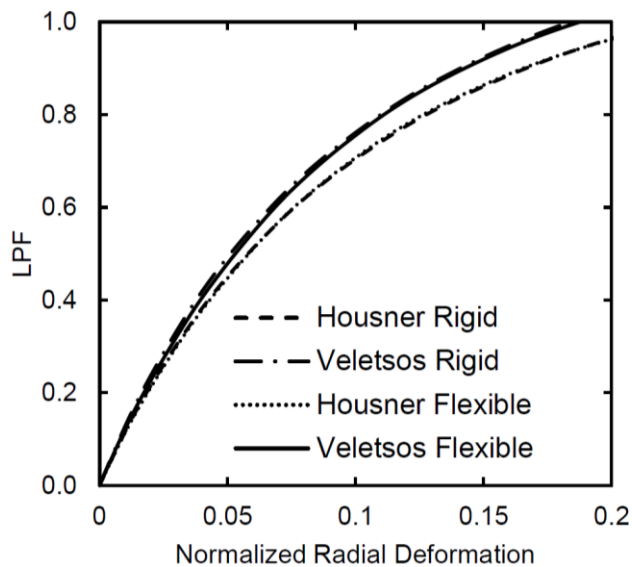


Figure 2-16: Normalized nonlinear behaviour of Tank-2 using Riks method. LPF represent the percentage of load applied. Deformation is measured from the point of maximum hoop stress; deformation is normalized to \sqrt{Rt} of the respective tank

This figure is originally presented in H. Bohra, E. Azzuni, and S. Guzey, "Seismic Analysis of Open-Top Storage Tanks With Flexible Foundation," *Journal of Pressure Vessel Technology*, vol. 141 no. 4, p. 041801, 2019. Reproduction of the figure has been permitted by ASME. The author would like to acknowledge ASME for granting the permission.

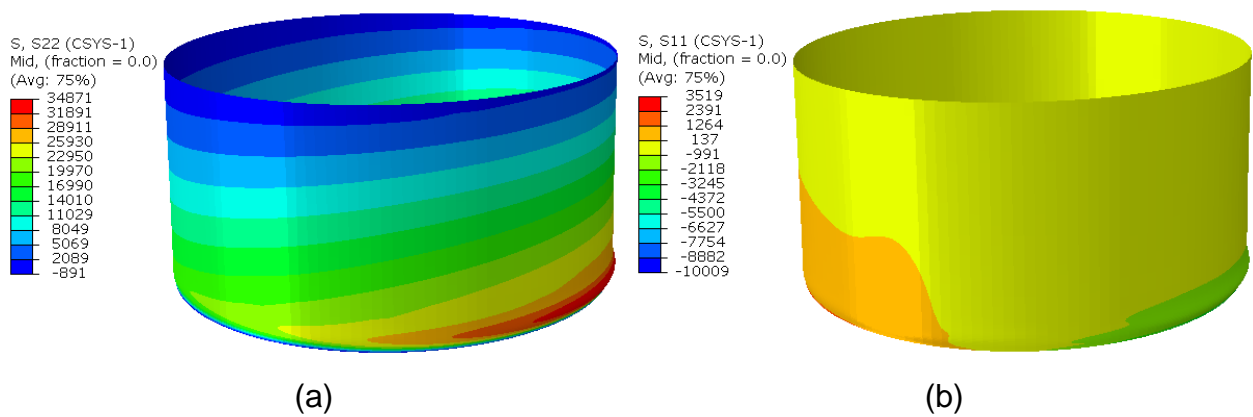


Figure 2-17: (a), Hoop stress and (b) Longitudinal stress with deformation Tank-2 under hydrostatic, gravity and hydrodynamic loads. Stress values shown are in psi; to convert them to MPa, multiply stress in psi by 6.9×10^{-3}

This figure is originally presented in H. Bohra, E. Azzuni, and S. Guzey, "Seismic Analysis of Open-Top Storage Tanks With Flexible Foundation," *Journal of Pressure Vessel Technology*, vol. 141 no. 4, p. 041801, 2019. Reproduction of the figure has been permitted by ASME. The author would like to acknowledge ASME for granting the permission.

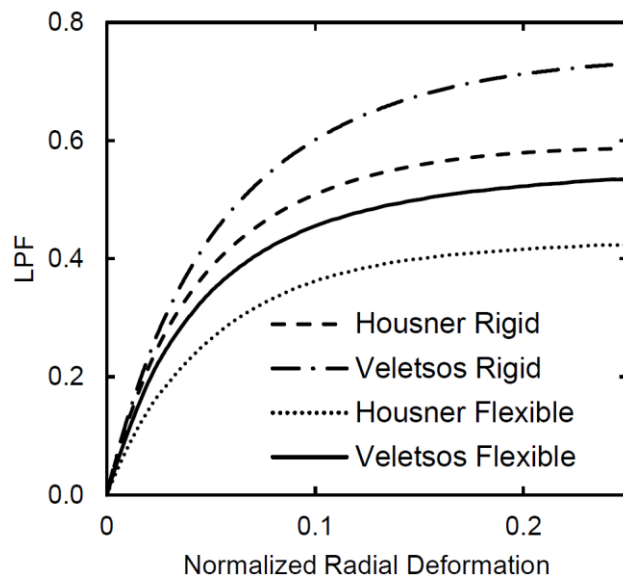


Figure 2-18: Normalized nonlinear behaviour of Tank-3 using Riks method. LPF represent the percentage of load applied. Deformation is measured from the point of maximum hoop stress; deformation is normalized to \sqrt{Rt} of the respective tank

This figure is originally presented in H. Bohra, E. Azzuni, and S. Guzey, "Seismic Analysis of Open-Top Storage Tanks With Flexible Foundation," *Journal of Pressure Vessel Technology*, vol. 141 no. 4, p. 041801, 2019. Reproduction of the figure has been permitted by ASME. The author would like to acknowledge ASME for granting the permission.

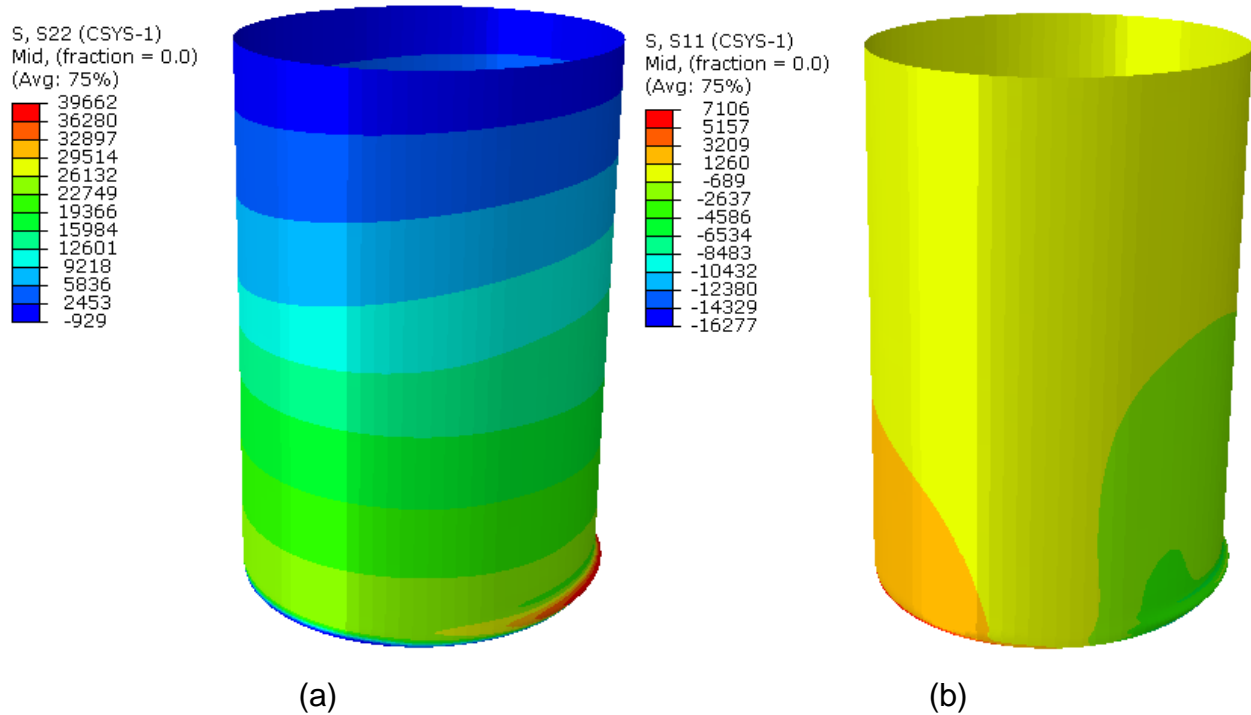


Figure 2-19: (a), Hoop stress and (b) Longitudinal stress with deformation of Tank-3 under hydrostatic, gravity and hydrodynamic loads. Stress values shown are in psi; to convert them to MPa, multiply stress in psi by 6.9×10^{-3}

This figure is originally presented in H. Bohra, E. Azzuni, and S. Guzey, "Seismic Analysis of Open-Top Storage Tanks With Flexible Foundation," *Journal of Pressure Vessel Technology*, vol. 141 no. 4, p. 041801, 2019. Reproduction of the figure has been permitted by ASME. The author would like to acknowledge ASME for granting the permission.

3. FITNESS-FOR-SERVICE OF OPEN-TOP STORAGE TANKS SUBJECTED TO DIFFERENTIAL SETTLEMENT

Summary

A method for evaluating the mechanical integrity of open-top cylindrical storage tanks subjected to a differential settlement is given. The settlement profile underneath the bottom circumference of the tank shell can be transformed into different harmonic components using the Fourier transformation. The existing method in American Petroleum Institute's standard API 653, which is currently used by the industry in North America does not differentiate the effect of different harmonic components. Nevertheless, the proposed method evaluates a cumulative damage factor by considering the effects of first five harmonic components individually. The paper further discusses other limitations of the existing method in API 653 document. Numerous finite element analysis (FEA) simulations are conducted to formulate and validate the proposed method by employing geometric nonlinear algorithm with nonlinear plastic material properties (GMNA) in ABAQUS finite element software. The trend for limiting settlement values with respect to different harmonic components under consideration and different tank geometries are discussed. The proposed method is validated by performing FEA using four actual settlement data profiles on different tank geometries. Lastly, the comparison is drawn between the FEA results, the existing API 653 method and the proposed method. The results of the allowable settlement indicate that the existing method is not consistent with the FEA findings. For some of the actual settlement data, the existing method results in overly conservative values and for others it gives non-conservative values. Thus, the existing method may not capture the true behavior of tanks under settlement and needs modifications. The results of allowable settlement from the proposed method are found to be consistent with the FEA results for all different settlement data and tank geometries. Therefore, it is recommended that the new method is used instead of the existing method.

Keywords: Foundation settlement; Storage tanks; Finite element analysis; Harmonic settlement; Differential settlement; API 653

3.1 Introduction

Open-top tanks with a floating roof are used for storing a variety of liquid petroleum products such as crude oil, gasoline, diesel oil, and other similar liquids. These tanks are generally built on a relatively soft soil or concrete ring wall foundation, which makes them susceptible to failure due to foundation settlement. The settlement below the tank shell can cause failure due to buckling or yielding of the tank shell. It can also cause serviceability issue due to excessive out of roundness of the tank shell which may inhibit the vertical movement of the floating roof of the tank, if there is one. For many years, researchers have been investigating how the settlement affects the overall structural stability. The settlement profile of the tank shell can be decomposed using a Fourier series as suggested by Malik et al. [1]. The Fourier series of a settlement profile along the tank circumference is shown in the following equation

$$u(\theta) = \sum_{n=0}^{n_{\max}} u_n \cos(n\theta + \phi_n) \quad (30)$$

where $u(\theta)$ is the settlement (vertical displacement) along the bottom circumference of the shell, n is the harmonic wave number, u_n is the Fourier coefficient, θ is the circumferential central angle, ϕ_n is the phase angle for n^{th} harmonic wave number and n_{\max} is the maximum harmonic wave number used for the Fourier transformation. From a practical design point, the settlement along the bottom circumference of the shell can be classified as uniform settlement ($n=0$), planar tilt ($n=1$), and nonplanar settlement ($n \geq 2$).

Malik et al. [1] related the radial displacement at the top of the shell to the vertical displacement (settlement) at the bottom edge of the tank using inextensional linear thin shell theory and formulated the following equation

$$w + \frac{DH}{2} \left(\frac{\partial^2 u}{\partial y^2} \right) = 0 \quad (31)$$

where D is the diameter of the tank, H is the height of the tank, w is the radial displacement, u is the settlement at the edge and y is the y -coordinate as shown in Figure 1.

In Malik et al. [1] formulation, the shell thickness was assumed to be uniform, and the effect of fluid present in the tank was ignored. In addition to the analytical work, they performed controlled physical experiments of the scaled models to validate their theory. They carried out experiments for various settlement profiles such as tilt, twist, diametric fold, and local settlement using sine functions. They concluded that the uniform settlement ($n=0$) and planar tilt ($n=1$) did not cause any stresses to the tank. They used this formulation to calculate a maximum allowable settlement by limiting the maximum allowable radial displacement.

Later, Marr et al. [2] proposed a different procedure for the allowable foundation settlement of a tank. This procedure is based on a formulation of failure due to rupture of the tank material, which is a strength limit state and not a serviceability limit state. The formulation combines the DeBeer relationship [3] and the classical beam theory. DeBeer related out of plane distortion at a point to the radius of curvature at the point. The beam theory relates to the radius of curvature at a point with the stresses. Combining the DeBeer relationship and beam theory, Marr and coworkers established a relationship between the differential settlement at a given point on the shell circumference and the stress at a point as shown in the following equation

$$S = \frac{11L^2Y}{EH} \quad (32)$$

where S is the differential settlement in ft, L is the arc length between the measurement settlement points in ft, Y is the yield strength of the shell material in ksi, E is the Young's modulus in ksi and H is the height of the tank in ft. This equation is based on limiting value of strain to 0.014, which corresponds to initiation of strain hardening of a carbon steel material having a yield stress of 36 ksi [2]. Their procedure is currently used in the API 653 standard [4] with an additional factor of safety. The Eq. (32) is modified by dividing it with a factor of two in API 653 that results in the limiting strain value to 0.007, still beyond yielding of a carbon steel material. This modified Marr and coworkers' method used by API 653 is referred as "method-1" in the present paper.

Kamyab and Palmer [5] concluded that Malik et al. [1] assumption of inextensional theory is valid only for smaller harmonic wave numbers. The limitation of inextensional theory was resolved by recommending a membrane and long wave solution for higher harmonic wave numbers. Also, Palmer [6] observed that for localized settlement profiles, the inextensional theory does not give

accurate results when the settlement is occurring along a small arc, typically less than 60° of the shell circumference.

Later, Jonaidi and Ansourian [7] performed finite element analysis (FEA) for tanks with step thickness. They found that the assumption of uniform thickness using membrane theory gave conservative results for harmonic wave numbers between 5 and 10 for open-top tanks. Most of the tanks build have step thickness rather than uniform thickness for a more economical design. They also found that the effect of differential settlement causes bending at the junction of the primary wind girder and the shell and, at the tip of the girder, which ultimately causes the failure of the tank material.

Meanwhile, Godoy and Sosa [8] also studied the behavior of tanks under localized settlement using FEA. They used a geometric nonlinear algorithm with linear material model and found that there is a significant gap in the equilibrium path between linear and geometric nonlinear analysis. The nonlinear analysis showed that the model becomes unstable whereas in the linear analysis no such behavior was observed. In addition, they performed physical experiments on a small-scale model, which validated that the tanks, in reality, follow the nonlinear behavior [9].

Holst and Rotter [10] looked into the buckling of cylindrical shells under combined axial compression and localized settlement using FEA. They considered the effect of localized settlement as an imperfection to the tank and then applied uniform axial compression to determine the buckling strength. The results show that buckling strength is reduced because of the formation of dimple due to the localized settlement.

Zhao et al. [11] investigated the behavior of floating roof tanks under harmonic settlement using FEA with a linear static algorithm. They did a parametric study for various tank radius to thickness ratios, tank height to radius ratios, and bending rigidity of wind girders. A simple approximation for relating the radial displacement at the top of the tank with the vertical settlement was developed using regression analysis on FEA results.

Later, Cao and Zhao [12] further investigated the buckling strength for different harmonic wave numbers and included the effect of eigenmode-affine geometric imperfections. They found that the critical harmonic settlement decreases with the increase in the wave number and the critical

value depends not only on the wave number but also on the tank height to radius ratio. A similar study was done by Gong and coworkers [13] for conical roof tanks observing similar results. Gong and coworkers [14] also studied the behavior for open-top tanks and compared the results with tanks having a conical roof. Later, Gong and coworkers [15] investigated the effect of the top stiffener ring on open-top tanks subjected to harmonic settlement. They found that with the top stiffener ring the critical settlement decreases compared to a tank without a top stiffener ring. Gong and coworkers [16] did another FEA study and investigated the effect of hydrostatic pressure due to liquid in the tank on the buckling behavior under the local settlement.

Having studied the effect of harmonic settlement, Zhao and coworkers [17] worked on actual settlement data. Based on their study, the actual tank settlement could be classified into global or local settlement. For the global differential settlement with a smaller height to radius ratio, local buckling at the wind girder with a stable post buckling behavior was observed and for higher height to radius ratio, unstable snap through buckling was observed. In case of local differential settlement with large central angle, such as 60° the behavior is similar to global differential settlement and for small central angle, such as 15° snap through buckling at the tank wall takes place.

Fan and coworkers [18] suggested the use of the Poisson curve method for prediction of settlement. The method uses the least square approach and Lagrange quadratic interpolation to predict the future settlement profile. Fan and coworkers [19] also performed a study to relate the impact of the settlement on the axial buckling capacity of the tank. Settlement directly does not result in tank failure but it acts like imperfection to tank. The FEA results agreed showing a reduction in buckling capacity with an increase in differential settlement. Further, the effect of liquid stored was also investigated. The hydrostatic pressure due to the liquid pushes the shell outwards hindering the inward deformation caused by the settlement. Thus, increasing the buckling capacity of the tank.

Many researchers have studied the effect of the settlement on the tank. The settlement profile can be classified into global and local settlement. The results show that the effect of a global settlement profile can be understood effectively by decomposing the settlement into its harmonic components. However, the current provisions of API 653 (method-1) consider only the zero and first harmonics and do not differentiate the effect of higher harmonics. Thus, the current provisions are not

consistent with the available research findings for global settlement profile. Each harmonic wave number has a different effect and allowable settlement. Andreani and Carr [20] proposed an alternative method to evaluate the allowable settlement based on a parametric FEA study. Their proposed method was added in the API 653 provisions as an alternative to the original Marr at el. [2] method (method-1). However, the results from their study do not represent the true behavior of a global settlement profile, as their study was primarily focused on local settlement profiles with different degree of localization. Therefore, there is a need of a refined approach to determine allowable settlement of storage tanks under the global settlement profile by considering the effect of higher harmonics individually.

This authors' aims to formulate a new method to evaluate the fitness of the tank under global settlement profiles, taking the effect of higher harmonics into account for a vertical, aboveground, steel, open-top, flat bottom liquid storage tanks. The proposed method considers the effect of the higher harmonics wave numbers $n=2, 3$ and 4 in addition to $n=0$ and 1 . Various FEA simulations were conducted with different tank geometries to formulate and validate the proposed method. The geometric nonlinear analysis with nonlinear plastic material properties was conducted. The limiting settlement values were found for different harmonic wave numbers under consideration. The proposed method was validated by using the actual settlement data reported by Gong et al. [21]. Finally, the results from the FEA of the actual settlement data were compared with the proposed method and the existing provisions of API 653 (method-1) for allowable differential settlement.

3.2 Settlement calculation model

The approach used for formulating the proposed method is presented. The selection of tank geometries and design of open-top tank used in the formulation are discussed. Next, the criterion proposed by the authors and its execution in FEA for the evaluation of limiting settlement values for different harmonic wave numbers are presented. Finally, the FEA results are given and discussed.

3.2.1 Tank geometry

The tank geometry for open-top tank is defined by the tank diameter D , the tank height H , the shell thicknesses and the wind girder detail. Tank geometries were selected based on two criteria; (1) geometric ratio and (2) aspect ratio. The geometric ratio is defined as D^2/H and aspect ratio is defined as H/D . The allowable settlement according to method-1 is proportional to L^2/H , where L is linearly dependent on D . Therefore, the tank geometries for developing the proposed method were selected to have a unique geometric ratio (D^2/H). Also, majority of the tanks studied in the literature have aspect ratios ranging between 0.25 to 1 as reported in a recent study conducted by Pantousa and Godoy [22]. Based on the two criteria 18 different tank geometries were selected representing seven different aspect ratios ranging between 0.25 to 1 and 18 different geometric ratios ranging between 40 to 640.

Three different tank heights typically used in the industry in North America; 40 ft (12.2 m), 48 ft (14.6 m) and 56 ft (17.1 m) were selected and the tank diameter was varied from 40 ft (12.2 m) to 160 ft (48.8 m). The notation used to refer each tank geometry is shown in Table 1. The tank model name is referred as TK- D^2/H . For example a tank with diameter of 40 ft (12.2 m) and height 40 ft (12.2 m) is referred as TK-40 because D^2/H is 40.

3.2.2 Tank Design

The tanks were designed in accordance with API 650 [23]. The design of tank shell wall thicknesses is depended on the specific gravity, G of the stored liquid and the material specification used for tank construction. The tank was assumed to contain a liquid having a specific gravity of 0.9 and the design liquid height was taken as the tank height, H .

The material specifications used for modeling the shell and the wind girder were ASTM A516 Grade 70 steel [24] and ASTM A36 [25] steel specifications, respectively. The material specifications A516 Grade 70 and A36 were selected because they are typically used in the North American industry for construction of tank shell and wind girder, respectively. The A516 Grade 70 steel has an allowable stress for design, S_d , of 25.3 ksi (173 MPa), an allowable stress for hydrostatic test, S_t , of 28.5 ksi (195 MPa), a yield stress, F_y , of 38 ksi (260 MPa), and an ultimate

tensile strength, F_u , of 70 ksi (485 MPa). ASTM A36 steel has an F_y of 36 ksi (250 MPa) and an F_u of 58 ksi (400 MPa).

The tank shell thicknesses were sized in conformance with section 5.6 of API 650. The more economical set of shell thicknesses calculated using the one-foot and the variable design point methods was taken as design thicknesses. For all the tank models the variable design point method resulted in a more economical set of thicknesses. The width of shell courses was taken as 8 ft (2.4 m) because many of the tanks are constructed using this width in North America. Furthermore, the tanks were assumed to be open-top, having no fixed roof. The tank shell thicknesses are listed in Appendix A, Table A.1.

The top and intermediate wind girders were sized using sections 5.9.6 and 5.9.7 of API 650, respectively. The 3-sec gust design wind speed of 90 mph (40 m/s) was taken as the design wind speed, V_d . All the tanks were required to have a top wind girder because they are open-top tanks. Only TK-192 and TK-224 required an intermediate wind girder. However, the intermediate wind girder was not provided because the primary focus of study was to investigate the effect of settlement and not wind. The wind girder detail ‘e’ was provided because of its applicability to varying geometries and for consistency. To incorporate the influence of the wind girder detail, the models TK-40 and TK-90 were modelled with the wind girder detail type ‘c’ as well and referred as TK-40c and TK-90c. Similarly, the model TK-108 was modelled with the wind girder detail ‘d’ as well and referred as TK-108d. In Figure 3-2 different wind girder details are shown. The required elastic section modulus S_x , the provided elastic section modulus S_p , the sizes of wind girders and the location of wind girder for each tank model are given in Appendix A Table A.2.

3.2.3 Criterion for the limiting settlement

The limiting settlement for a given harmonic wave number n is defined as the settlement value at which the tank failure takes place and the tank is not fit for use in the current state. The tank failure can be due to buckling, yielding of material, a certain stress or strain value. The Annex B of API 653 provisions have two procedures and corresponding two criteria for the maximum allowable settlement. The first criterion is based on limiting the strain level to 0.007, using Marr et al. [2] approach (named as method-1 in the present paper) and the second criterion is based on limiting the plastic strain level to 0.03 formulated by Andreani and Carr [20]. The probability of a tank

failure with the tank material going beyond yield is relatively high. It can result in unexpected failure given that the evaluation of tank settlement is a “point in time” analysis, which does not include the future settlement. In addition, there are other possible environmental loadings such as wind or earthquake that are not taken into consideration in maximum allowable settlement limits in Marr et al. [2] or Andreani and Carr [20]. Thus, the existing two API 653 design criteria may not be sufficiently safe as it allows material to go beyond yielding. For this reason the maximum membrane stress level is limited to the yield stress of the material in the proposed method. So that there is a reserved capacity beyond yielding point for future settlement and unaccounted additional environmental loadings.

The membrane stress is defined as the mid-surface stress of the tank cylinder, stiffening ring flange and web components. Similarly, membrane plus bending stress is the inside and outside surface stress on the tank cylinder and stiffening ring flange and web components. Thus, membrane stress is not the global membrane stress of the combined section of the stiffening ring and tank shell. For this reason, there will be some additional membrane plus bending stresses (surface stresses) in the outside and inside surfaces of the tank cylinder and stiffening ring. However, these surface stresses would be slightly higher than mid-surface membrane stresses because of the relatively small thickness of the shell and stiffening ring. The combined cross section of the wind girder and the contributing shell is under in-plane bending along the stiffener ring plane. The maximum thickness of the top shell course and wind girder is 0.313 inches. Therefore, the membrane plus bending stresses measured at the outer surfaces of the shell and wind girder are not significantly higher compared to the membrane stresses measured at the mid surface of the shell and wind girder. Moreover, the allowable stress value for membrane plus bending stress as indicated in ASME Section VIII-2 [26] is at least 1.5 times the allowable membrane stress. Hence, the membrane stress values are used for the limiting settlement evaluation.

The corresponding limiting settlement values for each harmonic wave numbers under consideration are found using the FEA. The critical settlement due to buckling failure for small n values ($n < 10$) were found to be relatively high in the literature [14, 15]. Thus, the buckling of the shell and wind girder for small harmonic wave numbers, $n = 2, 3$ and 4 , would not likely to take place before the yielding of the material.

The limiting settlement is dependent on the tank's geometry, the harmonic wave number and material properties as discussed in the literature [2, 11, 12, 17, 20]. Thus, the limiting settlement values were evaluated for different harmonic wave numbers and different tank geometries using FEA. The material specifications used in the current study are A36 and A516 Grade 70. The material A36 has a lower yield stress value of 36 ksi (250 MPa). Thus, the limiting membrane stress value was taken as 36 ksi (250 MPa) in the current study.

3.2.4 FEA procedure

FEA was performed using Abaqus CAE 2018 [26]. Twenty-one tank geometries were modeled. Each of the tank models was subjected to pure harmonic settlement profiles for n values of 2, 3 and 4, as $\cos(n\theta)$ along the bottom circumference of the shell to obtain limiting settlement value. The limiting settlement is similar to allowable settlement, the criteria for the limiting settlement is discussed in section 3.2.3.

The tank shell was modeled using material properties of ASTM A516 Grade 70 steel and the wind girder was modeled using material properties of A36 steel in the FEA. The nonlinear plastic behavior for both of the material specifications was obtained using the ASME Boiler and Pressure Vessel Code, Section VIII, Division 2 [27] procedure for the true stress-strain behavior. Figure 3-3 shows the true stress-strain diagrams for A516 and A36 material specifications. Both of the materials were modeled as isotropic materials with modulus of elasticity $E = 29,000$ ksi (200 GPa), Poisson's ratio $\nu = 0.3$, and density $\rho = 490$ lb/ft³ (7800 kg/m³). The yield and the ultimate tensile stress values of these materials are given in section 3.2.1.

The four node, doubly curved, quadrilateral shell element with reduced integration and hourglass control, S4R element was used. The FEA mesh of model TK-360 is shown in Figure 3-4. The length of a typical shell element, a , was calculated using the following equation

$$a = 0.5\sqrt{Rt} \quad (33)$$

where R is the tank radius and t is the thickness of the thinnest shell course. This mesh size was decided after performing a mesh convergence study. Thus, the global mesh size ranged between 3 in. (7.6 cm) to 8 in. (20.3 cm) depending on the tank geometry. A refined mesh is used near the

top location and at the girder to capture the stress distribution more accurately as shown in Figure 3-4. The mesh size was reduced to have minimum of three elements near the shell and wind girder junction, and on each surface of the wind girder.

The geometric nonlinear analysis considering nonlinear plastic material properties (GMNA) was conducted. The imperfection was not included in the analysis because the failure criterion is yielding rather than buckling and the yielding failure is not sensitive to imperfection. The analysis was conducted in two steps. In the first step, the gravity load was applied with pinned boundary conditions along the bottom circumference of the shell. The tanks subjected to the differential settlement are more vulnerable when they are empty as observed by Gong et al. [16]. Therefore, the hydrostatic liquid pressure was not considered to be acting on the tank walls. In the second step, the settlement profile was applied with the translation in both the radial and the circumferential directions constrained and displacement in the vertical direction was applied as a settlement profile at the bottom of the shell cylinder. The boundary conditions at the bottom of the shell cylinder were assumed to be pinned (translational degree of freedoms fixed and rotational degree of freedoms free). A study was conducted to investigate the influence of rotational boundary conditions on the limiting settlement value given in the Appendix C. The boundary condition at top of the shell cylinder was free because it is an open-top tank. The settlement profile was applied using the Riks method to capture the nonlinear geometric effects, which can affect the results significantly as shown by Godoy and Sosa [9].

3.2.5 FEA limiting settlement results

Twenty-one different tank models are studied using FEA. For each tank model, limiting settlement values were found for harmonic wave numbers $n=2, 3$ and 4 . The limiting values for all the different tank models were similarly obtained and are plotted for harmonic wave numbers $n=2, 3$ and 4 in Figure 3-5, Figure 3-6, and Figure 3-7, respectively. Appendix D discusses details on how the Figure 3-5, Figure 3-6, and Figure 3-7, were obtain form FEA. In all of these figures the horizontal axis represents the geometric ratio and vertical axis represents the limiting settlement amplitude. The horizontal axis is displayed on a logarithmic scale (base 10) for a better visualization. Each solid circle corresponds to the limiting settlement value of a tank model obtained from the FEA. The solid curve represents the best fit curve found from multiple curve

fitting models/regression analysis. The best fit curve for a given harmonic wave number, n is found to be a power function as shown in Eq. (5).

$$U_n^* = U_n \left(\frac{D^2}{H} \right)^{p_n} \quad (34)$$

Where U_n^* is the limiting settlement for the n^{th} harmonic wave number in in. (mm). The U_n and p_n are constants tabulated in Table 3-2. The constant U_n is unit dependent, therefore, both US customary and SI unit versions of the U_n listed in Table 3-2. In Eq. (5), D and H are also unit sensitive. Thus, D and H should be in feet for US customary units and in meters in SI units. The coefficient of determination (R^2) value of curves for $n=2, 3$ and 4 are found to be 0.98, 0.97 and 0.98, respectively. The R^2 , measures statistically the goodness of the curve fit. The value of R^2 closer to 1.0 implies that the approximation is closer to the actual data points.

It is observed that with the increase in geometric ratio the limiting settlement increases for all harmonic wave numbers. Furthermore, as the harmonic wave number increases, there is a decrease in the limiting settlement value. Thus, under the application of a pure harmonic settlement profile, the tank failure takes place at a lesser settlement magnitude for a higher n value. It is observed that the maximum allowable settlement is inversely proportional to the square of the harmonic wave number, n . Therefore, the differentiation between the limiting settlement values for different harmonic wave numbers is required, which is missing in Marr et al. [2] formulation and API 653 method-1.

The location of the maximum stress was found to be at the tip of the wind girder for all the cases. The FEA results for limiting settlement and von Mises membrane stresses for TK-90c are shown in Figure 3-8 and Figure 3-9, respectively for different harmonic wave numbers $n= 2, 3$ and 4 . . In Figure 3-8 and Figure 3-9 total displacement magnitude is plotted which includes radial and axial displacements. The vertical displacement at the bottom causes a radial displacement at the top of the tank. According to the study conducted by Kamyab and Palmer [6] the radial displacement at the top of the tank is proportional to the square of the vertical displacement at the tank bottom. Consequently, we observed that maximum displacement takes place at the top of the tank. This therefore, results in maximum stresses at the wind girder which is resisting the radial displacement.

Furthermore, as observed from the Figure 3-8 the number of locations for maximum displacement magnitude and stresses are proportional to the harmonic wave number, n .

3.3 Validation of the proposed method

In this section the methodology adopted for validation of the proposed method is discussed. First, the criteria for selecting different tank models and the actual settlement profiles used for validation are presented. Then the application of actual settlement data in the FEA using the Fourier transformation is discussed and the proposed method is given. Finally, the results of the FEA are compared with the results of the proposed method for validation.

3.3.1 Tank models for the validation of the proposed method

Three different sets of tank models were subjected to four different measured natural settlement profiles in order to validate the proposed method. The set-1 consist of four tank models with a constant tank height of 40 ft (12.2 m) and different tank diameters (TK-40, 90, 250, and 640) to examine the effect of the aspect ratio (H/D). The set-2 consist of three tank models with the same aspect ratio but different tank heights to investigate the effect of the tank height (TK-160,192 and 224). The set-3 consist of four tank models selected using random design parameters. The tank height, tank diameter, basic wind speed (V_b) and specific gravity of the liquid stored (G) were randomly selected using the random function in Microsoft Excel for set-3 models. These random values were rounded up or down to have realistic parameters. The details of design parameters and tank IDs for set-3 tank models are listed in Table 3-3. The tank design procedure adopted for all of the tanks in set-3 is the same as described in section 2.2.

3.3.2 Modeling measured actual settlement in FEA

The measured actual settlement data was used to validate the proposed method for evaluating the allowable settlement. There was a total of four different measured settlement profiles considered for the validation. The measured settlement data is reported in Table 3-4 and was taken from Gong et al. [21]. The data corresponds to tank structures having capacity of approximately 10,000 m³ (2.6 million gallons) to 125,000 m³ (33 million gallons). This settlement data was used in the present study to have realistic settlement profiles.

The settlement data for each profile was measured at 16 discrete measuring points which were equally spaced along the tank circumference. However, the actual settlement along the circumference is a continuous function of central circumferential angle, θ and cannot be applied on discrete points. In order to study the behavior of a tank under the natural settlement, the data is required to be a continuous function along the bottom circumference of the shell. Based on the prior research work [5, 17, 19, 21], the transformation of the discretely measured data can be done to a continuous settlement profile using the Fourier transformation as discussed in section 3.3.2.1.

The settlement profiles for validation were selected such that the R^2 value with the Fourier fit is at least 0.99 so that the profile applied in the FEA closely approximates the actual settlement profile. The FEA modelling was the same as discussed in section 3.2.2 with the exception of measured settlement profiles applied along the bottom circumference of the shell in the second step of FEA using the Fourier fit curve as settlement profile rather than a single $\cos(n\theta)$ profile.

3.3.2.1 The Fourier transformation of settlement data

The settlement data was collected at different locations which were equally spaced along the tank circumference. The locations are numbered from 1 to N , where N is the total number of measurement points. The API 653 [4] requires a minimum of eight points equally spaced and the maximum spacing between two points should be less than 32 ft (9.8 m) measured along the shell circumference. The settlement along the bottom shell circumference can be written as a function of the central circumferential angle θ , with respect to a coordinate system having the origin at the center of the tank bottom and first measurement point corresponding to $\theta=0^\circ$. The Fourier transformation of the data can be done as shown in the following equation

$$z(\theta) = z_{\text{avg}} + \sum_{n=1}^k [A_n \cos(n\theta) + B_n \sin(n\theta)] \quad (35)$$

where n is harmonic wave number, z_{avg} is the arithmetic average value of the measured settlement, k is the cut-off harmonic wave number considered for the transformation. A_n and B_n are the Fourier coefficients for the n^{th} harmonic wave number which can be calculated using the following equations

$$z_{\text{avg}} = \frac{1}{N} \sum_{i=1}^N z_i \quad (36)$$

$$A_n = \frac{2}{N} \sum_{i=1}^N z_i \cos\left(\frac{2\pi n(i-1)}{N}\right) \quad (37)$$

$$B_n = \frac{2}{N} \sum_{i=1}^N z_i \sin\left(\frac{2\pi n(i-1)}{N}\right) \quad (38)$$

where z_i is the settlement of the i^{th} data point. The series can be simplified and converted into a function of only cosine series as the following expression

$$z(\theta) = z_{\text{avg}} + \sum_{n=1}^k C_n \cos(n\theta - \phi_n) \quad (39)$$

where the coefficients C_n and the phase angles ϕ_n are calculated using the following equations

$$C_n = \sqrt{A_n^2 + B_n^2} \quad (40)$$

$$\phi_n = \tan^{-1}\left(\frac{B_n}{A_n}\right) \quad (41)$$

The Fourier transformation of a settlement profile using the Eq. (39) can be done for any value of k . Nonetheless, it has been suggested to limit the k value to n_{lim} based on a study was conducted by Gong et al. [21] to evaluate the number of harmonic components that should be considered to get meaningful results. The n_{lim} , depends on the number of measurement points N , and can be calculated using the following equation

$$n_{\text{lim}} = \text{floor}\left[\frac{N}{3}\right] \quad (42)$$

where the floor function gives the greatest integer less than or equal to the input value as output. In most of the tanks, the number of measurement points used is generally equal to or less than 16. Thus, the n_{lim} was found to be five. Therefore, the transformation should be done for the first five

components ($n= 0, 1, 2, 3, 4$), resulting in the cut-off value of k as four. Additionally, for global settlement profiles the Fourier coefficients of harmonic wave number greater than 4 are smaller than the least count of the measuring instruments. Moreover, the higher components ($n>4$) add noise to the data rather than enriching the data to obtain better information. The Fourier transformation results, the values of C_n and ϕ_n of the settlement profiles used in this study are tabulated in Table 3-5. The C_0 correspond to $n= 0$ and thus equal to z_{avg} . The values of ϕ_n are reported between 0 to 2π rather than $-\pi/2$ to $\pi/2$ for better visualization. Also, the coefficient of determination (R^2) and the maximum absolute error between the measured settlement data and the curve fit are tabulated in Table 3-5. The storage tanks are subjected to relatively large uniform hydrostatic pressure on the tank bottom due to stored liquid, which results in uniform settlement of the tank foundation. The maximum settlement value for profiles 2, 3 and 4 is about 1 m, which is typical for tanks built on soft unconsolidated soil without having a concrete ring-wall or pile foundation. For these type of tanks majority of the settlement is due to uniform settlement as observed in the Table 3-5.

The measured settlement profiles considered for validation of the proposed method have R^2 value of 0.99 or greater so that almost exact settlement profile was applied in FEA. Additionally, the method-1 can be used if there is a well defined rigid plane. Well defined rigid plane means that a single cosine curve together with uniform settlement (harmonic components of $n=0$ and 1) accurately fits the measured settlement data. The goodness of the fit is measured using the R^2 value, which should be greater than or equal to 0.90 for the plane to be considered as well defined [4]. Method-1 is used for global settlement profiles. Consequently, the R^2 value for the approximated settlement profile with higher harmonic should also be at least 0.90 for a profile to be considered as a global settlement profile. The measured settlement data points and the Fourier curve fit profile used in the FEA are plotted in Figure 3-10 for all the four profiles.

3.3.3 Proposed method for the evaluation of allowable differential settlement

The following procedure is proposed to evaluate the allowable differential settlement.

Step 1: Transform the measured settlement data into Fourier series using the procedure given in section 3.3.2.1 and calculate the R^2 value. If the R^2 value of the approximated settlement profile with first five harmonic components is greater than 0.90, it is a global settlement profile. Therefore,

the procedure in step 2 to step 5 should be used. If R^2 is smaller than 0.90, it is a localized settlement and the Andreani and Carr [20] procedure suggested in Annex B.3.2.2 of API 653 should be followed.

Step 2: Obtain the limiting allowable settlement (U_n) for harmonic wave numbers $n=2, 3$, and 4. The allowable settlement is directly proportional to yield strength and inversely proportional to the modulus of elasticity as mentioned in API 653 [4]. Therefore, the values obtained from curve fitting given in Table 2 are normalized with Y/E of A36 material specification to obtain the Eqs. (43)-(45) for US customary units

$$U_2 = 47.53 \frac{Y}{E} \left(\frac{D^2}{H} \right)^{0.984} \quad (43)$$

$$U_3 = 11.28 \frac{Y}{E} \left(\frac{D^2}{H} \right)^{0.912} \quad (44)$$

$$U_4 = 6.444 \frac{Y}{E} \left(\frac{D^2}{H} \right)^{0.815} \quad (45)$$

where U_n is limiting settlement for n^{th} harmonic wave number in in. (mm), Y is yield strength of the material in ksi (MPa), E is the modulus of elasticity of the material in ksi (MPa) and D^2/H in ft (m). For using SI units the constant coefficients for U_2 , U_3 , and U_4 in the Eqs. (43)-(45) should be replaced to 375, 96.7 and 62.0 from 47.53, 11.28, and 6.444, respectively. In case more than one material is used for construction of the tank shell or the wind girder than the material with the minimum ratio of yield stress to modulus of elasticity (Y/E) should be used to calculate the U_n . The Eq. (43)-(45) are used to calculate the limiting allowable settlement for harmonic wave numbers $n=2, 3$, and 4.

Step 3: Calculate the maximum absolute error, E_{max} between the measured settlement data and the curve fitted with first five harmonic wave components ($n=0, 1, 2, 3, 4$). Evaluate the allowable differential settlement S using the Eq. (32) proposed by Marr [2].

Step 4: Compute the cumulative damage factor, CDF by adding the normalized amplitude of each harmonic wave number obtained from step 1 and the ratio of E_{max} to S obtained from step 3. The

normalization of amplitude is done by dividing the amplitude (C_n) with its respective limiting allowable settlement value (U_n) obtained from step 2 as shown in Eq. (46)

$$CDF = \frac{C_2}{U_2} + \frac{C_3}{U_3} + \frac{C_4}{U_4} + \frac{E_{\max}}{S} \quad (46)$$

Step 5: The CDF represents the combined contribution of the first five harmonic wave numbers towards yielding of the tank material with an additional error term. The harmonic wave numbers $n=0$ and 1 do not cause stresses in the tanks, and therefore their contributions toward yielding is taken as zero. If the value of CDF obtained in step 4 is less than 1.0 it implies that the tank is fit for usage otherwise the tanks is not fit and either a more refined analysis should be performed or the tank should be releveled.

3.3.4 FEA results for validation

In accordance with the proposed method the tank is not good for service when the maximum stress reaches the yield stress. Therefore, in the FEA the settlement profile under consideration was scaled until the maximum membrane stress in the tank reaches the yield stress, 36 ksi (250 MPa). The settlement scaling factor, λ is a scaler constant relating the transformed settlement profile obtained from the measured settlement data, $z(\theta)$ and the failure settlement profile $z_f(\theta)$ corresponding to tank yielding in FEA, as shown in the following equation

$$z_f(\theta) = \lambda z(\theta) \quad (47)$$

Next, in order to validate the method, the CDF value was calculated corresponding to the failure settlement level of $z_f(\theta)$ using the procedure given in section 3.3.3.

The allowable value of the CDF as defined in Eq. (46) is 1. Therefore, the CDF corresponding to the failure settlement profile, $z_f(\theta)$ should be greater or equal to 1.0 for the proposed procedure to be conservative and valid to use. Theoretically, if the proposed method is perfect it should estimate the failure level CDF exactly as 1.0 irrespective of the tank geometry and settlement profile. The CDF values for each of the profile for three different sets of tank models are plotted in Figure 3-11, Figure 3-12, and Figure 3-13, respectively. For all the figures CDF value for the $z_f(\theta)$ profile is plotted on the vertical axis and the dotted line represent the CDF value of 1.0.

The set-1 has tank models with different aspect ratios ranging from 0.25 to 1. The horizontal axis in the Figure 3-11 shows the aspect ratio. From Figure 11 we observe that for all the models in set-1 CDF is greater than 1. The minimum CDF value is found to be 1.18 for Model TK-90 corresponding to settlement profile-2. The set-2 has tank models with different tank heights. The horizontal axis in the Figure 3-12 shows the tank height. From Figure 12 we observed that the CDF value initially increases with increase in height but then decreases with increase in height. We observe that for all the models in set-2, the CDF is greater than 1 and the minimum value of CDF is found to be 1.07 for Model TK-224 corresponding to settlement profile-2. The set-3 has tank models with randomly selected design parameters. The horizontal axis in the Figure 3-13 shows the tank model ID. The minimum value of CDF is found to be 1.01 for Model TK-302 corresponding to settlement profile-2.

As observed, irrespective of the tank aspect ratio, tank height or design parameters such as wind speed, specific gravity the CDF is always found to greater than 1 at the failure settlement profile. Hence, the proposed method is relatively conservative and valid for all cases studied. It must be noted that the level of conservatism varies depending on the settlement profile and tank models. Primary reason for variation of conservatism with different profile is that the proposed method assumes the worse possible scenario in which all the harmonic components are such that the maximum amplitude occurs simultaneously at one location. The harmonic component can be both additive and subtractive in nature depending upon the phase difference. The method ignores the phase difference to avoid analysis of multiple possible combinations. Our primary objective is to have a method which is able to capture the behavior of shell better than the existing method-1, but at the same time is also simple and easy to use by practicing engineers without the need to rigorous analysis such as finite element analysis

3.4 Comparison between the existing API method and the proposed method

In this section, results are presented for the settlement scaling factor based on method-1 ($\lambda_{f,API}$) and proposed method ($\lambda_{f,P}$). All three different sets of tank models as discussed in section 3.3.1 subjected to four different measured settlement profiles are compared. The settlement scaling factor obtained from FEA (λ) is used as a benchmark and to normalize $\lambda_{f,API}$ and $\lambda_{f,P}$ for comparison.

3.4.1 API 653 method-1 settlement amplitude

The method-1 can be used if there is a well defined rigid plane. For the settlement profiles-2 and 3 and 4, this criterion was satisfied thus, method-1 was used for evaluation. However, for the settlement profile-1 this criterion was not satisfied, as the R^2 value with single cosine fit and uniform settlement is only 0.70 which is less than required R^2 value of 0.90 as discussed earlier. Therefore, the API 653 method-1 could not be used for profile-1.

For method-1 maximum allowable differential settlement is independent of the settlement profile. The allowable settlement depends on the height, diameter, arc length between two data points, and material properties. The arc length for each model is calculated such that it satisfies these two criteria: (1) there should be at least eight settlement measurement points, and (2) the maximum arc length should not be larger than 32 ft (10 m). Thus, the maximum allowable settlement obtained for profiles-2, 3 and 4 are the same for a given tank geometry. Nonetheless, the settlement scaling factor for each profile is different. For profiles-2, 3 and 4 maximum differential settlement for the initial $z(\theta)$ profile is 0.232 in. (0.59 cm), 0.361 in. (0.92 cm), and 0.386 in. (0.98 cm) respectively. The ratio of allowable differential settlement to respective maximum differential settlement for $z(\theta)$ profile, gives the settlement scaling factor based on method-1, $\lambda_{f,API}$. The values of $\lambda_{f,API}$ are reported in Table 3-6 for different models.

The allowable settlement increases with a decrease in the aspect ratio. However, after a certain tank diameter, the allowable differential settlement value for given tank height is capped because of the maximum allowable arc length of 32 ft (9.75 m). Therefore, the values for allowable settlement for TK-250 (aspect ratio 0.4) and TK-640 (aspect ratio 0.25) were found to be same. The allowable settlement as observed for set-2 models decreases with increase in tank height for a given aspect ratio.

3.4.2 Proposed method settlement amplitude

Based on the proposed method, the tank is not fit for use if for a settlement profile of which the CDF is greater than 1.0. Therefore, the settlement scaling factor based on the proposed method, $\lambda_{f,P}$ should be such that the resulting settlement profile has the value of CDF equal to 1.0. The $\lambda_{f,P}$ can be therefore calculated using the following equation

$$\lambda_{f,P} = \frac{1}{CDF_{\text{initial}}} \quad (48)$$

where CDF_{initial} is the CDF corresponding to the initial $z(\theta)$ profile. The values of $\lambda_{f,P}$ for all different tank models and profiles are reported in Table 3-7. We observe that the settlement scaling factor increase with decrease in aspect ratio similar to method-1. However, for a given aspect ratio as in set-2 tank models, the settlement scaling factor increases with increase in tank height unlike the observation made in method-1. Moreover, the proposed method can be used for profile-1 unlike method-1 which do not permit to evaluate a tank with the settlement profile-1.

3.4.3 Comparison of the API 653 method-1 and the proposed method

The settlement scaling factor obtained from method-1 $\lambda_{f,API}$ and proposed method $\lambda_{f,P}$ are normalized with respect to vertical axis the settlement scaling factor λ obtained from FEA analysis presented in section 3.3.4. The normalized settlement scaling factor for method-1 and proposed method are plotted in Figure 3-14, Figure 3-15, and Figure 3-16. The vertical axis in all the figures represent normalized settlement scaling factor. The dotted solid line represents the normalized settlement scaling factor value of 1.0. The tank would be safe at the recommended allowable settlement scaling factor if the normalized settlement scaling factor is less than 1.0 otherwise the tank would fail before reaching the recommended allowable settlement scaling factor. Since the criteria used for formulation of the method-1 and the proposed method are different we cannot have a direct comparison. Nonetheless, we still investigate how does the allowable settlement based on method-1 would vary for different tank models and settlement profile when compared against the allowable stress value of yield stress.

In the Figure 3-14 the normalized settlement scaling factor is shown for the set-1 tanks with different aspect ratios for profile-2 and profile-3. We observe that for profile-2, the method-1 prediction of tank is fit-to-service is similar to FEA only for a smaller aspect ratio of 0.25 and not correct for higher aspect ratios. For model TK-90 (aspect ratio= 0.67), the method-1 overestimates the allowable settlement by 60% compared to the FEA. The method-1 is based on higher allowable strain level, therefore, we would expect the allowable settlement value to be higher compared to the FEA results which is based on a lower allowable strain level. But, in case of profile-3 we

observe that the method-1 is overly conservative as the settlement scaling factor is as small as 18% for TK-640 (aspect ratio =0.25) of the FEA results. For profile-3 we observe that the proposed method is also conservative, but it always results in higher allowable settlement and is closer to capacity calculated using FEA compared to the method-1

In Figure 3-15 the normalized settlement scaling factor is shown for the set-2 tanks with different tank height and the same aspect ratios for profile-2, and profile-3. For profile-2 the method-1 is found to be estimate higher allowable settlement for all the models in set-2 with an average settlement scaling factor overestimation of 30% compared to FEA. The proposed method on the other hand is found to be conservative with an average estimation of 80% of the settlement scaling factor obtained from FEA. For profile-3 the method-1 underestimates the settlement scaling factor. The allowable settlement proposed by method-1 is only one-third of the capacity found from FEA for model TK-192 ($H=48$ ft).

In Figure 3-16 the normalized settlement scaling factor is shown for the set-3 tank models for profile-2 and profile-4. For profile-2 the method-1 overestimates the settlement scaling factor by 33%, 92% and 16% for model TK-302, TK-106 and TK-197 respectively. The proposed method for profile-2 is found to match almost the actual capacity estimated by the FEA for tank models in set-3. For profile-4 we observe the method-1 to be comparable for only two tank models (TK-302 and TK-106) whereas the proposed method is found to be conservative for all the models.

Based on the findings, the API 653 method-1 allowable settlement is inconsistent with the FEA results. The method overestimates the settlement capacity by a factor of two for some cases (TK-106, profile-2) and also underestimates the settlement capacity by a factor of five for some cases (TK-640, profile-3). The proposed method is found to be consistently acceptable and closer to the FEA results compared to method-1.

3.5 Conclusion

The authors' presents an approach for evaluation of allowable differential settlement for open-top, vertical, above ground storage tanks by using higher order harmonics of the settlement profile. The understanding of tanks behavior under differential settlement has improved because of extensive investigations conducted in the last two decades. Nonetheless, the current foundation settlement

provision in API 653 (method-1) is still based on prior research work. The authors propose a new method for evaluating the allowable differential settlement as an attempt to bridge the gap between the latest research and industrial practice. The approach proposed by the authors was validated using actual measured settlement data. A comparison between the existing provisions of API 653 was also conducted and limitations of the method-1 are highlighted. The limiting settlement values for different aspect ratios were found for different harmonic wave numbers. Based on the FEA the following conclusions can be drawn from the study:

1. The limiting settlement for different harmonic component vary significantly for a given aspect ratio and geometry. Thus, each harmonic component should be analyzed individually for evaluating the fitness of the tank. However, this is not performed in the existing API 653 method-1 and it leads to unconservative results for some settlement profiles and overly conservative results for other settlement profiles. Therefore, the current API 653 method-1 may not able to capture the true behavior.
2. The existing API 653 method-1 cannot be used for global settlement profiles if a well-defined tilt plane is not observed. This limits the number of settlement profiles which can be analyzed using this method such as profile-1. Furthermore, if a well-defined tilt plane is observed the allowable settlement is independent of the settlement profile.
3. A proposed method for evaluating the allowable differential settlement is proposed for the global settlement profile which individually accounts for the effect of higher harmonic wave numbers $n= 2, 3$ and 4. This proposed method is applicable for a wider range of global settlement profiles compared to the existing API 653 method-1. The proposed method is validated using FEA for tanks with different tank geometries, randomly selected design parameters and subjected different settlement profiles.
4. The existing API 653 method-1 is based on beam theory and cannot capture the true shell behavior. The proposed method is based on FEA which is formulated using thin shell theory. The shell theory is better able to capture the true shell behavior. Thus, the proposed method is more accurate compared to the existing method.

5. The limiting harmonic settlement was found to increase with an increase in geometric ratio (D^2/H). For a given geometric ratio the higher harmonic wave number has a lesser limiting settlement, and thus are more prone to failure. For smaller harmonic wave numbers $n=2, 3$ and 4 the material yielding was found to take place before the buckling of the shell and the wind girder under pure harmonic settlement profile. Thus, the failure is governed by yielding of the material.
6. The proposed method is currently applicable to only open-top tanks, a similar study should be conducted for fixed roof tanks.

3.6 Appendix A: Shell thickness and wind girder details

The design shell thicknesses for each shell course and the wind girder details used in all of the tank models are presented in Table A.1 and Table A.2, respectively.

Table A.1: Tank ID and design shell thicknesses for different tank geometries

Tank-ID	Course number (bottom to top) with 8 ft (2.4 m) course height						
	Course 1 [in.]	Course 2 [in.]	Course 3 [in.]	Course 4 [in.]	Course 5 [in.]	Course 6 [in.]	Course 7 [in.]
TK-40	0.250	0.188	0.188	0.188	0.188	-	-
TK-48	0.250	0.188	0.188	0.188	0.188	0.188	-
TK-56	0.285	0.250	0.250	0.250	0.250	0.250	0.250
TK-62.5	0.250	0.250	0.250	0.250	0.250	-	-
TK-75	0.261	0.250	0.250	0.250	0.250	0.250	-
TK-87.5	0.356	0.303	0.252	0.250	0.250	0.250	0.250
TK-90	0.250	0.250	0.250	0.250	0.250	-	-
TK-108	0.313	0.259	0.250	0.250	0.250	0.250	-
TK-126	0.427	0.362	0.301	0.250	0.250	0.250	0.250
TK-160	0.289	0.250	0.250	0.250	0.250	-	-
TK-192	0.417	0.342	0.273	0.250	0.250	0.250	-
TK-224	0.570	0.478	0.397	0.316	0.250	0.250	0.250
TK-250	0.361	0.284	0.250	0.250	0.250	-	-
TK-300	0.522	0.424	0.338	0.313	0.313	0.313	-
TK-350	0.712	0.592	0.491	0.391	0.313	0.313	0.313
TK-360	0.433	0.338	0.313	0.313	0.313	-	-
TK-432	0.626	0.504	0.401	0.313	0.313	0.313	-
TK-640	0.577	0.443	0.328	0.313	0.313	-	-
TK-302	0.441	0.344	0.256	0.250	0.250	-	-
TK-106	0.250	0.250	0.250	0.250	0.250	-	-
TK-197	0.890	0.741	0.615	0.489	0.364	0.250	0.250
TK-408	0.811	0.650	0.516	0.383	0.313	0.313	-

^aTo convert to millimeters (mm) multiply the value in inches (in.) by 25.4

Table A.2: Top wind girder design details in accordance with API 650

	S_x , [in ³]	S_p , [in ³]	leg “b” width or angle size [in.]	Location from top [in.]
TK-40	3.6	3.7	3	5
TK-40c	3.6	4.1	L4 x 3 x 5/16	5
TK-48	6.2	6.6	5	6
TK-56	9.9	12.4	6	7
TK-62.5	7.4	7.5	4	6
TK-75	9.7	9.9	5	7
TK-87.5	15.4	17.7	8	7
TK-90	8.1	10.6	5	6
TK-90c	8.1	10.6	L6 x 4 x 3/8	6
TK-108	14.0	15.1	7	7
TK-108d	14.0	16.2	L5 x 3 x 5/16	7
TK-126	22.2	23.2	10	7
TK-160	14.4	15.1	7	6
TK-192	24.9	26.1	11	7
TK-224	39.5	41.7	16	7
TK-250	22.5	23.3	10	6
TK-300	38.9	45.1	16	7
TK-350	61.7	68.8	22	8
TK-360	34.4	34.7	13	7
TK-432	56.0	56.9	19	7
TK-640	57.6	60.5	20	7
TK-302	27.2	29.0	12	6
TK-106	16.9	17.7	8	6
TK-197	38.7	38.4	15	7
TK-408	65.3	69.2	22	7

^a To convert section modulus value to cubic millimeter (mm³) multiply the value in cubic inches (in³) by 16,400

^b To convert the leg width and angle size value to millimeters (mm) multiply the value in inches (in) by 25.4

3.7 Appendix B: Example problem to use the proposed method

Example problem: A storage tank with height, $H= 40$ ft (12.2 m) and diameter, $D= 160$ ft (48.8 m) with shell settlement survey as given in profile-4 given in Table 3. The material specification of the tank is A36, with an assumed modulus of elasticity of 29,000 ksi (200 GPa) and yield strength of 36 ksi (248 MPa). Using the proposed method determine the fitness of the tanks.

Step 1: Determining the type of settlement. The settlement data is transformed into Fourier series using the procedure described in section 2.3.1. The R^2 value obtain for the settlement profile is 0.99 which is greater than 0.9. Therefore, the settlement profile is a global settlement profile and this proposed method can be used. The Fourier coefficients and maximum absolute error obtained are as followed:

- $n=0, C_1= 995.7$ mm (Uniform settlement)
- $n=1, C_2= 203.78$ mm
- $n=2, C_2= 3.46$ mm
- $n=3, C_2= 1.62$ mm
- $n=4, C_2= 2.69$ mm
- $E_{\max}= 6.27$ mm (maximum absolute error)

Step 2: Obtain the limiting settlement for each harmonic wave number, the geometric ratio (D^2/H) of the tank is 640 ft. The following limiting settlement values are obtained using the Eqs. (43)-(45) for the corresponding geometric ratio:

- $n=2, U_2= 34.05$ in (865 mm)
- $n=3, U_2= 5.08$ in (129 mm)
- $n=4, U_2= 1.55$ in (39 mm)

Step 3: Calculate the allowable settlement S using Eq. (3)

$N= \max(8, \pi D/32) = 16$, the number of measurement points required for calculation of L

$L= \pi D/N = 31.4$ ft

$$S = \frac{11L^2Y}{EH} = 11 \times (31.4)^2 \times \frac{36}{29000 \times 40} = 0.337 \text{ ft} = 4.043 \text{ in (102.6 mm)}$$

Step 4: Calculate the cumulative damage factor, CDF

$$CDF = \frac{C_2}{U_{2,limit}} + \frac{C_3}{U_{3,limit}} + \frac{C_4}{U_{4,limit}} + \frac{E_{max}}{S}$$

$$CDF = \frac{3.46}{865} + \frac{1.62}{129} + \frac{2.69}{39} + \frac{6.27}{102.6} = 0.146$$

Step 5: $CDF < 1$. Therefore, the tank is fit for use.

3.8 Appendix C: Study on effect of rotational boundary condition

The model TK-300 was subjected to two types of boundary conditions at the bottom of the shell cylinder: pinned and fixed. Based on the results we observed that the rotational constrains at the tank bottom lead to an increase in bending stresses near the bottom of the tank shell as shown in Figure Appendix C 1. However, there is no significant influence of the rotational constrain at the top of the tank shell. The displacement corresponding to yielding level at the top stiffener and shell were found to be the same for all the harmonic wave numbers. Based on this observation we concluded that the limiting settlement value does not depend on the rotation boundary condition at the tank bottom. The primary cause of the stresses at the top is the radial displacement, which takes place because of the vertical displacement at the bottom. The stresses at the top stiffener and shell remains unaffected with the rotational constrains. Therefore, the problem is independent of the rotational constrains.

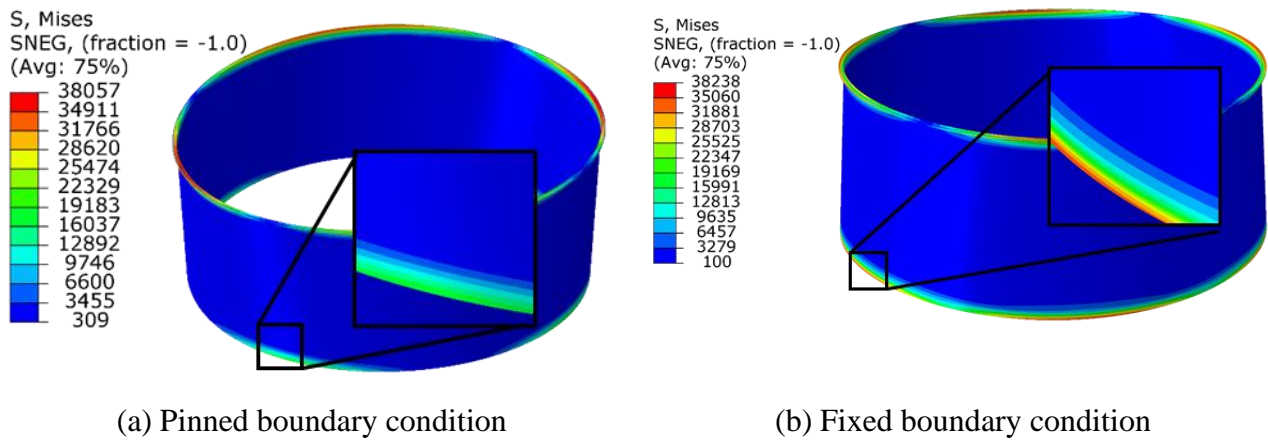
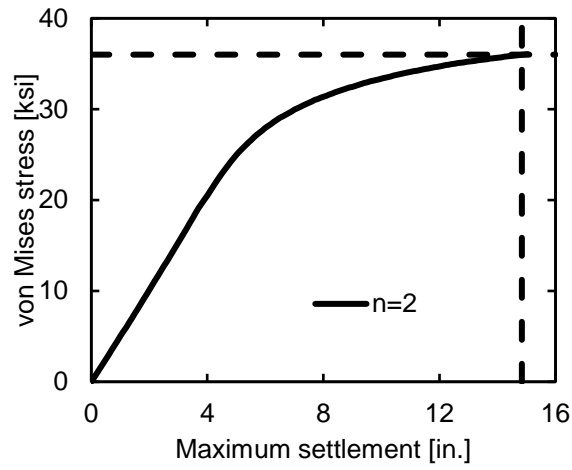


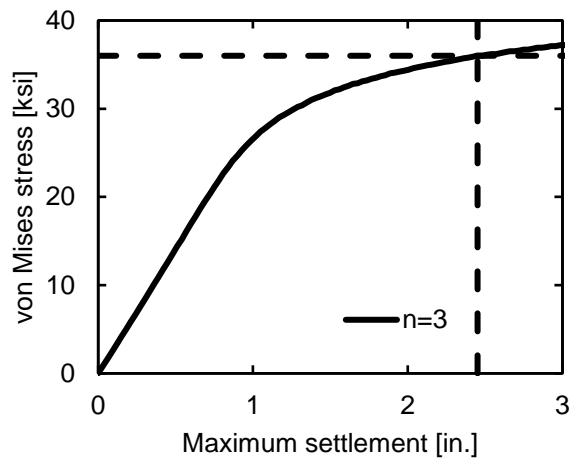
Figure Appendix C 1: von Mises membrane plus bending stresses for harmonic wave number $n=2$ of model TK-300 with (a) pinned boundary condition and (b) fixed boundary condition

3.9 Appendix D: Limiting settlement value from FEA

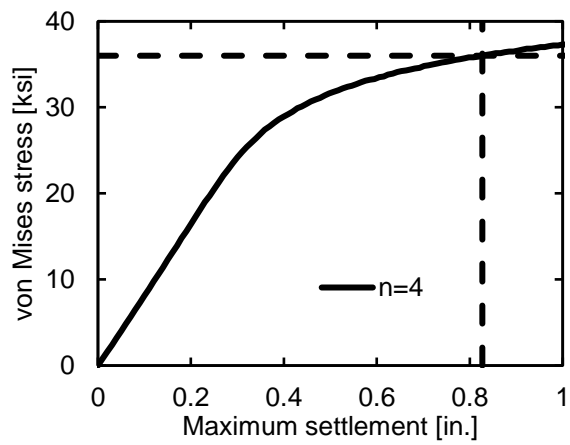
The limiting settlement value corresponds to the settlement at which the maximum membrane stress in the tank reaches the yield stress of 36 ksi (250 MPa). In the Figure Appendix D 1 the plots are shown for settlement vs von Mises membrane stress for different harmonic wave numbers for model TK-300. The settlement corresponding to membrane stress of 36 ksi is the limiting settlement value. For each tank model these values are evaluated to plot the Figure 3-5, Figure 3-6, and Figure 3-7.



(a) $n=2$



(b) $n=3$



(c) $n=4$

Figure Appendix D 1: Settlement vs von Mises membrane stress for different harmonic wave numbers (a) $n=2$, (b) $n=3$ and (c) $n=4$ of tank model TK-300

3.10 Tables

Table 3-1: Notation to identify tank geometry, aspect ratio and geometric ratio for each tank considered

Tank ID	H [ft]	D [ft]	H/D	D^2/H [ft]
TK-40	40	40	1.00	40
TK-40c	40	40	1.00	40
TK-48	48	48	1.00	48
TK-56	56	56	1.00	56
TK-62.5	40	50	0.80	63
TK-75	48	60	0.80	75
TK-87.5	56	70	0.80	88
TK-90c	40	60	0.67	90
TK-90	40	60	0.67	90
TK-108d	48	72	0.67	108
TK-108	48	72	0.67	108
TK-126	56	84	0.67	126
TK-160	40	80	0.50	160
TK-192	48	96	0.50	192
TK-224	56	112	0.50	224
TK-250	40	100	0.40	250
TK-300	48	120	0.40	300
TK-350	56	140	0.40	350
TK-360	40	120	0.33	360
TK-432	48	144	0.33	432
TK-640	40	160	0.25	640

^a To convert to meters (m) multiply the value in feet (ft) by 0.3048

Table 3-2: Constant U_n and p_n of power functions corresponding to limiting settlement for different harmonic wave numbers

n	U_n [US customary units]	U_n [SI units]	p_n
2	0.059	0.466	0.984
3	0.014	0.120	0.912
4	0.008	0.077	0.815

Table 3-3: Tank-ID and randomly selected design parameters for tank models used in validation of proposed method

Tank ID	H [ft]	D [ft]	G	V_b [mph]	V_d [mph]
TK-302	40	110	1.0	142	110
TK-106	40	65	0.8	157	120
TK-197	56	105	1.5	127	95
TK-408	48	140	1.2	135	100

^a To convert to meters (m) multiply the value in feet (ft) by 0.3048

^b To convert to m/s multiply the value in mph by 0.447

Table 3-4: Measured natural settlement data in mm taken from Gong et al. [21]

Measurement point	Profile-1	Profile-2	Profile-3	Profile-4
1	0	897	914	1088
2	8	920	942	1020
3	38	944	969	936
4	52	979	1001	874.5
5	34	1001	1026	813
6	2	1007	1045	797
7	-25	1013	1054	800
8	-47	1008	1046	832
9	-60	991	1036	896
10	-77	964	999	980
11	-62	937	970	1051
12	-31	915	942.5	1125
13	3	887	915	1181
14	26	876	895	1202
15	18	874	896	1190
16	4	881	901	1146

Table 3-5: Fourier transformation coefficients, C_n , phase angles, ϕ_n , corresponding maximum error and R^2 values for measured settlement data

		$n=0$	$n=1$	$n=2$	$n=3$	$n=4$	R^2	Maximum Error [mm]
Profile-1	C_n [mm]	-7.31	44.49	26.83	11.22	2.58	0.998	2.82
	ϕ_n [radian]	-	0.40	3.33	2.94	5.11	-	-
Profile-2	C_n [mm]	943.3 8	70.91	0.42	1.21	2.24	0.999	3.00
	ϕ_n [radian]	-	2.28	3.70	4.26	5.18	-	-
Profile-3	C_n [mm]	971.9 7	79.94	2.21	0.35	1.21	0.998	4.96
	ϕ_n [radian]	-	2.36	5.47	2.56	4.92	-	-
Profile-4	C_n [mm]	995.7 2	203.7 8	3.46	1.62	2.69	0.999	6.27
	ϕ_n [radian]	-	5.21	2.66	2.42	1.52	-	-

Table 3-6: The settlement scaling factor based on method-1 for different tank models and settlement profiles

Tank ID	H [ft]	D [ft]	Allowable settlement [in]	$\lambda_{f,API}$ Profile-2	$\lambda_{f,API}$ Profile-3	$\lambda_{f,API}$ Profile-4
Set-1						
TK-40	40 ^a	40	0.505 ^b	2.179	1.401	1.309
TK-90	40	60	1.137	4.902	3.153	2.945
TK-250	40	100	2.022	8.716	5.605	5.236
TK-640	40	160	2.022	8.716	5.605	5.236
Set-2						
TK-160	40	80	2.022	8.716	5.605	5.236
TK-192	48	96	1.553	6.694	4.305	4.021
TK-224	56	112	1.497	6.454	4.151	3.877
Set-3						
TK-302	40	110	2.022	8.716	5.605	5.236
TK-106	40	65	1.335	5.754	3.700	3.457
TK-197	56	105	1.316	5.672	3.648	3.408
TK-408	48	140	1.685	7.263	4.671	4.364

^a To convert to meters (m) multiply the value in feet (ft) by 0.3048

^b To convert to millimeters (mm) multiply the value in inches (in.) by 25.4

Table 3-7: The settlement scaling factor based on proposed for different tank models and settlement profiles

Tank ID	H [ft]	D [ft]	$\lambda_{f,P}$ Profile-2	$\lambda_{f,P}$ Profile-3	$\lambda_{f,P}$ Profile-4
Set-1					
TK-40	40 ^a	40	1.270	1.783	0.895
TK-90	40	60	2.544	3.679	1.820
TK-250	40	100	5.713	7.856	4.035
TK-640	40	160	10.415	11.860	6.850
Set-2					
TK-160	40	80	4.157	6.132	3.005
TK-192	48	96	4.553	6.195	3.199
TK-224	56	112	5.020	6.587	3.481
Set-3					
TK-302	40	110	6.508	8.646	4.541
TK-106	40	65	2.917	4.242	2.093
TK-197	56	105	4.490	5.858	3.105
TK-408	48	140	7.572	9.060	5.076

^a To convert to meters (m) multiply the value in feet (ft) by 0.3048

3.11 Figures

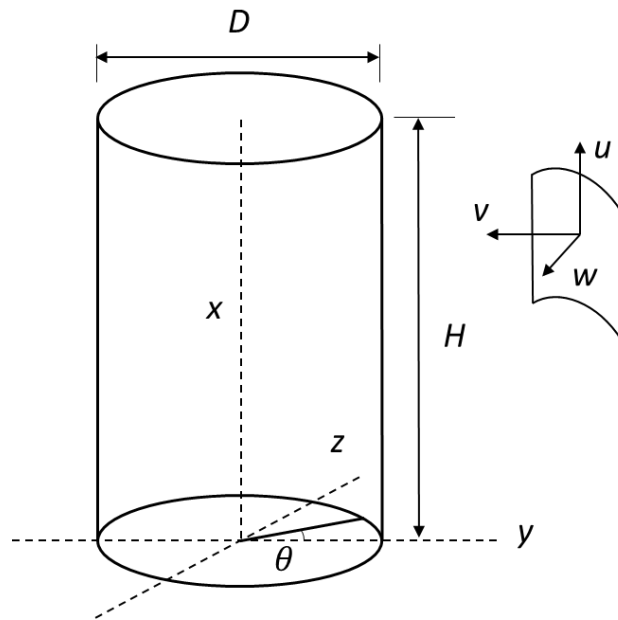


Figure 3-1: Coordinate system for the cylindrical shell model

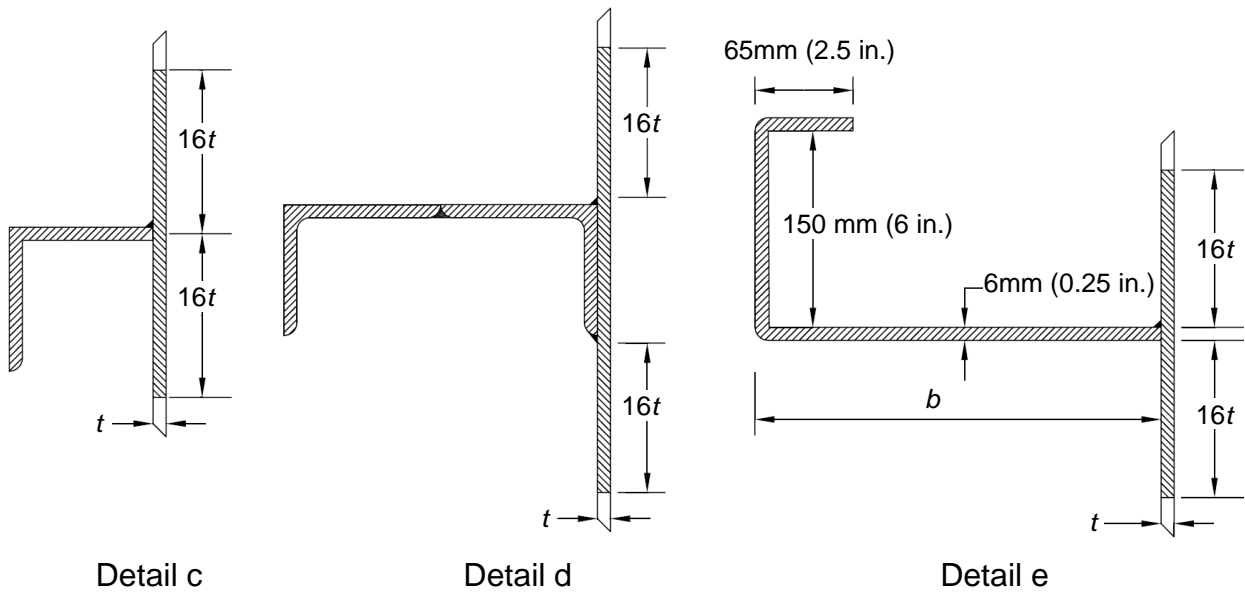


Figure 3-2: Wind girder details in accordance with API 650 [23]

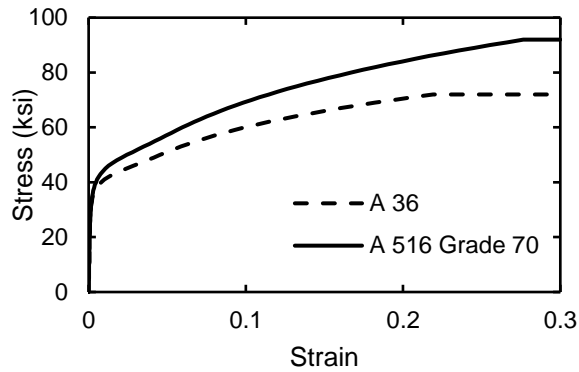


Figure 3-3: True stress-strain diagram for A36 and A516 Grade 70 material specifications; to convert stress values to MPa multiply stress in ksi by 6.9

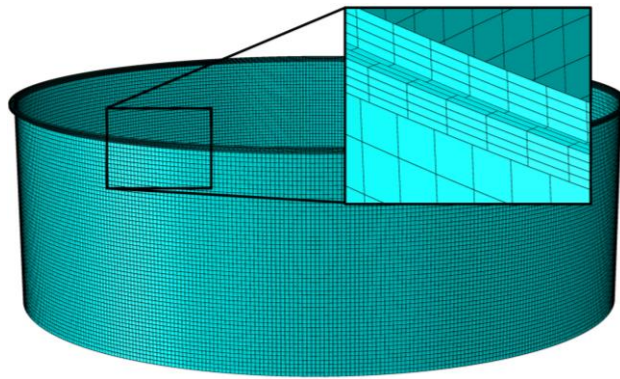


Figure 3-4: FEA mesh for TK-360 with a close-up view to the top wind girder

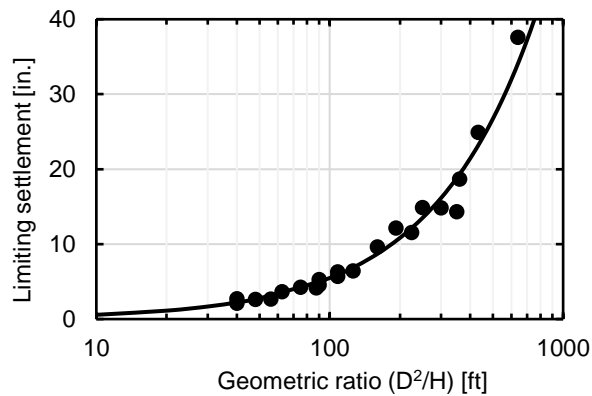


Figure 3-5: Limiting settlement for different geometric ratios for harmonic wave number $n=2$. The settlement values are shown in inches; to convert settlement values to mm, multiply values in inches with 25.4.

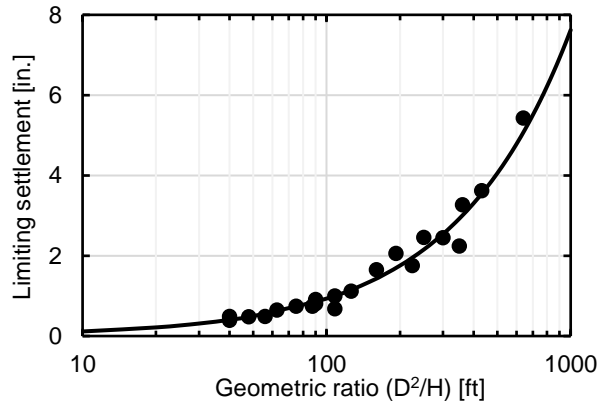


Figure 3-6: Limiting settlement for different geometric ratios for harmonic wave number $n=3$. The settlement values are shown in inches; to convert settlement values to mm, multiply values in inches with 25.4.

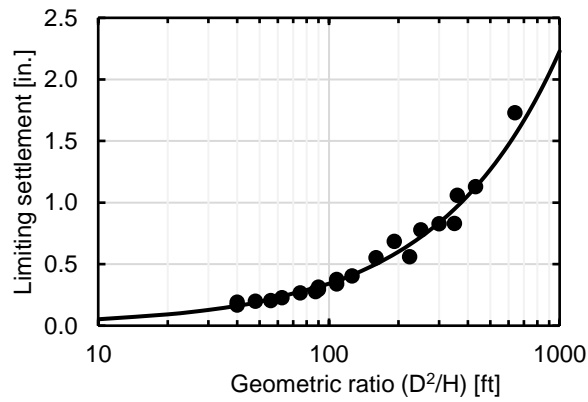
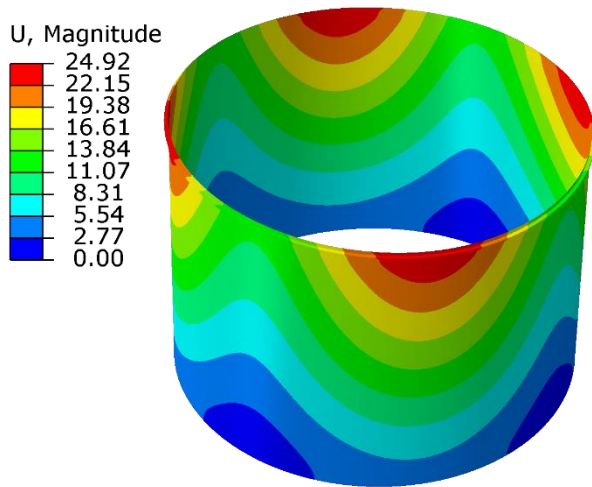
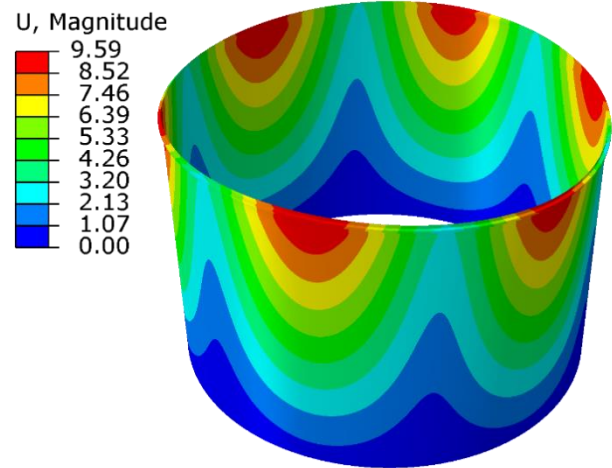


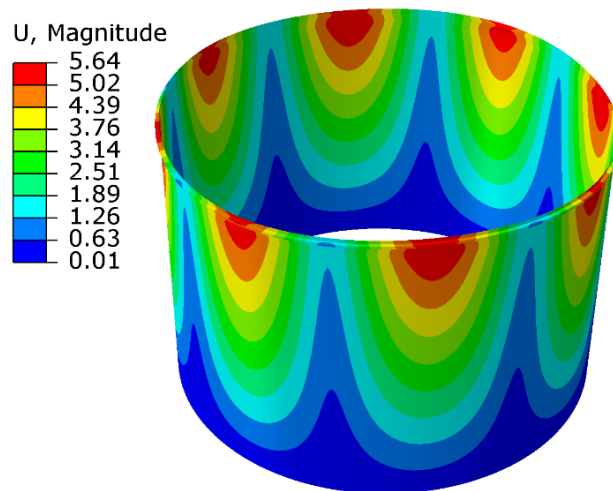
Figure 3-7: Limiting settlement for different geometric ratios for harmonic wave number $n=4$. The settlement values are shown in inches; to convert settlement values to mm, multiply values in inches with 25.4.



(a) $n=2$ at maximum settlement value of 4.52 in.

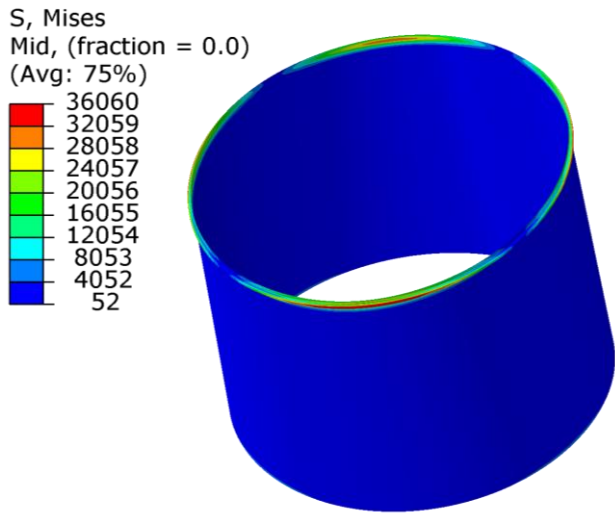


(b) $n=3$ at maximum settlement value of 0.808 in.

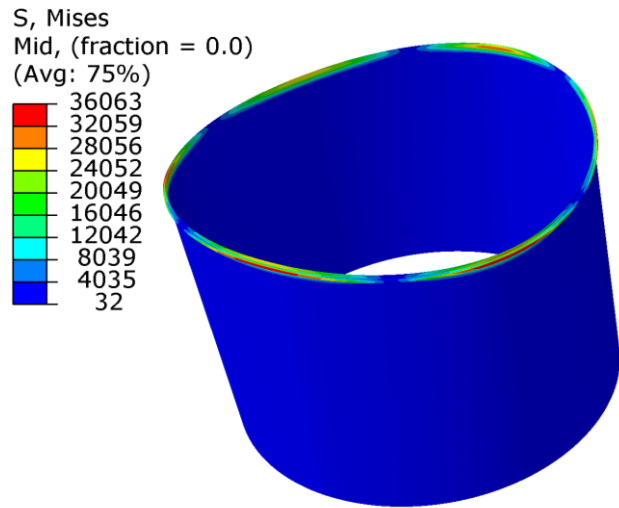


$n=4$ at maximum settlement value of 0.296 in.

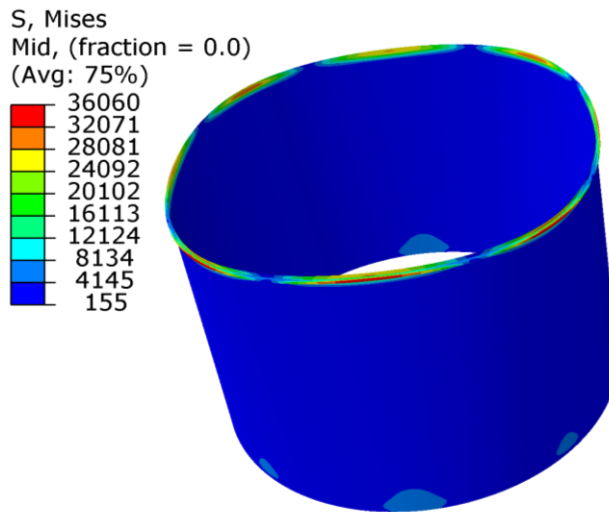
Figure 3-8: Deformed tank TK-90c under application of pure harmonic settlement profile for (a) $n=2$, (b) $n=3$ and (c) $n=4$. The total displacement magnitude values are shown in inches; to convert displacement values to mm, multiply values in inches with 25.4.



(a) $n=2$ at maximum settlement value of 4.52 in.

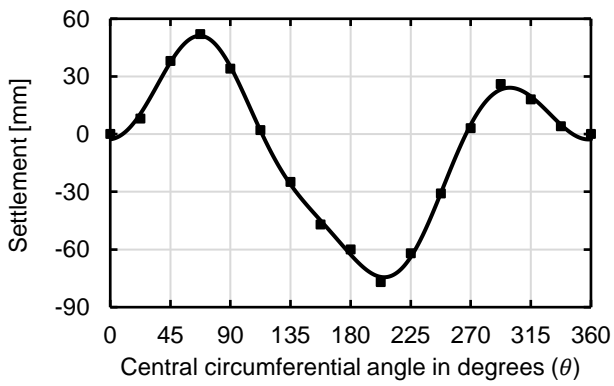


(b) $n=3$ at maximum settlement value of 0.808 in.

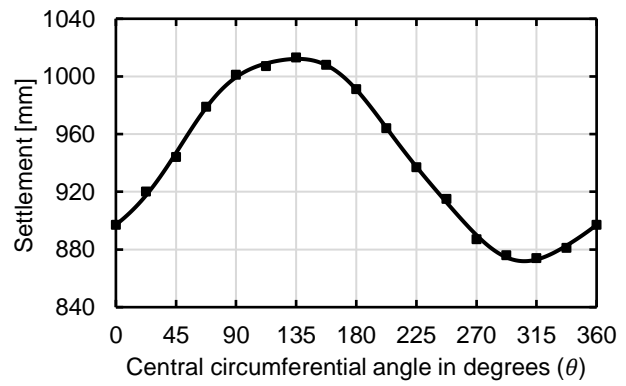


(c) $n=4$ at maximum settlement value of 0.296 in.

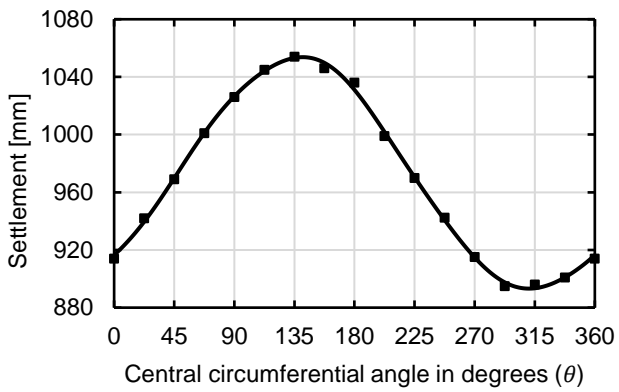
Figure 3-9: Von Mises membrane stresses with deformation for tank TK-90c under application of a pure harmonic settlement profile for (a) $n=2$, (b) $n=3$ and (c) $n=4$. The stress values are shown in psi; to convert the stress value to MPa, multiply the stress in psi by 6.9×10^{-3}



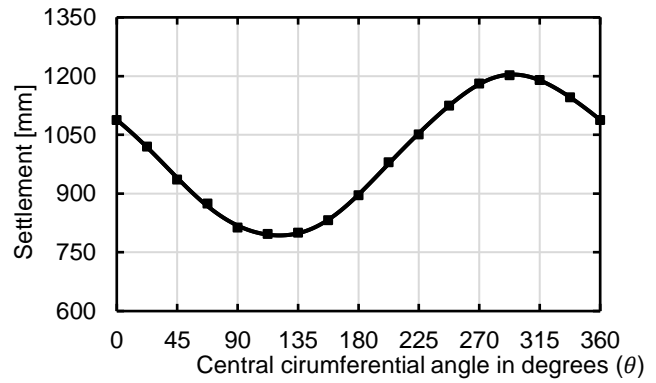
(a) Profile-1



(b) Profile-2



(c) Profile-3



(d) Profile-4

— Approximate profile ■ Actual data

Figure 3-10: The approximated settlement profile using Fourier transformation and actual measured data for (a) Profile-1, (b) Profile-2, (c) Profile-3, and (d) Profile-4

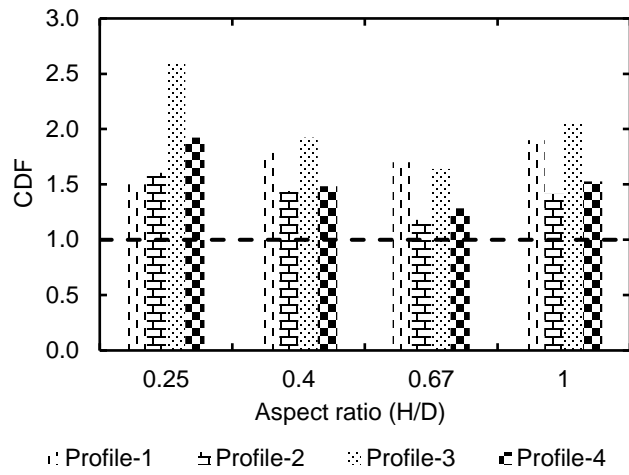


Figure 3-11: CDF value at failure settlement profile level of $z_f(\theta)$ for the set-1 tanks

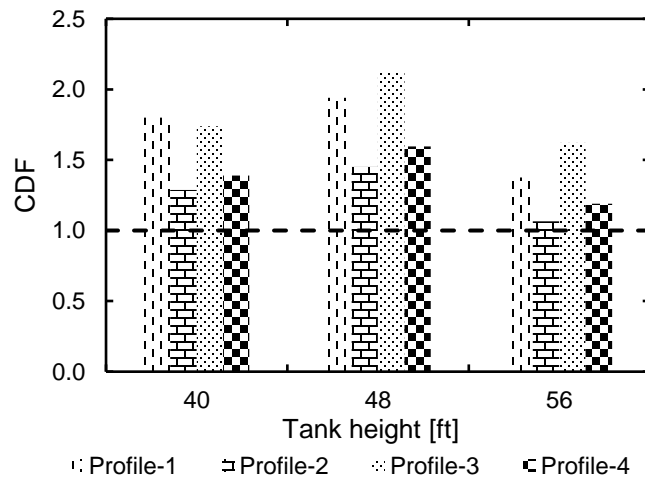


Figure 3-12: CDF value at failure settlement profile level of $z_f(\theta)$ for the set-2 tanks

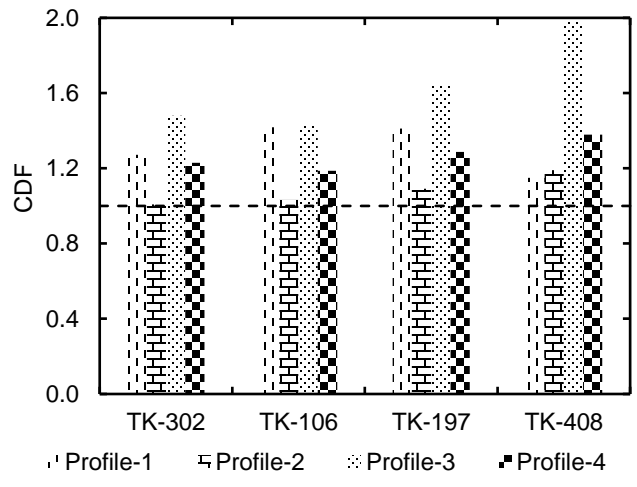
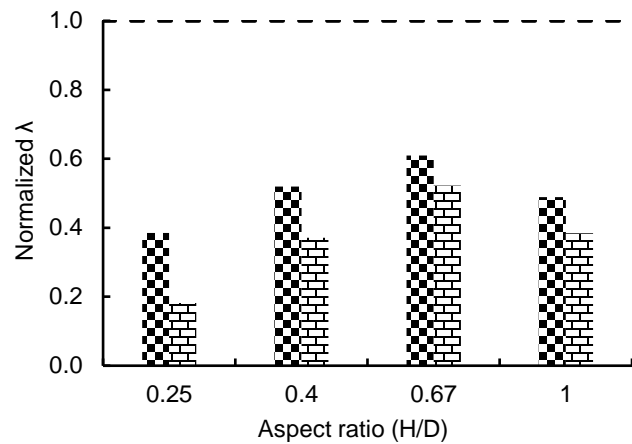
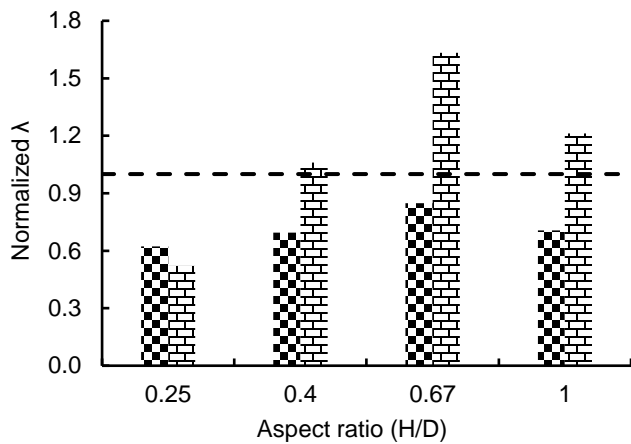


Figure 3-13: CDF value at failure settlement profile level of $z_f(\theta)$ for the set-3 tanks



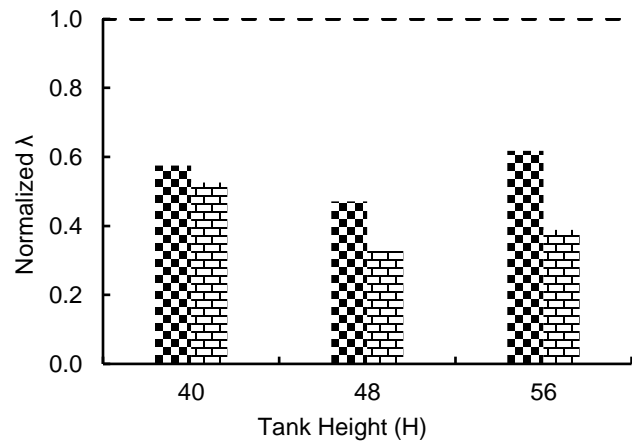
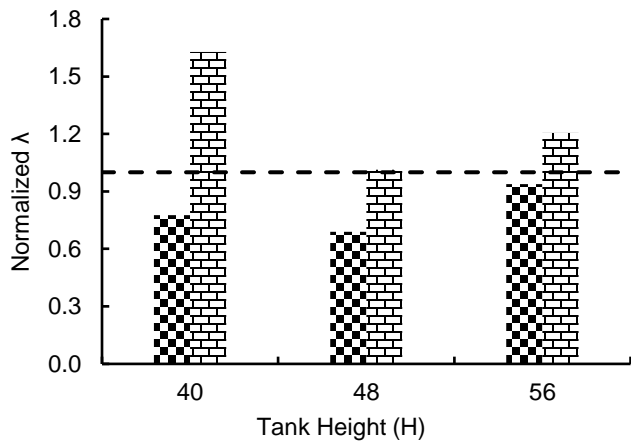
■ Normalized Proposed method ▨ Normalized API method

■ Normalized Proposed method ▨ Normalized API method

(a) Profile-2

(b) Profile-3

Figure 3-14: Normalized settlement scaling factor for (a) Profile-2 and (b) Profile-3 for the set-1 tanks with different aspect ratio. The normalization is done with respect to settlement scaling factor obtained from FEA



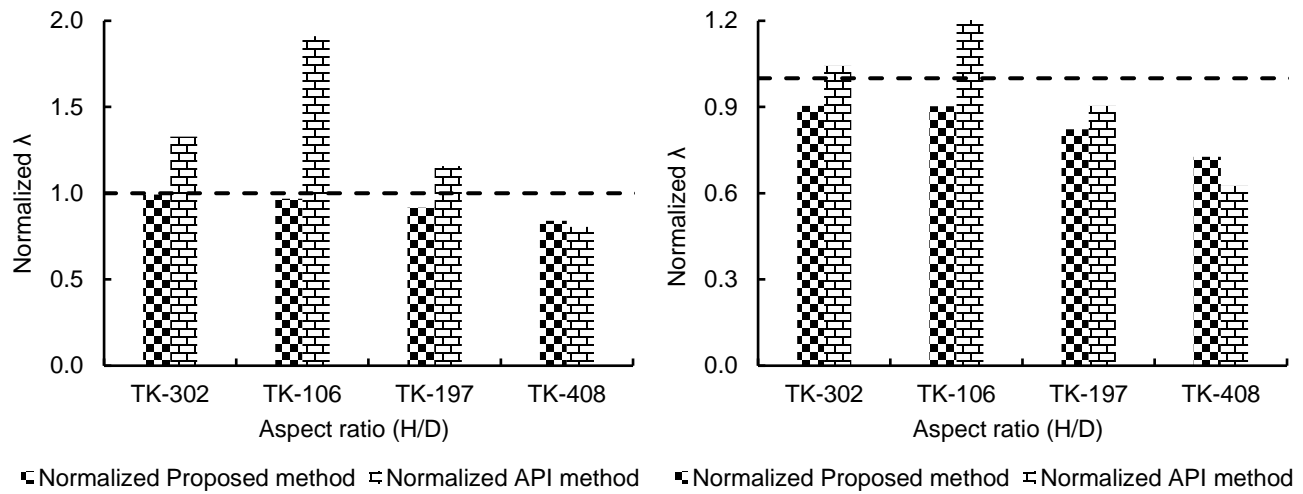
■ Normalized Proposed method ▨ Normalized API method

■ Normalized Proposed method ▨ Normalized API method

(a) Profile-2

(b) Profile-3

Figure 3-15: Normalized settlement scaling factor for (a) Profile-2 and (b) Profile-3 for the set-2 tanks with same aspect ratio. The normalization is done with respect to settlement scaling factor obtained from FEA



(a) Profile-2

(b) Profile-4

Figure 3-16: Normalized settlement scaling factor for (a) Profile-2 and (b) Profile-4 for the set-3 tanks with different aspect ratio. The normalization is done with respect to settlement scaling factor obtained from FEA

3.12 References

- [1] Z. Malik, J. Morton, and C. Ruiz, "Ovalization of cylindrical tanks as a result of foundation settlement," (in English), *The Journal of Strain Analysis for Engineering Design* *The Journal of Strain Analysis for Engineering Design*, vol. 12, no. 4, pp. 339-348, 1977.
- [2] W. A. Marr, J. A. Ramos, and T. W. Lambe, "Criteria for settlement of tanks," *Journal of the Geotechnical Engineering Division*, vol. 108, no. 8, pp. 1017-1039, 1982.
- [3] E. E. DeBeer, "Foundation problems of petroleum tanks," *Annales de L'Institut Belge du Petrole*, vol. 6, pp. 25-40, 1969.
- [4] American Petroleum Institute (API) Standard, "API 653: Tank inspection, repair, alteration and reconstruction," 5th ed, Addendum 1: American Petroleum Institute, Washington, DC, 2018.
- [5] H. Kamyab and S. C. Palmer, "Analysis of Displacements and Stresses in Oil Storage Tanks Caused by Differential Settlement," *Proceedings of the Institution of Mechanical Engineers, Part C: Mechanical Engineering Science*, vol. 203, no. 1, pp. 61-70, 1989.
- [6] S. C. Palmer, "Stresses in Storage Tanks Caused by Differential Settlement," *Proceedings of the Institution of Mechanical Engineers, Part E: Journal of Process Mechanical Engineering*, vol. 208, no. 1, pp. 5-16, 1994.
- [7] M. Jonaidi and P. Ansourian, "Harmonic settlement effects on uniform and tapered tank shells," *Thin-Walled Structures*, vol. 31, no. 1, pp. 237-255, 1998.
- [8] L. A. Godoy and E. M. Sosa, "Localized support settlements of thin-walled storage tanks," *Thin-Walled Structures*, vol. 41, no. 10, pp. 941-955, 2003.
- [9] L. A. Godoy and E. M. Sosa, "Deflections of thin-walled storage tanks with roof due to localized support settlement," Seoul, Korea, 2002: II International Conference on Advances in Structural Engineering and Mechanics.

- [10] J. Mark F. G. Holst and J. M. Rotter, "Axially compressed cylindrical shells with local settlement," *Thin-Walled Structures*, vol. 43, no. 5, pp. 811-825, 2005.
- [11] Y. Zhao, Q.-s. Cao, and X.-y. Xie, "Floating-roof steel tanks under harmonic settlement: FE parametric study and design criterion," *J. Zhejiang Univ. - Sci. A Journal of Zhejiang University-SCIENCE A : Applied Physics & Engineering*, vol. 7, no. 3, pp. 398-406, 2006.
- [12] Q.-s. Cao and Y. Zhao, "Buckling strength of cylindrical steel tanks under harmonic settlement," *Thin-Walled Structures*, vol. 48, no. 6, pp. 391-400, 2010.
- [13] J. Gong, W. Cui, S. Zeng, and T. Jin, "Buckling analysis of large scale oil tanks with a conical roof subjected to harmonic settlement," *Thin-Walled Structures*, vol. 52, pp. 143-148, 2012.
- [14] J. Gong, J. Tao, J. Zhao, S. Zeng, and T. Jin, "Buckling analysis of open top tanks subjected to harmonic settlement," *Thin-walled structures.*, vol. 63, pp. 37-43, 2013.
- [15] J. Gong, J. Tao, J. Zhao, S. Zeng, and T. Jin, "Effect of top stiffening rings of open top tanks on critical harmonic settlement," *Thin-Walled Structures*, vol. 65, pp. 62-71, 2013.
- [16] J. Gong, S. Zeng, and T. Jin, "Effect of Hydrostatic Pressure on Buckling Behavior of Storage Tanks Under Local Support Settlement," *Proceedings of the ASME 2013 Pressure Vessels and Piping Conference. Volume 3: Design and Analysis. Paris, France. July 14–18, 2013.*
- [17] Y. Zhao, X. Lei, Z. Wang, and Q. s. Cao, "Buckling behavior of floating-roof steel tanks under measured differential settlement," *Thin-walled structures.*, vol. 69, pp. 70-80, 2013.
- [18] H. Fan, Z. Chen, J. Cheng, P. Jiao, J. Shen, and D. Chen, "Buckling of steel tanks under measured settlement based on Poisson curve prediction model," *Thin-Walled Struct Thin-Walled Structures*, vol. 106, pp. 284-293, 2016.
- [19] Z. Chen, H. Fan, J. Cheng, P. Jiao, F. Xu, and C. Zheng, "Buckling of cylindrical shells with measured settlement under axial compression," *Thin-Walled Structures*, vol. 123, pp. 351-359, 2018.

[20] J. Andreani and N. Carr, "Final Report on the Study of Out-of-Plane Tank Settlement," Report to API SCAST, May 2007.

[21] J. G. Gong, Z. Q. Zhou, and F. Z. Xuan, "Buckling strength of cylindrical steel tanks under measured differential settlement: Harmonic components needed for consideration and its effect," *Thin-Walled Structures*, vol. 119, pp. 345-355, 2017.

[22] D. Pantousa and L. A. Godoy, "On the mechanics of thermal buckling of oil storage tanks," *Thin-Walled Structures*, vol. 145, p. 106432, 2019.

[23] American Petroleum Institute (API) Standard 650, *Welded steel tanks for oil storage*, 12th Edition, American Petroleum Institute. 2013.

[24] ASTM International, 2015, "Standard Specification for Pressure Vessel Plates, Carbon Steel, for Moderate- and Lower-Temperature Service," ASTM International, West Conshohocken, PA, Standard No. ASTM A516/A516M-10.

[25] ASTM, 2008, "Standard Specification for Carbon Structural Steel," ASTM International, West Conshohocken, PA, Standard No. ASTM A36.

[26] ABAQUS, 2017, *Abaqus Analysis User's Manual Version 6.14*, Dassault Systems Simulia Corp., Providence, RI.

[27] ASME Boiler and Pressure Vessel Code, 2019, "Section VIII, Alternative Rules for Construction of Pressure Vessels, Division 2," American Society of Mechanical Engineers, New York, NY.

4. CONCLUSION

Two independent studies were conducted to investigate the current design and analysis provisions of above ground storage tanks as per API 650 and API 653 standards for seismic design and differential settlement, respectively. In the first study, the assumption of rigid foundation for seismic design was investigated for different tank geometries. In the second study, numerous FEA were conducted to propose and validate an alternative method for determining the fitness-for-service of an open top above ground storage tank subjected to differential settlement.

In the first study, the assumption of having rigid base and smaller uplift magnitude was found to be acceptable for the broad tank geometry, however for the nominal and slender geometries this assumption was found to be unacceptable. Having a flexible foundation allowed the tank to uplift during seismic excitation unlike the rigid foundation which has zero uplift. The uplift reduces the contact area and therefore results in higher vertical reaction to balance the horizontal moment due to the hydrodynamic forces. This resulted in higher longitudinal stresses in flexible foundation compared to rigid foundation, which was evident in case of slender tank models. Furthermore, it was observed that the difference between the hoop stresses and longitudinal stresses of the tank cylinder, for a rigid base model compared to a flexible base model increases with the increase in aspect ratio (H/D). The combination of higher hoop stresses along with higher longitudinal stresses in nominal and slender tanks having flexible foundation resulted in an earlier failure through rupture or elephant foot buckling. Thus, resulting in a lower load carrying capacity. Based on the findings, it is recommended that the API 650 Annex E for seismic design guidelines should incorporate the effect of uplift and flexible foundation in the design provisions for nominal and slender tank geometries.

In the second study, the limiting foundation settlement values were found to decrease significantly with increase in harmonic wave number for a given tank geometry. Moreover, limiting settlement values for a given harmonic wave number were found to increase with an increase in the geometric ratio (D^2/H). Therefore, the damage contribution because of each harmonic component should be individually evaluated. However, in the existing API 653 method there is no such provision. The

existing method does not differentiate between effect of different harmonic component and thus, not able to correctly determine the mechanical integrity of the tank. The proposed method is tailored such that the individual damage because of first five harmonic components is calculated and cumulative damage factor is then evaluated. The proposed method is applicable to larger set of global settlement profiles as it does not require a well-defined tilt. The FEA were conducted for multiple tank models subjected to four different actual settlement profiles. The fitness-for-service evaluation based on the proposed method was found to be consistently conservative with the FEA results. The existing method on the other hand was found to be inconsistent with the FEA results, in some cases overestimating allowable settlement by a factor of two and in some other cases underestimating the allowable settlement by a factor of 5. Therefore, it was concluded that the proposed method shall be used in the API 653 for determining the fitness-for-service of open-top above ground storage tank subjected to differential settlement.

The method proposed in the second study is applicable for open top tanks, a future study should be conducted for fixed roof tanks. Also, the effect of differential settlement on reduction in load carrying capacity under seismic and wind load should be investigated. The differential settlement can induce imperfection in tank geometry and results in lower buckling capacity.